UNIVERSITY OF CALIFORNIA,
IRVINE

Disentangling Coastal Carbon Reservoirs Using Carbon Isotopes

DISSERTATION

submitted in partial satisfaction of the requirements
for the degree of

DOCTOR OF PHILOSOPHY

in Earth System Science

by

Niels Egilsson Hauksson

Dissertation Committee:
Professor Ellen Druffel, Chair (UCI)
Professor Tomoko Komada (SFSU)
Professor Adam Martiny (UCI)
Professor Francois Primeau (UCI)

2023

DEDICATION

To

Auren and Laurella

May we build a future worthy of you.

TABLE OF CONTENTS

LIST OF FIGURES

LIST OF TABLES

ACKNOWLEDGEMENTS

I would like to express the deepest appreciation to my committee chair, Professor Ellen R.M. Druffel. She has taught me so much about being a scientist and navigating the challenges of the academic world. It has been an honor to have you as a mentor and to become part of the collective effort to respond to climate change. Thank you also for helping me through becoming a working parent and all of the challenges that it brings.

I would like to thank my committee members. Thank you to Professor Tomoko Komada for being a co-author on my first paper, for helping me refine my writing, and for helping me navigate the peer review process. Thank you to Professor Adam Martiny for advising me on career pathways and how to claim a space in academia. Thank you to Professor Francois Primeau for answering all my questions on physical oceanography and statistics and for showing how to ask questions that get to the heart of a scientific problem.

I would like to the thank the members of my lab, without whose help, none of the work would have been accomplished. Thank you to our lab manager Sheila Griffin. She has taught me to organize a research project from start to finish, and I know that I will continue using those skills for my entire career. Thank you to Dr. Christian Lewis, the graduate student before me, was an invaluable colleague who pushed me on refining my experimental design and scientific thinking. Finally, thank you to Katie Thomas, our undergraduate research assistant, for her tireless work on processing all the samples that I brought into the lab from my field work. It is truly a joy to be part of the Druffel lab family.

I would like to thank my other colleagues in the Earth System Science department at UC Irvine. Thank you to Dr. Xiaomei Xu for teaching me what feels like everything there is to know about carbon isotope analysis. The precision and quality with which she works is

an inspiration and it will continue to be the standard against which I hold myself. Thank you to Dr. John Southon, director of the Keck CCAMS laboratory, for teaching me how to run a particle accelerator and for how to properly scrutinize our data. Thank you to all of the other researchers in the Keck CCAMS laboratory including Professor Claudia Czimczik, Dr Guaciara Santos, Professor Sue Trumbore, Dr Patrick Rafter, Chanda Bertrand, Hector Martinez, and Nassib Shamas, for all their help in entering the wonderful world of radiocarbon. Thank you to Dr. Julie Ferguson for her mentorship in transitioning from the world of K-12 education to university education. Thank you to all of the ESS graduate students for their comradery and insightful lunch time conversations during my time at UCI.

Chapter 2 of this dissertation is a reprint of the material as it appears in (Hauksson, N., Lewis, C.B., Komada, T. and Druffel, E.R.M. (2023), Effect of marine sediment on the phase partitioning and isotopic content of riverine DOC. Limnol Oceanogr, 68: 2008-2021. https://doi.org/10.1002/lno.12403), used with permission from John Wiley and Sons. Minor edits have been made to fix typographic errors. The co-authors listed in this publication are Christian B. Lewis, Tomoko Komada, and Ellen R.M. Druffel.

Chapter 3 of this dissertation is a reprint of the material as it appears in (Hauksson NE, Xu X, Pedron S, et al. TIME SERIES OF SURFACE WATER DISSOLVED INORGANIC CARBON ISOTOPES FROM THE SOUTHERN CALIFORNIA BIGHT. Radiocarbon. 2023:1-16. doi:10.1017/RDC.2023.73). The article was published by Cambridge University Press under a creative commons license (https://creativecommons.org/licenses/by/4.0/). Minor edits have been made to fix typographic errors. The co-authors listed in this publication are Xiaomei Xu, Shawn Pedron, Hector A. Martinez, Christian B. Lewis, Danielle

S. Glynn, Christopher Glynn, Noreen Garcia, Alessandra Flaherty, Katherine Thomas, Sheila Griffin, and Ellen R. M. Druffel.

Financial support was provided by the University of California, Irvine, NSF Grant OCE–1951073 and the Jenkins Foundation.

VITA

Niels Egilsson Hauksson

Education

2018-2023	University of California, Irvine	Earth System Science Ph.D.
2018-2020	University of California, Irvine	Earth System Science M.S.
2013-2015	University of California, Irvine	Teaching Credential
2013-2015	University of California, Irvine	Chemistry M.S.
2008-2012	University of California, Santa Cruz	Biochemistry B.S.

Professional Positions

2018-2023	Graduate Student Researcher: University of California, Irvine
2017-2018	Project Coordinator: Strategic Energy Innovations
2015-2017	Science Teacher: Huntington Beach Union High School District
2013-2014	Teaching Assistant: University of California, Irvine
2013-2016	Operations Manager: Parker Anderson Enrichment, Orange County
2010-2012	Undergraduate Researcher: University of California, Santa Cruz
2011	Summer Research Assistant: Children's Hospital Los Angeles
2005-2013	Youth Development Specialist: Tom Sawyer Camps

Peer Reviewed Publications

1. Druffel, E.R.M.; Lewis, C.B.; Griffin, S.; Flaherty, A.; Rudresh, M.; Hauksson, N.E.; Key, R.M.; McNichol, A.P.; Walker B.D. 2023 Dissolved organic radiocarbon in the West Indian Ocean. *Geophysical Research Letters,* 50, e2023GL104732., *https://doi.org/10.1029/2023GL104732*
2. Hauksson, N.E.; Xu, X.; Pedron, S; Martinez, H.A.; Lewis, C. B.; Glynn, D.S.; Glynn, C; Garcia, N; Flaherty, A; Thomas, K; Griffin, S; Druffel, E.R.M. 2023, Time series of surface water dissolved inorganic carbon isotopes from the Southern California Bight, *Radiocarbon,* 1-16. http://dx.doi.org/10.1017/RDC.2023.73
3. Hauksson, N.; Lewis, C.B.; Komada, T.; Druffel, E.R.M. 2023, Effect of Marine Sediment on the Phase Partitioning and Isotopic Content of Riverine DOC, *Limnol. Oceanogr. 9999, 2023, 1–14 https://doi.org/10.1002/lno.12403*
4. Druffel, E. R. M.; Griffin, S.; Lewis, C. B.; Rudresh, M.; Garcia, N. G.; Key, R. M.; McNichol, A. P.; Hauksson, N. E.; Walker, B. D. 2021 Dissolved organic radiocarbon in the Eastern Pacific and Southern Oceans. *Geophys. Res. Lett. 48:* (10), e2021GL092904. https://doi.org/10.1029/2021GL092904
5. Turner, R. A., Hauksson N. E., Gripe J. H., and Lokey. R. S., Selective, On-resin N-methylation of peptide N-trifluoroacetamides, Org. Lett. Vol. 15, pp. 5012-5015, September 2013, https://doi.org/10.1021/ol402341u

Invited Talks

1. Disentangling Riverine Organic Carbon Pools Using Carbon Isotopes, Caltech Geoclub Seminar, November 2023

Meeting Presentations

1. Hauksson, N; Thomas, K; Druffel, E; Organic Carbon Cycling at the Mouth of the Santa Clara River During the 2021-2022 La Niña. Poster Presentation. Gordon Research Conference, Chemical Oceanography, July 2023
2. Hauksson, N; Griffin, S; Xu, X; Martinez, H.A.; Pedron, S.; Druffel, E.R.M. Long term time series of surface water dissolved inorganic carbon isotopes from the Southern California Bight. Poster Presentation. 24th Radiocarbon Conference September 2022. Zürich, Switzerland
3. Niels Hauksson, Christian Lewis, Ellen Druffel, Effects of marine sediment on the solubility and carbon isotopes of terrigenous organic matter. Virtual Oral Presentation. Ocean Sciences Meeting, February 2022
4. Niels E. Hauksson, Christian Lewis, Ellen R. M. Druffel, Effect of marine sediment on DOC solubility and radiocarbon isotopes. Virtual Poster Presentation. Radiocarbon in the Environment III Conference, July 2021. Gliwice, Poland.
5. Niels Hauksson, Christian Blair Lewis, and Ellen R M Druffel, Effect on the chemical and isotopic composition of marine dissolved organic matter by adsorption to deep sea sediment. Poster Presentation. Ocean Sciences Meeting, February 2020. San Diego, United States
6. Ellen R M Druffel, Sheila Griffin, Ning Wang, Christian Blair Lewis, Noreen Garcia, Niels Hauksson, Ann P McNichol, Robert M Key and Brett Walker, Radiocarbon in dissolved organic carbon and inorganic carbon in the Pacific Ocean, Poster Presentation. Ocean Sciences Meeting, February 2020. San Diego, United States

Academic Awards and Certifications

June 2022	Earth System Science Outstanding Teaching Assistant Award, UC Irvine
March 2021	Course Design Certificate, UC Irvine
June 2020	Division of Teaching Excellence and Innovation Graduate Fellow, UC Irvine
June 2017	Permanent California Teaching Credential in Biology, Chemistry, and Physics
June 2015	Preliminary California Single Subject Teaching Credential, UC Irvine
June 2012	Honors in the Major, UC Santa Cruz
May 2012	Joseph F. Bunnet award for undergraduate research in chemistry, UC Santa Cruz

Teaching Experience

2021(Fall)	UCI, ESS 40a, Laboratory Instructor, Earth System Chemistry
2021(Spring)	UCI, ESS 1, Teaching Assistant, Introduction to Earth System Science
2020 (Fall)	UCI, ESS 40a, Teaching Assistant, Earth System Chemistry
2020 (Spring)	UCI, ESS 40c, Teaching Assistant, Introduction to Earth System Physics

2020 (Winter)	UCI, ESS 3, Teaching Assistant, Oceanography
2019 (Fall)	UCI, ESS 40a, Teaching Assistant, Earth System Chemistry
2015-2017	Edison High School, Teacher, Physics
2015-2017	Edison High School, Teacher, Chemistry
2014-2015	Ocean View High School, Student Teacher, Chemistry
2014 (Summer)	UCI, CHEM 1a, Teaching Assistant, General Chemistry
2014 (Spring)	UCI, CHEM 1lc, Teaching Assistant, General Chemistry Laboratory
2014 (Winter)	UCI, CHEM 1c, Teaching Assistant, General Chemistry
2013 (Fall)	UCI, CHEM 1b, Teaching Assistant, General Chemistry

Undergraduate Mentorship

2021-2023	Katherine Thomas - Undergraduate Researcher, UC Irvine. Current Position: Ph.D. student, USC, Department of Geological Sciences
2019-2021	Alessandra Flaherty - Undergraduate Researcher, UC Irvine. Current Position: Ph.D. candidate Caltech, Division of Geological and Planetary Sciences
2018-2019	Noreen Garcia - Undergraduate Researcher, UC Irvine. Current Position: Ph.D. NSF Fellowship; Scripps Institution of Oceanography

Synergistic Activities

2021	Ran laboratory classes for ESS 40a, Earth System Chemistry.
2019	Wrote laboratory lessons for ESS 40a, Earth System Chemistry.
2019	Taught at the UCI Radiocarbon Short Course on Marine research of DOC.
2018	Design workshops for the Dr. Lucy Jones Center for Science and Society.
2015-2018	Develop curriculum that integrates environmental topics with K-12 science.
2017-2018	Assist with local high school science lessons as a guest speaker.
2017-2018	Organized and implemented teacher trainings on sustainability curriculum.
2016-2017	Designed courses for the Academy of Sustainability Education at Edison High School.

Field Work:

October 2018	Newport Beach Pier, Orange County CA. Collected surface DIC.
Dec 2021-Jun 2022	Santa Clara River, Ventura, CA. Collected suspended POC and DOC in river water, and sediment.
Feb 2023	Santa Ana River, Orange County, CA. Collected suspended POC, DOC, and DIC in river water, and sediment.

ABSTRACT OF THE DISSERTATION

Disentangling Coastal Carbon Reservoirs using Carbon Isotopes

by

Niels Egilsson Hauksson

Doctor of Philosophy in Earth System Science

University of California, Irvine, 2023

Professor Ellen R.M. Druffel, Chair

Coastal waters connect the terrestrial and marine carbon cycles and are the location of a large portion of the organic carbon (OC) burial in the ocean. Anthropogenic activity has affected the carbon (C) cycling in these waters. However, the heterogeneity of these systems makes generating global estimates challenging. Thus, detailed information about the mechanisms and long-term trends of C fluxes and storage are needed to assess past and future changes to the coastal C cycle.

This dissertation examines the mixing of multiple pools of C in coastal waters using C isotopes (^{13}C and ^{14}C). First, we performed a series of laboratory experiments that examined whether sorption of riverine dissolved OC to sediments could be isotopically selective. We found that compounds with higher $\Delta^{14}C$ values and lower $\delta^{13}C$ values were selectively sorbed by the sediments. Lignin phenols and black C were suspected as possible sorbed compounds. Second, we report a timeseries of $\Delta^{14}C$ and $\delta^{13}C$ values from dissolved inorganic C at the Newport Beach Pier, CA. This record showed a steady decrease in the $\Delta^{14}C$ and $\delta^{13}C$ values over the study period that indicates an increasing quantity of fossil

fuel derived CO_2 dissolved in the surface waters. Third, we compare the magnitude and composition of particulate OC and sedimentary OC from the Santa Clara River Estuary during periods of extreme precipitation and extreme drought. The results mirror the change in the C isotope values of atmospheric CO_2 and show that even in low precipitation years, significant quantities of eroded petrogenic OC are exported by this watershed. The amount of recently produced plant- and algae-derived OC is highly variable in the estuary while the amount petrogenic OC is relatively stable over the study period. Together, these studies enhance our understanding of the processes that control C cycling within coastal waters.

Chapter 1. INTRODUCTION

1.1 **Significance of coastal systems for carbon cycling**

Coastal waters (<200m depth) are hot spots of carbon (C) cycling that link terrestrial systems, the atmosphere, and the open ocean (Cole et al., 2007). These waters account for 85% of total oceanic burial flux of organic carbon (OC) to sediments (Dunne et al., 2007) and they emit significant quantities of CO_2 to the atmosphere from the remineralization of OC and from outgassing of C-rich, upwelled waters (Smith and Hollibaugh, 1993; Bauer et al., 2013). Global estimates of coastal C fluxes are not well constrained due to the limited studies and the heterogeneity of these ecosystems (Bauer et al., 2013). Improving our understanding of mechanisms that underlie coastal C fluxes and the effect of anthropogenic activity on them is key for understanding the future fate of the global C cycle.

Coastal waters are part of the land-ocean aquatic continuum (LOAC), which is the system of waters that interface between the terrestrial biosphere and the open ocean (Billen et al., 1991). Currently, about 2.9 Pg C yr^{-1} from terrestrial systems is entrained by LOAC and 0.95 Pg C yr^{-1} of this flux is exported to the ocean (Global Carbon Project, 2022). The remainder is either buried in lake and river sediments or remineralized (Aufdenkamp et al., 2011). About 1.0 Pg C yr^{-1} of the flux from the terrestrial biosphere to the LOAC is the result of human activity (Regnier et al., 2013). Of this anthropogenic flux, roughly 40% is remineralized and outgassed, 50% buried in sediments, and 10% exported to the open ocean (Regnier et al., 2013). Human activities have and will continue to alter the morphology and biogeochemistry of these waters, which will subsequently impact the fate of the C that moves through them.

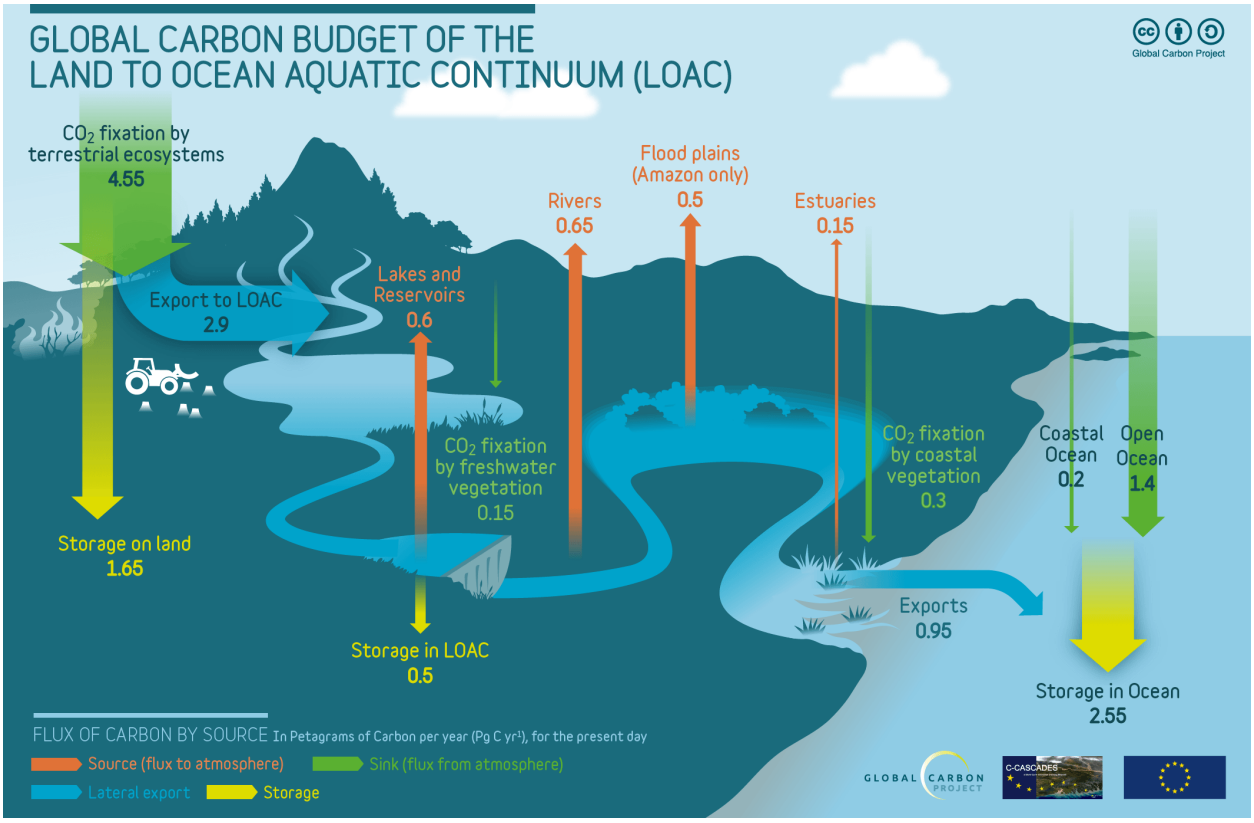

Figure 1.1: C budget of the LOAC, terrestrial ecosystems, and ocean (Global Carbon Project, 2022).

Despite intense C cycling in coastal waters, between 1993 and 2012 dissolved CO_2 concentrations in coastal waters have not increased as much as those in the open ocean (Bourgeois et al., 2016). This is due in part to anthropogenic inputs of macronutrients and sediments that increase C fixation and burial in these regions and drive down dissolved CO_2 concentrations (Dai et al., 2022). Additionally, the shallow depths and relatively low flow in coastal waters limit the rate at which new CO_2 poor waters from the open ocean can replace waters enriched in CO_2 by the coastal heterotrophy (Bourgeois et al., 2016). The already high rates of remineralization of OC that occur in these waters also limits the atmospheric CO_2 uptake in these regions (Ver et al., 1999). It has been estimated that the coastal ocean acts as a carbon sink of 0.25 ± 0.05 Pg C yr^{-1} (Dai et al., 2022).

Human construction within watersheds as also altered the amount of OC exported to the coasts. By the 1990s, human activity increased soil erosion resulting in an additional 2.3 ± 0.6 billion metric tons of sediment per year transported by rivers compared to prehuman estimates (Syvitski et al., 2005). However, dams and reservoirs have reduced the flux of sediment reaching the ocean by 1.4 ± 0.3 billion metric tons per year over this same period (Syvitski et al., 2005). It has been estimated that between 1970 and 2000 the trapping of sediment by dams reduced the flux of OC to oceans by 13% (0.05 Pg C yr^{-1}) (Maavara et al., 2017).

Storms are a major driver of particulate OC (POC) export from rivers to the ocean (Hilton et al., 2008). As storm frequency and intensity increase with climate change this may amplify the OC exported to coasts to either be remineralized or buried. These anthropogenic disturbances are spatially and temporally heterogenous, and therefore will require a fine-tuned understanding of their mechanisms and significant monitoring to predict their future impact.

1.1 The use of carbon isotopes in studying carbon cycling

Naturally occurring C isotopes are invaluable tools for measuring environmental C cycling, source apportionment, reactivity, and age. The ratio between the two naturally occurring stable carbon isotopes ($^{13}C/^{12}C$) in a substance is primarily controlled by the kinetic and equilibrium isotope effect. The heavier mass of ^{13}C means that molecules with ^{13}C atoms have different reaction rates and equilibrium constants than molecules with only ^{12}C atoms (Wolfsberg, 1969; Bigeleisen et al., 1973). Thus, variations of the $^{13}C/^{12}C$ ratios of a sample can be used to infer the chemical history of that sample. For example, OC has

characteristic $^{13}C/^{12}C$ ratios based on the photosynthetic pathway of the organism that fixed the C as well as the $^{13}C/^{12}C$ ratio of the CO_2 feedstock and the temperature at which the organism lived (Sternberg et al., 1984; Mook, 1986).

The unstable C isotope, radiocarbon (^{14}C), has a half-life of 5730 ± 40 yr (Godwin 1962). ^{14}C is generated in the upper atmosphere when cosmic radiation generates high energy neutrons that react with nitrogen nuclei. The ^{14}C nucleus then reacts with atmospheric oxygen to create a $^{14}CO_2$ molecule. The ^{14}C atoms from these molecules become fixed by primary producers or are dissolved into surface waters. Even though ^{14}C undergoes radioactive decay, a system that exchanges CO_2 with the atmosphere will contain a relatively constant amount of ^{14}C. When the exchange stops (e.g., an organism dies or a water parcel moves below the mixed layer), the $^{14}C/^{12}C$ ratio within the system will decrease. ^{14}C measurements by AMS correct for isotopic fractionation and therefore, reflect only the changes due to radioactive decay.

Since the Industrial Revolution, humans have altered the C isotopic ratios of the major above-ground C reservoirs through two main mechanisms. First, humans have added massive quantities of CO_2 to the atmosphere that is predominantly derived from the combustion of fossil fuels and land use changes. The emitted CO_2 has lower $^{14}C/^{12}C$ and $^{13}C/^{12}C$ ratios than atmospheric CO_2 and the mixing of this excess CO_2 into the atmosphere have lowered the overall $^{14}C/^{12}C$ and $^{13}C/^{12}C$ ratios of atmospheric CO_2. This dilution of atmospheric C isotopes is known as the generalized Suess Effect (Keeling 1979). Second, between 1945 and 1963, above ground nuclear weapons testing doubled the ^{14}C content of atmospheric CO_2 in the northern hemisphere. With the passage of the Limited Test Ban Treaty in 1962, above ground tests nearly stopped. Since that time, exchange of CO_2 with

the ocean and the biosphere and the continued emission of fossil fuel CO_2 has drastically reduced the ^{14}C content of the atmosphere, while raising the ^{14}C content of the terrestrial biosphere and the surface ocean. The presence of bomb-radiocarbon has enabled numerous experiments that improved our understanding of C cycling on decadal scales (Jain et al., 1995; Lassey et al., 1995; Wang et al., 2019). As of 2022, atmospheric CO_2 has approximately the same $^{14}C/^{12}C$ ratio as the pre-bomb atmosphere, and this ratio is expected to continue to decline as more fossil fuel CO_2 is emitted (Graven et al., 2022). As the bomb ^{14}C becomes more evenly distributed between the atmosphere, the terrestrial biosphere, and the ocean, the emission of fossil fuel CO_2 will become the major forcing on changes in C isotopic ratios.

A key use of ^{13}C and ^{14}C in aquatic settings is source apportionment. Many of the different sources of C in coastal systems have distinct isotopic ratios. The isotopic ratio of a heterogenous, environmental sample will be the weighted average of the isotopic values of its components. If the isotopic value of the different end members is known, the proportion of each end member can be estimated through calculation. This method has been used in a variety of ways. For example, it has shown that exported riverine OC is derived from plant matter and soils or from eroded petrogenic material (Masiello and Druffel, 2001; Galy et al., 2015). It has also been demonstrated that despite the significant input of riverine DOC to the open ocean, marine DOC appears to be predominantly derived from marine phytoplankton (Hansell et al., 2009; Druffel and Griffin, 2015). Even the mixing of ocean and riverine waters can be observed by changes in the isotope ratios of dissolved inorganic carbon (Hinger et al., 2010). This method is powerful and can be applied to a number of aspects of the coastal C cycle.

1.2 Summary of the dissertation

This dissertation reports three studies that use C isotopes to examines different pools of C in coastal systems. The first chapter describes a series of laboratory studies that examine how sediment sorption affects the isotopic content of riverine dissolved OC (DOC). A riverine organic matter standard was mixed with marine sediments and the C isotopic ratios of the POC and the DOC were measured. This is the first quantitative study of how sediment sorption affects the isotopic content of complex heterogenous DOC.

The second chapter presents an 18-year time series of C isotopes in the surface dissolved inorganic C (DIC) at the Newport Beach Pier in Orange County, CA. The sampling location is in the Southern California Bight. This is a region with complex hydrology, seasonal upwelling, and extensive marine ecosystems. This study examines seasonal and long-term variability and the distribution of bomb-derived ^{14}C and anthropogenic CO_2 in this region.

The third chapter describes the particulate OC (POC) exported by the Santa Clara River during the relatively dry 2021-2022 rainy season and compares it to previous high precipitation (1997-1998) and normal precipitation (2002-2003) years. The Santa Clara River is the largest and least developed river in Southern California, and is responsible for significant terrestrial C export and burial in the Santa Barbara Basin during the last several millennia (Biroski, 2006; Sarno et al., 2020). It has experienced rapid change due to development of the watershed and the region's changing climate. The results of this study will help determine the response of this region to its changing precipitation patterns.

1.4 References

Aufdenkampe, A. K., Mayorga, E., Raymond, P. A., Melack, J. M., Doney, S. C., Alin, S. R., Aalto, R. E., & Yoo, K. (2011). Riverine coupling of biogeochemical cycles between land, oceans, and atmosphere. Frontiers in Ecology and the Environment, 9(1), 53–60. https://doi.org/10.1890/100014

Bauer, J. E., Cai, W.-J., Raymond, P. A., Bianchi, T. S., Hopkinson, C. S., & Regnier, P. A. G. (2013). The changing carbon cycle of the coastal ocean. Nature, 504(7478), Article 7478. https://doi.org/10.1038/nature12857

Bigeleisen, J., Lee, M. W., & Mandel, F. (1973). Equilibrium Isotope Effects. Annual Review of Physical Chemistry, 24(1), 407–440 https://doi.org/10.1146/annurev.pc.24.100173.002203

Billen, G., Lancelot, C., Meybeck, M., Mantoura, R.F., Martin, J.M., & Wollast, R. (1991). N, P and Si retention along the aquatic continuum from land to ocean.

Birosik, S. (2006). *State of the Watershed – Report on Surface Water Quality: The Santa Clara River Watershed* (RB-AR22181). California Regional Water Quality Control Board, Los Angeles Region.

Bourgeois, T., Orr, J. C., Resplandy, L., Terhaar, J., Ethé, C., Gehlen, M., & Bopp, L. (2016). Coastal-ocean uptake of anthropogenic carbon. Biogeosciences, 13(14), 4167–4185. https://doi.org/10.5194/bg-13-4167-2016

Cole, J. J., Prairie, Y. T., Caraco, N. F., McDowell, W. H., Tranvik, L. J., Striegl, R. G., Duarte, C. M., Kortelainen, P., Downing, J. A., Middelburg, J. J., & Melack, J. (2007). Plumbing the Global Carbon Cycle: Integrating Inland Waters into the Terrestrial Carbon Budget. Ecosystems, 10(1), 172–185. https://doi.org/10.1007/s10021-006-9013-8

Dai, M., Su, J., Zhao, Y., Hofmann, E. E., Cao, Z., Cai, W.-J., Gan, J., Lacroix, F., Laruelle, G. G., Meng, F., Müller, J. D., Regnier, P. A. G., Wang, G., & Wang, Z. (2022). Carbon Fluxes in the Coastal Ocean: Synthesis, Boundary Processes, and Future Trends. Annual Review of Earth and Planetary Sciences, 50(1), 593–626. https://doi.org/10.1146/annurev-earth-032320-090746

Druffel, E. R. M., & Griffin, S. (2015). Radiocarbon in dissolved organic carbon of the South Pacific Ocean. Geophysical Research Letters, 42(10), 4096–4101. https://doi.org/10.1002/2015GL063764

Dunne, J. P., Sarmiento, J. L., & Gnanadesikan, A. (2007). A synthesis of global particle export from the surface ocean and cycling through the ocean interior and on the seafloor. Global Biogeochemical Cycles, 21(4). https://doi.org/10.1029/2006GB002907

Galy, V., Peucker-Ehrenbrink, B., & Eglinton, T. (2015). Global carbon export from the terrestrial biosphere controlled by erosion. Nature, 521(7551), Article 7551. https://doi.org/10.1038/nature14400

Global Carbon Budget 2022, by Pierre Friedlingstein, Michael O'Sullivan, Matthew W. Jones, Robbie M. Andrew, Luke Gregor, Judith Hauck, Corinne Le Quéré, Ingrid T. Luijkx, Are Olsen, Glen P. Peters, and others (2022), Earth System Science Data, 14, 4811–4900, 2022, DOI: 10.5194/essd-14-4811-2022.

Graven H, Keeling R, Xu X. 2022. Radiocarbon Dating: Going Back in Time. *Nature* 607(7919):449–449.

Hansell, D., Carlson, C., Repeta, D., & Schlitzer, R. (2009). Dissolved Organic Matter in the Ocean: A Controversy Stimulates New Insights. Oceanography, 22(4), 202–211. https://doi.org/10.5670/oceanog.2009.109

Hilton, R. G., & West, A. J. (2020). Mountains, erosion and the carbon cycle. Nature Reviews Earth & Environment, 1(6), Article 6. https://doi.org/10.1038/s43017-020-0058-6

Hinger, E. N., Santos, G. M., Druffel, E. R. M., & Griffin, S. (2010). Carbon Isotope Measurements of Surface Seawater from a Time-Series Site Off Southern California. Radiocarbon, 52(1), 69–89. https://doi.org/10.1017/S0033822200045045

Jain, A. K., Kheshgi, H. S., Hoffert, M. I., & Wuebbles, D. J. (1995). Distribution of radiocarbon as a test of global carbon cycle models. Global Biogeochemical Cycles, 9(1), 153–166. https://doi.org/10.1029/94GB02394

Keeling, C. D. (1979). The Suess effect: 13Carbon-14Carbon interrelations. Environment International, 2(4), 229–300. https://doi.org/10.1016/0160-4120(79)90005-9

Mook WG. 1986 13C in Atmospheric CO2. *Netherlands Journal of Sea Research* 20(2/3): 211-223

Lapierre, J.-F., Guillemette, F., Berggren, M., & del Giorgio, P. A. (2013). Increases in terrestrially derived carbon stimulate organic carbon processing and CO2 emissions in boreal aquatic ecosystems. Nature Communications, 4(1), Article 1. https://doi.org/10.1038/ncomms3972

Lassey, K. R., Enting, I. G., & Trudinger, C. M. (1996). The earth's radiocarbon budget. Tellus B: Chemical and Physical Meteorology, 48(4), 487–501. https://doi.org/10.3402/tellusb.v48i4.15928

Maavara, T., Lauerwald, R., Regnier, P., & Van Cappellen, P. (2017). Global perturbation of organic carbon cycling by river damming. Nature Communications, 8(1), Article 1. https://doi.org/10.1038/ncomms15347

Masiello, C. A., & Druffel, E. R. M. (2001). Carbon isotope geochemistry of the Santa Clara River. Global Biogeochemical Cycles, 15(2), 407–416. https://doi.org/10.1029/2000GB001290

Regnier, P., Friedlingstein, P., Ciais, P., Mackenzie, F. T., Gruber, N., Janssens, I. A., Laruelle, G. G., Lauerwald, R., Luyssaert, S., Andersson, A. J., Arndt, S., Arnosti, C., Borges, A. V., Dale, A. W., Gallego-Sala, A., Goddéris, Y., Goossens, N., Hartmann, J., Heinze, C., … Thullner, M. (2013). Anthropogenic perturbation of the carbon fluxes from land to ocean. Nature Geoscience, 6(8), Article 8. https://doi.org/10.1038/ngeo1830

Sarno, C. T., Benitez-Nelson, C. R., Ziolkowski, L. A., Hendy, I. L., Davis, C. V., Tappa, E. J., & Thunell, R. C. (2020). The Impacts of Flood, Drought, and Turbidites on Organic Carbon Burial Over the Past 2,000 years in the Santa Barbara Basin, California. Paleoceanography and Paleoclimatology, 35(7), e2020PA003849. https://doi.org/10.1029/2020PA003849

Sternberg, L. O.; Deniro, M. J.; Johnson, H. B. 1984. Isotope Ratios of Cellulose from Plants Having Different Photosynthetic Pathways. *Plant Physiol. 74:* (3), 557–561. https://doi.org/10.1104/pp.74.3.557.

Smith, S. V., and Hollibaugh, J. T. (1993), Coastal metabolism and the oceanic organic carbon balance, Rev. Geophys., 31(1), 75–89, doi:10.1029/92RG02584.

Syvitski, J. P. M., Vörösmarty, C. J., Kettner, A. J., & Green, P. (2005). Impact of Humans on the Flux of Terrestrial Sediment to the Global Coastal Ocean. Science, 308(5720), 376–380. https://doi.org/10.1126/science.1109454

Ver, L. M. B., Mackenzie, F. T., & Lerman, A. (1999). Carbon cycle in the coastal zone: Effects of global perturbations and change in the past three centuries. Chemical Geology, 159(1), 283–304. https://doi.org/10.1016/S0009-2541(99)00042-X

Wang, N., Shen, C., Sun, W., Ding, P., Zhu, S., Yi, W., Yu, Z., Sha, Z., Mi, M., He, L., Fang, J., Liu, K., Xu, X., & Druffel, E. R. M. (2019). Penetration of Bomb 14C Into the Deepest Ocean Trench. Geophysical Research Letters, 46(10), 5413–5419. https://doi.org/10.1029/2018GL081514

Wolfsberg, M. (1969). Isotope Effects. Annual Review of Physical Chemistry, 20(1), 449–478. https://doi.org/10.1146/annurev.pc.20.100169.002313

Chapter 2. Effect of Marine Sediment on the Phase Partitioning and Isotopic Content of Riverine DOC

2.1 Abstract

Rivers discharge significant quantities of dissolved organic carbon (DOC) to the ocean, yet biomarker and isotope studies suggest that terrigenous DOC makes up only a small amount DOC in the ocean. One of the removal pathways proposed for riverine DOC is sorption to marine sediments. This process is chemically selective, but whether sorption alters the isotopic composition of riverine DOC is unknown. Because there is isotopic variability across different organic compound classes, sorptive removal of DOC could also alter the isotopic composition of DOC. As a first step in addressing this question, we examined phase partitioning and isotopic composition of a riverine DOC standard in the presence of marine sediment particles. In a series of controlled experiments, the standard was mixed with marine sediment in 35‰ NaCl solution, then separated into particulate and dissolved phases for analyses of mass, $\delta^{13}C$, and $\Delta^{14}C$ of organic carbon (OC). Across a range of sediment OC to DOC mass ratios (from <0.1 to ~3), we found that: (1) sediment sorbed 0.8μg OC per mg of sediment; and (2) DOC compounds with higher $\Delta^{14}C$ and lower $\delta^{13}C$ values relative to the bulk DOC was preferentially removed from solution. In effect, mixing a riverine DOC standard with marine sediment resulted in decreased $\Delta^{14}C$ and increased $\delta^{13}C$ of the DOC that remained in solution. These results show that sorption of DOC to sediment can alter the isotopic content of riverine DOC.

2.2 Introduction

Rivers transport 0.25 PgC of dissolved organic carbon (DOC) and 0.15 PgC of particulate organic carbon (POC) to the ocean per year (Hedges et al., 1997). The

partitioning of OC between POC and DOC profoundly affects the chemical reactivity, microbial environment, and physical movement of the OC as it traverses riparian zones and estuaries (Hedges and Keil 1999). In particular, sorption has been shown to selectively remove certain compounds from DOC (Fox, 1983; Aufdenkamp et al., 2001; Mahamat Ahmat et al., 2016; Matiasek and Hernes, 2019). This chemical selectively may also result in isotopic selectivity because different compound classes often have distinct isotopic values (Close 2019), but the magnitude of this effect is not well constrained.

The global flux of riverine DOC is significant with respect to the size of the marine DOC pool (662 PgC) (Hansell et al., 2009). A DOC flux of 0.25 PgC yr^{-1} would support a marine DOC turnover time of ~2600 years (= 662 PgC/0.25 PgC yr^{-1}). However, the radiocarbon age of marine DOC ranges from 4900-6600 years in the deep ocean (Druffel et al., 2022). In this system, this discrepancy could occur if: (1) the contribution of riverine DOC to marine DOC is significantly less than 0.25 PgC yr^{-1} due to rapid removal of riverine DOC from seawater; (2) riverine DOC contributing to the marine DOC pool has an older radiocarbon age than modern photosynthetically produced compounds; (3) "young" riverine DOC is preferentially degraded in the ocean, leaving older riverine DOC; or (4) a combination of (1), (2), and (3). In rivers with broad DOC age distributions, sorption to sediment particles could contribute to both mechanisms; the sorption itself would reduce the total flux of riverine DOC to the open ocean, and if this sorption selectively removed compounds with a younger radiocarbon age, the radiocarbon age of remaining DOC would increase.

There is also a mismatch between the stable carbon isotope signatures ($\delta^{13}C$) of riverine DOC and those of marine DOC. Riverine DOC contains recently produced

compounds from local plants, aged material mobilized from soils and bedrock by weathering, or from anthropogenic inputs (Raymond and Spencer, 2015). The $\delta^{13}C$ values of the plant material depend on the photosynthetic pathway (-23‰ to -28‰ for C3, -12‰ to -16‰ for C4, -11‰ to -13‰ for CAM) (Sternberg et al., 1984). Petrochemical inputs have no measurable radiocarbon ($\Delta^{14}C$ = -1000‰) and $\delta^{13}C$ that is similar to C3 plants (-22‰ to -27‰) (Reed and Kaplan, 1977). In contrast, $\delta^{13}C$ values of marine DOC range from -18‰ to -23‰ at <1000 m depth, and from -21‰ and -23‰ at >1000 m depth (Druffel and Griffin, 2015; Druffel et al., 2021), similar to those of marine phytoplankton (-21‰) (Williams and Gordon 1970). This points to either significant removal or isotopic alteration of terrigenous DOC as it reaches the ocean. If sorption of DOC to sediments is isotopically selective, then this could contribute to the alteration of the $\delta^{13}C$ values and the masking of the terrigenous signal.

Sorption of DOC to sediments is mediated by various physiochemical interactions between the DOC and the sediments (Kleber et al., 2007). Cations within sediments can form ionic bonds with charged molecules in the DOC, such as carboxylic acids, or interact with the π-systems of aromatic rings (Keiluweit and Kleber, 2009; Kleber, et al., 2007). Additionally, organic molecules already bound to the sediment can interact with DOC through hydrophobic interactions, enabling attraction of long alkyl chains (Kleber, et al., 2007). Lignin monomers, long chain fatty acids, and *n*-alkanes, all biomarkers of terrestrial OC, contain either aromatic rings, carboxylic acids, or alkyl chains. These biomarkers are not found in abundance in pelagic environments but are found in estuarine and coastal sediments (Benner and Opsahl, 2001; Close 2019; Xing et al., 2011). Selective sorption of

these biomarkers to sediments could help explain their absence in the ocean, despite the large flux of riverine DOC to the ocean.

Carbon isotope signatures ($\Delta^{14}C$ and $\delta^{13}C$) are useful tracers of organic matter in complex environments. Chemical heterogeneity of a sample can result in isotopic heterogeneity, and consequently, any chemically specific processes could also affect the isotopic content of a sample. As a first step in examining how the isotopic content of terrigenous DOC could be affected by the presence of sediment particles, we carried out a series of controlled experiments where we combined a riverine DOC standard (Suwanee River Natural Organic Matter; SRNOM) with marine sediment from the eastern N. Pacific Ocean (Coppola et al., 2014) under fixed ionic strength, and measured the OC content and isotopic signatures in both the dissolved and particulate phases. Our specific objectives were to determine: (1) the amount and isotopic composition of SRNOM that is sorbed by marine sediment; and (2) the isotopic composition of SRNOM that remains in solution. We conducted this work as an initial investigation into isotopic fractionation during DOC sorption, and not as a simulation of riverine DOC loss in estuaries and the coastal ocean. We also note that these experiments were conducted during the height of the COVID-19 pandemic when field work was virtually impossible; experiments were therefore conducted using materials that were then readily available in our laboratory.

2.3 Methods

2.3.1 Site selection and sediment collection

The sediment used in this project was collected from 4100 m depth in the northeast Pacific Ocean in June 1994 at Station M, located 200 km west of Pt. Conception, CA

(34°50'N,123.0°W). This site was established to monitor multi-decadal time-series of the benthic boundary layer, features strong seasonal variability in surface primary productivity and minimal turbidity at abyssal depths, and offers ease of access for research vessels (Smith et al., 2016). Samples from Station M were selected for this study because our laboratory has previously conducted numerous isotopic studies at this location, and we had material from prior studies (Coppola et al., 2014; Hwang et al., 2005; Wang et al., 1996).

Sediments were collected with a box corer mounted on a free vehicle grab respirometer by Ken Smith and colleagues on the R/V New Horizon on 9 October 1996, stn #1309. A 10 cm diameter subcore was taken from the box core. The core was sub-sampled and sectioned on board ship, placed in precombusted, borosilicate bottles, and frozen at –20 ºC until analysis at UCI. Sediment from the 12-14 cm depth interval was used in the sorption experiments.

2.3.2 Riverine organic matter standard

Suwanee River Natural Organic Matter (SRNOM), 2R101N Humic Substances Society, was used for the experiments as riverine DOC. The chemical composition of this standard is well characterized, and it is used for assessing new dissolved organic matter related methodologies (Nwosu and Cook, 2015; Chen et al., 2016; Li et al., 2016). SRNOM was isolated from Suwanee River water using reverse osmosis and cation exchange chromatography, and lyophilized, recovering 94% of total DOC (Green et al., 2014). SRNOM was used as a type of DOC sample from temperate rivers, and its chemical and isotopic composition are not considered to be representative of all river systems. SRNOM was

chosen due to 1) its availability, 2) its widespread use in other laboratory studies of DOC, and 3) its high recovery from total DOC.

2.3.3 Sediment sorption experiments

Due to difficulty conducting field work during the COVID-19 pandemic, we elected to use sediments collected from the open ocean during prior field campaigns, and under ionic strength similar to that of seawater. We were primarily interested in the effect of the sediment on the DOC isotopes, so we chose to vary that parameter alone.

An overview of the sorption experiments is presented in Figure 2.1. All glassware and metal implements were precombusted at 540ºC for 2 hours prior to use. The sediment from Station M was homogenized, and aliquots ranging in size from ~5 mg to ~200 mg were weighed into borosilicate centrifuge tubes. Approximately 2 mg of SRNOM and 1 mL of 35‰ (w/w) NaCl in MilliQ water (from here on, referred to as "saltwater" for simplicity) were accurately quantified and placed in each tube. The NaCl was precombusted in the same manner as the glass and metal implements. The mixture was homogenized by swirling the tubes by hand for 5 minutes at room temperature and then stored overnight at 4ºC in the dark.

Samples were then centrifuged at 2600 x *g* for 60 minutes, and the supernatant was removed with a 2-mL glass pipette and vacuum filtered through a pre-combusted 0.7-µm 25-mm quartz fiber filter. Filter and filtrant were rinsed with an additional 1.5 mL of saltwater. The filtrate was acidified with 3 drops of 3% H_3PO_4 (Fisher Scientific, HPLC Grade), allowed to sit overnight at 4ºC to remove inorganic C, then transferred to 9-mm OD quartz combustion tubes and dried. Experiments with < 50 mg of sediment were dried by

lyophilization in a Labconco FreeZone 2.5 L benchtop freeze dry system. However, it was later discovered that this yielded a correctable, but significant amount of carbon contamination (54-75 μg C, $\Delta^{14}C$=-925‰). The likely cause of the contamination was oil fumes from the pump. The remaining samples (experiments with ≥50 mg of sediment) were dried directly on the vacuum line with lower blanks (2μg C, $\Delta^{14}C$=-383‰). The $\Delta^{14}C$ values were corrected for the contamination using the direct method described by Santos et al. (2010).

The sediment pellet and filter were acidified by HCl fumigation in a desiccator for 3 to 4 hours at room temperature to remove inorganic C (Komada et al., 2008), and transferred to separate quartz combustion tubes. Pre-combusted quartz wool was used to collect the sediment and transfer it from the centrifuge tube to the quartz tube. Samples were dried directly on a vacuum line before preparation for isotope analysis. The sediment pellet and supernatant filtrant were combined to represent the solid phase.

The experiments were repeated across a large range of sediment masses, from 5 mg to 205 mg. Insignificant amounts of SRNOM were sorbed in experiments with 5 mg of sediment, so we did not run experiments using smaller sediment masses. Experiments with 205 mg of sediment produced close to the maximum amount of CO_2 gas that could be safely measured on our vacuum line.

a

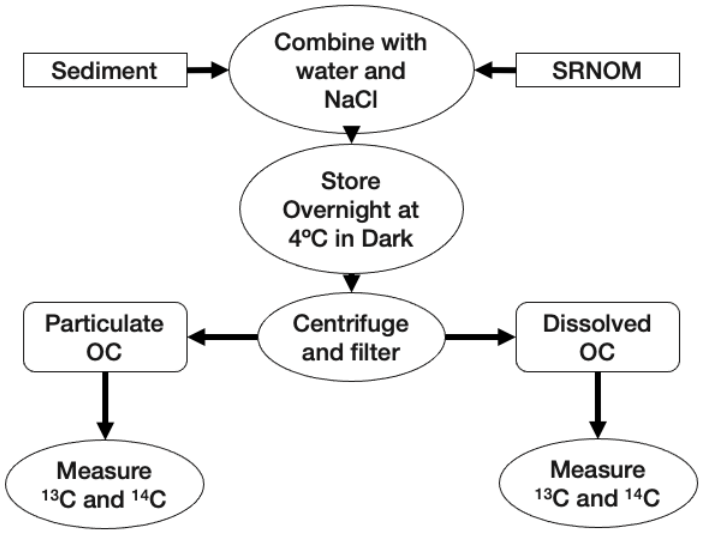

b

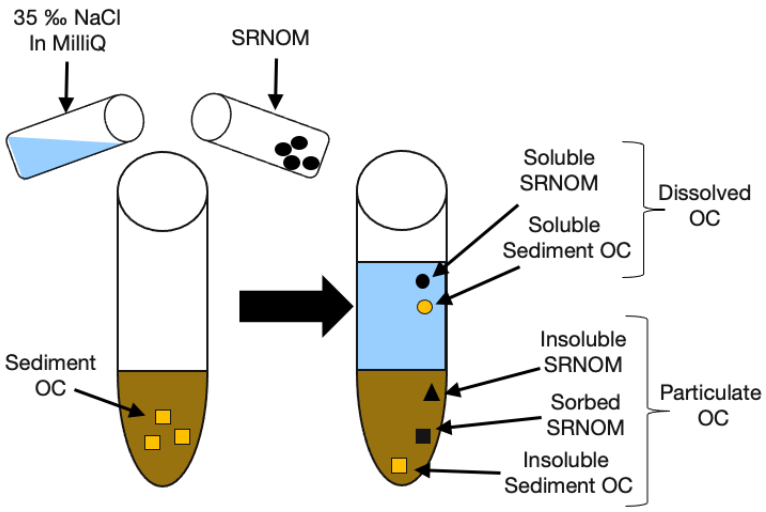

Figure 2.1. Procedural flowchart (a) and conceptual cartoon (b) for the sediment sorption experiments. In (b) black and orange indicate OC from Sta M sediment and SRNOM, respectively.

2.3.4 Control experiments

In addition to the sorption experiments, two sets of control experiments were performed to determine the solubility of SRNOM and marine sediment OC in saltwater. One set of control experiments (Table 2.2, SRNOM control) was performed in the absence of sediment to determine the mass and isotopic values of the salt-water soluble and insoluble components of SRNOM. Another set of control experiments (Table 2.2, sediment control) was performed in the absence of SRNOM to determine the mass and isotopic values of salt-water soluble and insoluble components of Station M sedimentary OC. 105±6 mg (n=3) of sediment was used. All conditions were otherwise same as sorption experiments.

2.3.5 Radiocarbon and stable carbon isotope analyses

All samples were sealed in quartz tubes under vacuum with cupric oxide and silver wire and combusted at 850ºC for 2 hours. The CO_2 produced (1- 757 μgC) was cryogenically separated from water and from gasses with boiling points < -196º C. The samples were then reduced to graphite on iron catalyst as described previously (Xu et al., 2007; Walker and Xu, 2019). Splits of the CO_2 were taken for $\delta^{13}C$ analysis (~20μgC). Each split was allowed to equilibrate for at least 2 minutes to avoid fractionation.

The ^{14}C analyses of the graphite samples were performed at the Keck Carbon Cycle AMS (KCCAMS) Laboratory at UCI (Santos et al., 2010). Direct process blanks, carbon produced from running an experiment with no sample, were used to correct for extraneous carbon added during the experiments. Indirect blank assessment was also used to correct for extraneous carbon added during combustion and graphitization of samples (Santos et al., 2010). Radiocarbon results are reported as $\Delta^{14}C$ corrected for collection date (Stuiver

and Polach, 1977). Uncertainties were determined by taking the pooled standard deviation of replicates (Druffel et al., 2013, McNaught and Wilkinson 1997). Radiocarbon measurements have the following uncertainties: DOC samples ±6‰; solid phase samples with <50mg of sediment: ±19 ‰; and solid phase samples with ≥50mg of sediment: ±2‰.

The ^{13}C analysis of the CO_2 splits was performed at UCI using a Gas Bench II coupled with a Thermo Electron Delta Plus XL isotope ratio mass spectrometer. $\delta^{13}C$ measurements have an uncertainty of ±0.1‰. This was determined by calculating the standard error of repeat measurements of the following standards: OX-1, glycine, and SRNOM. Because process blanks were too small to perform $\delta^{13}C$ measurements, we performed theoretical blank corrections using the masses of process blanks and assuming that the process b lanks had $\delta^{13}C$ values of -10‰ and -35‰. For both values, we found that the blank corrected $\delta^{13}C$ values were within 2 standard deviations of the uncorrected measurements. Due to the high blank and lower quantities of CO_2 obtained, OC from experiments with <50mg of sediment were only analyzed for $\Delta^{14}C$.

2.3.6 POC mass balance

We describe POC in the experimental slurries as the sum of three endmembers: OC indigenous to the marine sediment that is insoluble in saltwater ("insoluble sediment OC"), OC in SRNOM that is insoluble in saltwater (insoluble SRNOM), and OC in SRNOM sorbed by the sediment (sorbed SRNOM):

$$M_{POC} = M_{SedOC\_insoluble} + M_{SRNOM\_insoluble} + M_{SRNOM\_sorbed} \quad (1)$$

where M_i is the mass of OC from endmember i. The isotopic content of the solid phase OC can be defined by equation (2):

$$\Delta_{POC} M_{POC} = \Delta_{SedOC\_insoluble} M_{SedOC\_insoluble} + \Delta_{SRNOM\_insoluble} M_{SRNOM\_insoluble} + \Delta_{SRNOM\_sorbed} M_{SRNOM\_sorbed} \quad (2)$$

where Δ_i is the $\Delta^{14}C$ value of endmember i. Analogous equation can be written for $\delta^{13}C$ values. In solving equations (1) and (2), we assumed that an invariable fraction of sediment OC and SRNOM were insoluble in salt water, and that the isotopic composition of these insoluble fractions remained constant across all experiments. We used the results of the control experiments to determine the isotopic composition and masses of the insoluble sediment OC and insoluble SRNOM.

2.4 Results

2.4.1 Sediment control experiments

The sediment contained 12.1 ± 0.2 μg OC/mg sediment, and this OC had an average $\Delta^{14}C$ of -431 ± 2‰ (sd, n=3) and an average $\delta^{13}C$ of -22.1 ± 0.5‰ (n=3; Table 2.1). When suspended in salt water without SRNOM, OC in the dissolved phase increased by an amount equivalent to 0.08 ± 0.07 μg OC/mg sediment (n=3) and any change in the particulate phase was within analytical error of the total sediment OC (Table 2.1, 2.2). The salt-water soluble sediment OC had a $\Delta^{14}C$ of -181±13‰ (n=2; Table 2.1, 2.2); insufficient material was recovered to obtain a $\delta^{13}C$ measurement. The salt-water insoluble sediment OC had $\Delta^{14}C$ and $\delta^{13}C$ values that were indistinguishable from those of total OC (n=3; Table 2.1, 2.2).

2.4.2 SRNOM control experiments

SRNOM had an OC content of 428±25µg OC/mg of SRNOM, with a $\Delta^{14}C$ of 53±2‰ (n=6) and a $\delta^{13}C$ of -27.5 ± 0.1‰ (n=2) (Table 2.1). When suspended in salt water without sediment, 47±3µg OC/mg of SRNOM, or 10.9% of total OC, was recovered as POC (Tables 1 and 2). The remaining 89.1%, 381±22 µg OC/mg of SRNOM, was assumed to be DOC. When the SRNOM was initially collected, it was passed through a 0.45 µm filter, suggesting that this effect is primarily precipitation rather than aggregation to existing particles (Green et al., 2014). Because the same masses of SRNOM and water were used in all experiments, we assume that a constant fraction of insoluble OC was present in each experiment. The insoluble OC of the SRNOM had a $\Delta^{14}C$ of 37±7‰ (n=4) and a $\delta^{13}C$ of -28.2±0.1‰ (analytical error, n=1) (Tables 1 and 2). The salt-water soluble portion of SRNOM had an average $\Delta^{14}C$ value of 54±5‰ (n=5) and an average $\delta^{13}C$ value of -27.4±0.2‰ (n=2; Table 2.2).

Table 2.1: Masses, $\Delta^{14}C$, and $\delta^{13}C$ values for the sediment OC and SRNOM.

Station M Sediment		OC (μg/mg)	$\Delta^{14}C$ (‰)	$\delta^{13}C$ (‰)
Stn M Event 3109 12-14cm	Total OC	12.1 ± 0.2 n=3	-431 ± 2 n=3	-22.1 ± 0.5 n=3
	Salt Water Soluble OC*	0.08 ± 0.07 n=2	-181 ±13 n=2	not determined
	Salt Water Insoluble OC*	12.1 ± 0.2 n=3	-431 ± 2 n=3	-22.2 ± 0.2 n=3
Suwanee River Normal Organic Matter 2R101N		OC (μg/mg)	$\Delta^{14}C$ (‰)	$\delta^{13}C$ (‰)
	Total OC	428 ± 25 n=8	53 ± 2 n=6	-27.5 ± 0.1 n=2
	Salt Water Soluble OC†	381 ± 22 n=5	54 ± 5 n=5	-27.4 ± 0.2 n=2
	Salt Water Insoluble OC†	47 ± 3 n=4	37 ± 7 n=4	-28.2 ± 0.1 n=1‡

* Values were obtained by performing control experiments with no SRNOM present.
†Values were obtained by performing control experiments with no sediment present.
‡ Error based on IRMS analyses

2.4.3 OC mass partitioning in sorption experiments

Masses of total POC showed a strong positive correlation with the mass of sediment used in each experiment (R^2=0.99, p<<0.001; Table 2.2, Figure 2.2a). Masses of DOC (comprising salt water-soluble SRNOM and salt water-soluble sediment OC) ranged from 315 μg to 757 μg (Table 2.2, Figure 2.2b). A decrease in the mass of DOC with increasing sediment weight was observed in experiments containing 75 mg or more of sediment. Between 48-100% of the total OC introduced into each experiment (in the form of sediment OC and SRNOM) was recovered as the sum of POC and DOC (average of 87±12%, n=27) (Figure 2.2c). Between 48% to 99% of SRNOM OC was recovered (average of 81±13%, n=27; Figure 2.2d)

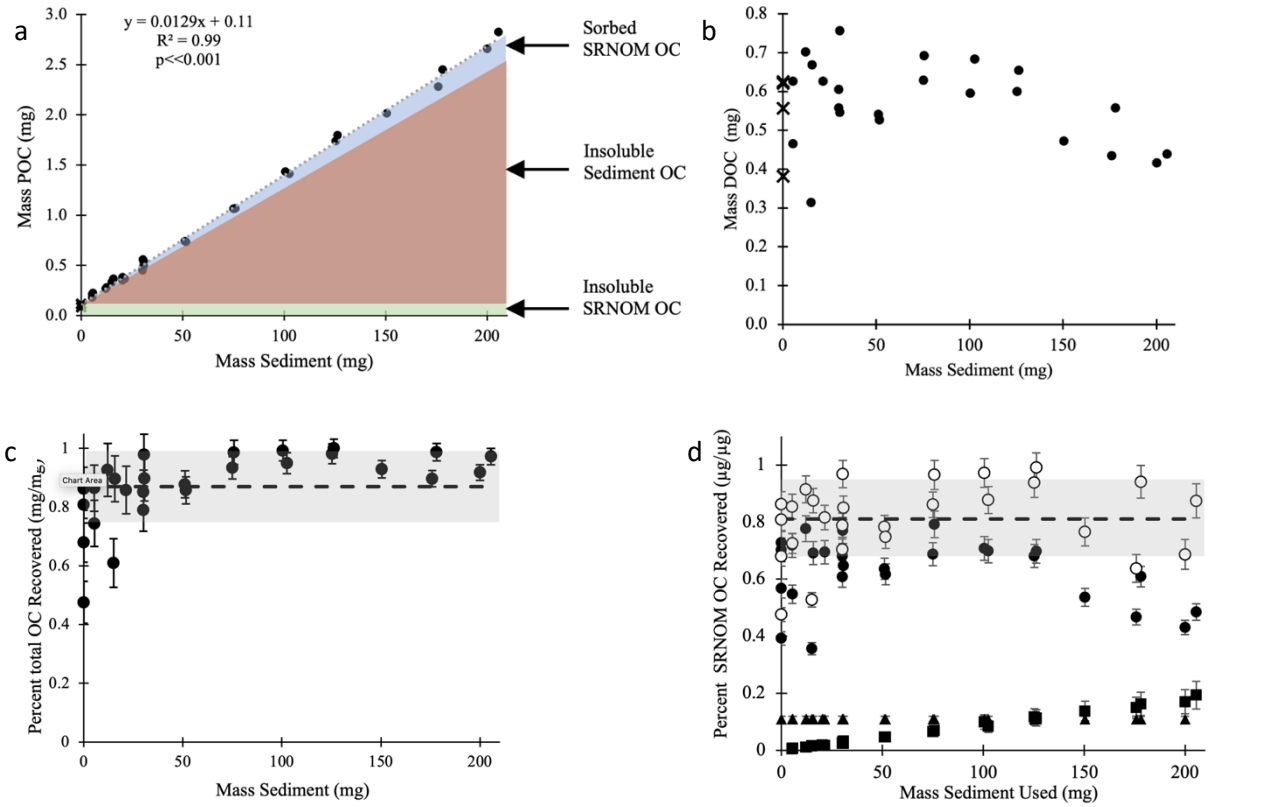

Figure 2.2: Panels a) and b) show mass of POC and DOC as function of mass of sediment in control (crosses) and sorption experiments (circles). Panels c) and d) show the fraction of total OC and SNROM OC recovered in each experiment. The mass of SRNOM used was kept constant throughout. In a) and b) error bars are smaller than the size of the symbols. Shaded portions in a) represent the three end members as described in the text and calculated using values in Table 2.1 and equation (1). The low DOC masses in b) in samples with <25mg of sediment suffered sample loss during lyophilization. Dashed lines in c) and d) show the average total OC and average total SRNOM OC recovered, respectively; shaded regions show ±1 standard deviation. Full details of the percent recovery calculations can be found in supplementary materials. Errors in c) and d) are propagated errors based on instrument precision. In d) filled circles show soluble SRNOM, triangles show insoluble SRNOM, squares show sorbed SRNOM, and empty circles show total SRNOM.

2.4.4 Isotopic content of DOC and POC in sorption experiments

The $\Delta^{14}C$ values of DOC ranged from 60±5‰ without sediment to 11±7‰ with 205 mg sediment (Figure 2.3a). These data were significantly correlated with sediment mass (R^2=0.93, p<<0.001). The $\delta^{13}C$ values of the recovered DOC ranged from -27.6±0.1‰ without sediment to -26.9±0.1‰ with 175 mg of sediment (R^2=0.54, p=0.005) (Figure 2.3b).

The $\Delta^{14}C$ values of POC ranged from 46±7‰ without sediment to -376±2‰ with 205 mg sediment (Table 2.2 and Figure 2.4a). The $\Delta^{14}C$ value decreased rapidly between 0 and 75 mg sediment, and then plateaued. Even though most of the OC in experiments conducted with >100 mg sediment is from sediment OC, its $\Delta^{14}C$ values were consistently higher than the sediment OC value of -431±2‰ and the expected values of insoluble SRNOM and insoluble sediment OC mixing (Figure A.1a, Appendix A).

The $\delta^{13}C$ values of POC range from -28.2±0.1‰ with 0 mg of sediment to -22.8±0.1‰ at 150 mg of sediment (Figure 2.4b). As with the $\Delta^{14}C$ data, these values are significantly offset from the Station M sediment OC $\delta^{13}C$ value of -22.2 ± 0.2‰ and from the expected values of insoluble SRNOM and insoluble sediment OC mixing (Figure A.1b, Appendix A).

Table 2.2. Masses of sediment and SRNOM used in each experiment, and masses and isotope values of POC and DOC recovered from each experiment. 1 mL of saltwater was used in all experiments.

	Mass Wet Sediment* (mg)	±	Mass SRNOM (mg)	±	Mass POC (mg)	±	UCID#	$\Delta^{14}C$ POC (‰)	±	$\delta^{13}C$ POC (‰)	±	Mass DOC (mg)	±	UCID#	$\Delta^{14}C$ DOC (‰)	±	$\delta^{13}C$ DOC (‰)	±
Sediment control	101.61	0.01	0		1.204	0.002	23476 & 23484	-429	2	-22.3	0.1	0.014	0.003	23492	-190	13		
	112.63	0.01	0		1.381	0.003	23527 & 23535	-432	2	-22.3	0.1	0						
	101.92	0.01	0		1.229	0.003	23528 & 23536	-431	2	-22.0	0.1	0.010	0.003	23544	-171	13		
SRNOM control	0		2.28	0.01	0.082	0.004	23360 & 23368	41	7			0.383	0.002	23376	60	6		
	0		2.29	0.01	0.110	0.003	23361 & 23369	46	7			0.556	0.002	23377	49	6		
	0		1.99	0.01	0.115	0.003	23226 & 23234	30	7			0.619	0.003	23242	50	6	-27.5	0.1
	0		2.02	0.01	0.096	0.003	23591 & 23595	32	7			0.585	0.002	23599	57	6		
	0		2.08	0.01	0.094	0.003	23590 & 23594			-28.2	0.1	0.625	0.002	23598	56	6	-27.6	0.1
Sorption experiments	5.31	0.01	2.04	0.01	0.183	0.004	23363 & 23371	-49	19			0.628	0.002	23379	52	6		
	5.38	0.01	1.99	0.01	0.216	0.004	23362 & 23370	-114	19			0.466	0.002	23378	55	6		
	5.66	0.01	2.20	0.01	0.227	0.004	23364 & 23372	-102	19									
	12.06	0.01	2.11	0.01	0.270	0.008	23126 & 23134	-209	19			0.702	0.003	23142	54	6		
	12.30	0.01	2.22	0.01	0.280	0.008	23127 & 23135	-192	19									
	15.06	0.01	2.06	0.01	0.333	0.007	23366 & 23374	-266	19			0.315	0.002	23382	49	6		
	15.08	0.01	2.16	0.01	0.334	0.007	23365 & 23373	-258	19									
	15.71	0.01	2.26	0.01	0.369	0.007	23367 & 23375	-239	19			0.669	0.002	23383	52	6		
	20.27	0.01	2.07	0.01	0.382	0.007	23229 & 23237	-267	19			0.407	0.003					
	20.30	0.01	2.02	0.01	0.353	0.007	23227 & 23235	-284	19									
	20.56	0.01	2.20	0.01	0.369	0.007	23228 & 23236	-275	19			0.629	0.003					
	21.38	0.01	2.10	0.01	0.368	0.008	23259 & 23265	-230	19			0.626	0.003	23271	44	6		
	30.13	0.01	2.14	0.01	0.452	0.007	23232 & 23240	-311	19			0.559	0.003	23248	48	6		
	30.15	0.01	2.07	0.01	0.460	0.007	23230 & 23238	-312	19			0.606	0.003	23246	51	6		
	30.39	0.01	2.29	0.01	0.561	0.008	23262 & 23268	-286	19			0.757	0.003	23274	46	6		
	30.64	0.01	1.96	0.01	0.541	0.008	23261 & 23267	-302	19			0.545	0.003	23273	44	6		
	30.77	0.01	2.35	0.01	0.497	0.007	23231 & 23239	-301	19			0.564	0.003					

	51.10	0.01	1.97	0.01	0.743	0.004	23592 & 23596	-347	2	-23.2	0.1	0.540	0.002	23600	46	6		
	51.60	0.01	1.98	0.01	0.735	0.004	23593 & 23597	-345	2	-23.3	0.1	0.526	0.002	23601	44	6	-27.5	0.1
	74.98	0.01	2.12	0.01	1.065	0.003	23470 & 23478	-359	2	-23.2	0.1	0.629	0.002	23486	40	6	-27.3	0.1
	75.82	0.01	2.03	0.01	1.068	0.004	23529 & 23537	-362	2	-23.0	0.1	0.694	0.002	23545	37	6	-27.2	0.1
	100.47	0.01	1.94	0.01	1.436	0.003	23471 & 23479	-363	2	-23.0	0.1	0.595	0.002	23487	36	6	-27.1	0.1
	102.52	0.01	2.26	0.01	1.413	0.004	23530 & 23538	-361	2	-23.0	0.1	0.683	0.003	23547	32	6	-27.1	0.1
	125.31	0.01	2.03	0.01	1.740	0.004	23531 & 23539	-370	2	-23.1	0.1	0.602	0.002	23547	35	6		
	126.24	0.01	2.16	0.01	1.798	0.003	23472 & 23480	-365	2	-22.9	0.1	0.655	0.002	23488	27	6	-27.2	0.1
	150.42	0.01	2.01	0.01	2.017	0.003	23473 & 23481	-373	2	-22.8	0.1	0.473	0.002	23489	27	6	-27.4	0.1
	175.80	0.01	2.11	0.01	2.281	0.003	23474 & 23482	-374	2	-22.9	0.1	0.436	0.002	23490	27	6	-27.2	0.1
	178.04	0.01	2.09	0.01	2.451	0.004	23533 & 23541	-371	2	-23.0	0.1	0.559	0.002	23549	17	6	-27.3	0.1
	199.95	0.01	2.17	0.01	2.657	0.003	23475 & 23483	-373	2	-22.9	0.1	0.415	0.002	23491	22	6	-27.0	0.1
	205.49	0.01	2.04	0.01	2.827	0.004	23534 & 23542	-376	2	-23.2	0.1	0.439	0.002	23550	11	6	-27.5	0.1

* We have determined that the percent water is 18 ± 3% n=5. This value is lower than the original 57%(w/w) water determined at the time of sampling, presumably because the samples dried out while in storage in the freezer for 24 years. Wet masses are used in all of our calculations and reported masses.

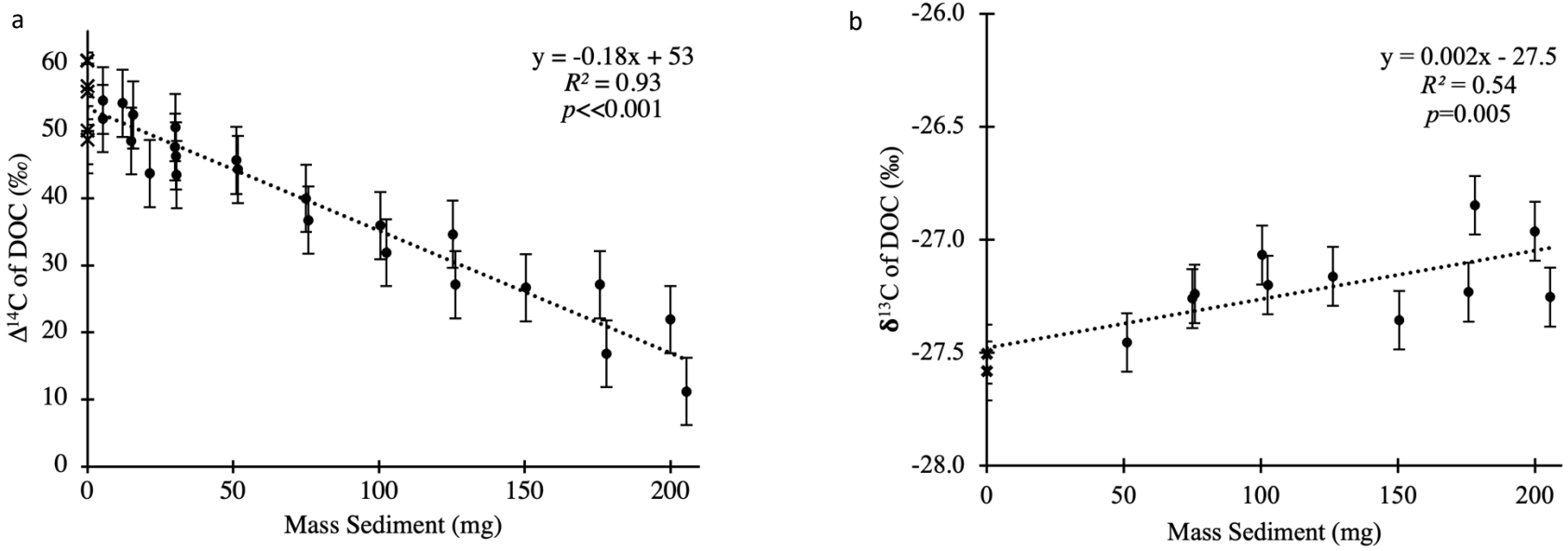

Figure 2.3: a) $\Delta^{14}C$ and b) $\delta^{13}C$ of DOC recovered after the control experiments (crosses) and sorption experiments (circles) as a function of sediment mass. Initial mass of SRNOM was kept constant throughout all experiments. Error bars represent pooled standard deviation of replicates.

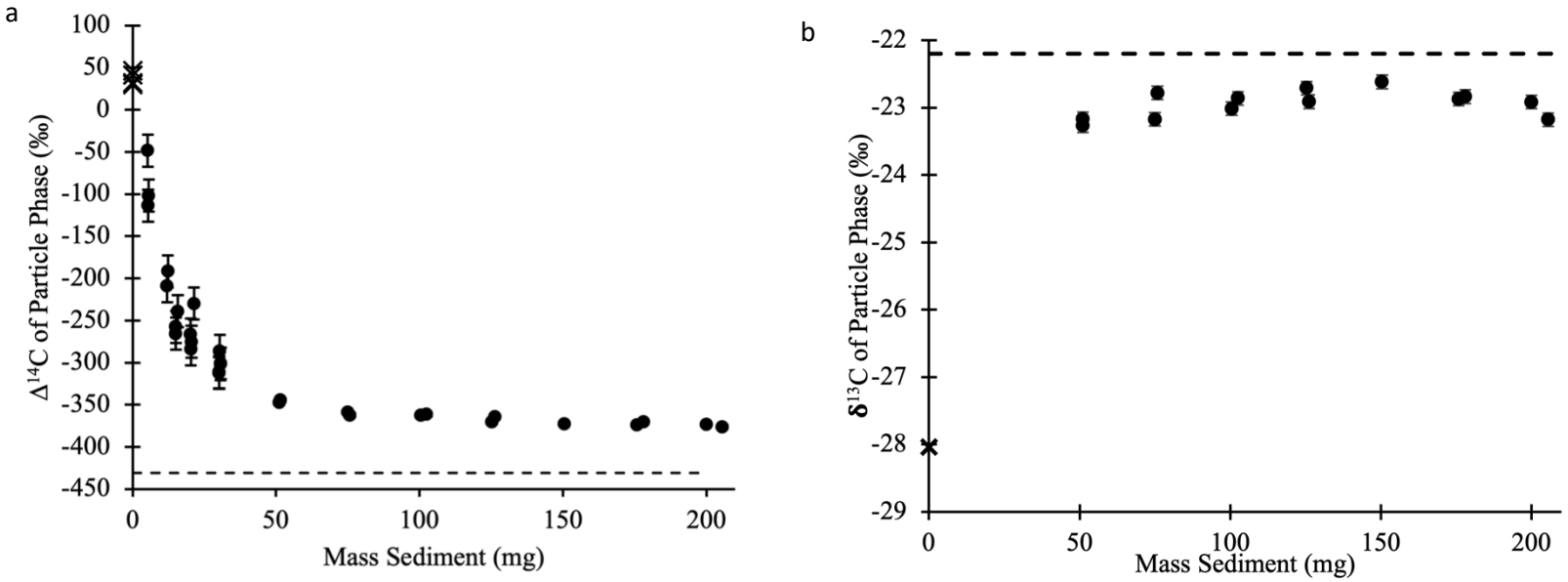

Figure 2.4: a) $\Delta^{14}C$ and b) $\delta^{13}C$ values of particulate OC recovered after control experiments (crosses) and sorption experiments (circles) as a function of increasing sediment mass used. Dashed lines indicate the a) $\Delta^{14}C$ and b) $\delta^{13}C$ values of insoluble sediment OC from the sediment control experiment. Error bars show the pooled standard deviation of replicates. Any error bars not visible are smaller than the size of the symbol. Initial masses of SRNOM were kept constant throughout the experiment.

2.5 Discussion

We hypothesized that the carbon isotope values of riverine DOC are altered in the presence of marine sediment due to selective sorption. Below, we test this hypothesis through (1) OC mass balance, and (2) isotope mass balance in DOC and POC.

2.5.1 OC mass balance

We applied a model 2 geometric mean regression to the relationship between the mass of sediment ($m_{sediment}$) and mass of POC (M_{POC}) (Figure 2.2a). This gave the following equation:

$$M_{POC} = 0.0129 \frac{mg\ OC}{mg\ sediment} \cdot m_{sediment} + 0.11\ mg\ OC \quad (3)$$

The intercept of this trendline (0.11±0.01 mg) is within error of the mass of insoluble SRNOM in the control experiments (Table 2.2). The slope, 12.9±0.1 µg particulate OC/mg sediment, is significantly larger than the OC content of insoluble sediment OC (12.1±0.2 µg particulate OC/mg sediment; Table 2.1); this was determined using a t-test assuming unequal variances (p=0.001).

We calculated the mass of sorbed SRNOM as follows. The total mass of POC (M_{POC}) was considered to be the sum of M_{SRNOM_sorbed}, $M_{SRNOM\_insoluble}$, and $M_{SedOC\_insoluble}$ (equation 1). $M_{SRNOM\_insoluble}$ was a constant value of 47±3µg OC/mg of SRNOM in each experiment (n=4) (Table 2.1). $M_{SedOC\_insoluble}$ was calculated by multiplying the saltwater insoluble OC content (12.1±0.2 µg OC/mg sediment; Table 2.1) by the total sediment mass used in each experiment (Table 2.2). M_{POC} was directly determined for each experiment as the total

mass of OC measured in the particulate phase (Table 2.2). M_{SRNOM_sorbed} was calculated using equation 1 and found to be 0.8±0.2 μg OC/mg sediment multiplied by the total sediment mass used in each experiment.

The amount of soluble sediment OC was small with respect to the amount of DOC from SRNOM. As the mass of sediment increased, the mass of DOC decreased and the mass of sorbed SRNOM correspondingly increased (Figure 2.2d). Overall, the masses of DOC and POC indicate that as more sediment is added to each experiment, more OC shifts from DOC to POC, implying sorption of the SRNOM to the sediment.

Percent yields of both total OC and SRNOM were within two standard deviations of 100% (Figures 2.2c and 2.2d). Given the high R^2 value of the POC mass with sediment (Figure 2.2a), we assume that most of the variability in yields was due to losses of the DOC during freeze drying. During lyophilization, DOC solution bubbled up and dried on the side of the tube, and some of the material on the side of the tubes was lost when the tubes were flame sealed. This effect is not isotopically selective, as evidenced by the fact that DOC samples with lower recoveries still had the same $\Delta^{14}C$ values as their replicates (Table 2.2, Figure 2.3a).

It should be noted that this study used solutions with high concentrations of sediment (5g/L-200g/L) and OC (~.9 g/L C). The higher concentration of sediment makes this system more similar to a pore water setting rather than suspended particles, which do tend to have higher OC concentrations than the overlying water. The high concentration of OC was chosen to ensure that the sediment would sorb as much OC as possible. This allowed us to examine how the isotopic content of the sorbed SRNOM changed as more of it was removed from solution. Given the linear response in the mass of sorbed SRNOM

(Figure 2.3a) this appears to have been successful. In a more dilute solution, we would expect more binding sites on the sediment to be available for sorbing the SRNOM. This would result in the isotopic content of the sorbed SRNOM to be similar to the experiments with the higher masses of sediment.

2.5.2 Changes in DOC isotopic composition

Though a significant percentage (10.9%) of the SRNOM OC is insoluble in the saltwater used here, the water-soluble fraction of the SRNOM had $\Delta^{14}C$ and $\delta^{13}C$ values (54±5‰, -27.4±0.2‰) that are less than one standard error apart from those of total SRNOM (53±2‰, -27.5±0.1‰) (Table 2.1). This indicates that the observed changes in the DOC isotopic values (Figure 2.3) are due to the presence of sediment.

Minimal OC from the sediment entered the dissolved phase under our experimental conditions (0.08 μg/mg sediment; Table 2.1). In the experiment with the largest mass of sediment (205 mg), we assume that 16 μg (=205 mg x 0.08 μg/mg) of sediment OC was soluble, with a $\Delta^{14}C$ of -181‰ (Table 2.1). The observed DOC from this experiment had a mass of 439 μg with a $\Delta^{14}C$ of 11‰ (Table 2.2). Using a mass balance equation to account for soluble sediment OC in this mixture yields a remaining DOC pool with a mass of 423 μgC and a $\Delta^{14}C$ of 17‰. This is still well below the SRNOM $\Delta^{14}C$ value of 53‰. Therefore, while dissolution of OC from the sediment does lower the $\Delta^{14}C$ of DOC, it cannot account for the observed departure from $\Delta^{14}C$ value of total SRNOM.

The highly correlated, linear decrease in DOC $\Delta^{14}C$ values with increasing sediment mass (Figure 2.3a) suggests that the sediment sorbs components of SRNOM with higher $\Delta^{14}C$ values than that of the total SRNOM. The $\delta^{13}C$ values of DOC show a weaker

correlation with sediment mass compared to the $\Delta^{14}C$ data (Figure 2.3b). All $\delta^{13}C$ values, however, are slightly higher relative to those of total SRNOM, indicating that the sediment sorbs compounds with lower $\delta^{13}C$ than that of total SRNOM.

Overall, these findings suggest that the addition of sediment resulted in sorption of compounds with higher $\Delta^{14}C$ values and lower $\delta^{13}C$ values than those of total SRNOM, thereby decreasing the $\Delta^{14}C$ values and increasing the $\delta^{13}C$ values of the remaining DOC.

2.5.3 Isotopic content of sorbed SRNOM

To further examine the composition of SRNOM that sorbed to sediment, we calculated the $\Delta^{14}C$ and $\delta^{13}C$ values of this pool as follows. Equation (2) represents an isotopic mass balance of the particulate phase. The masses from equation 1 and the isotopic values from the control experiments and the sediment sorption experiments were used (Tables 1 and 2). Due to the larger blank from the freeze dryer, experiments with <50 mg of sediment were excluded from this analysis. Equation (2) was then rearranged to solve for Δ_{SRNOM_Sorbed}. Figure 2.5 shows the results of these calculations. The average ± standard error of $\Delta^{14}C$ and $\delta^{13}C$ values of the sorbed OC are 135±20‰ (n=13) and -30.6‰±0.6 (n=13), respectively. A t-test assuming unequal variances showed that both $\Delta^{14}C$ and d ^{13}C values of the sorbed SRNOM were significantly different than those of the total SRNOM (p=0.002 and p=0.00007). This is consistent with the finding that sorption was isotopically selective in our experiments.

A model 2 geometric mean regression shows that the sorbed SRNOM $\Delta^{14}C$ values increased and $\delta^{13}C$ values decreased with increasing sediment mass in the experiments (Figure 2.5). The change in the sorbed SRNOM $\Delta^{14}C$ and $\delta^{13}C$ values with sediment mass

may indicate that the sorbed SRNOM contains multiple pools of OC with different isotopic content and sorption affinities. The OC with lower $\Delta^{14}C$ and higher $\delta^{13}C$ values was sorbed first, and as more sediment is added, another pool of OC with higher $\Delta^{14}C$ and lower $\delta^{13}C$ was removed from solution. This phenomenon is consistent with the molecular and isotopic heterogeneity of SRNOM.

2.5.4 Possible compounds sorbed by the sediment

Our data suggest that the component of SRNOM that sorbed to sediment had higher $\Delta^{14}C$ and lower $\delta^{13}C$ than those of the total SRNOM. The higher $\Delta^{14}C$ values observed in the sorbed material (Figure 2.5a) indicate the presence of bomb radiocarbon. This means that most of the compounds in the sorbed SRNOM would have been photosynthetically fixed sometime between 1957 and the date of collection in 2012 and are stable enough to survive on annual to decadal timescales. Sorption also requires a chemical structure that can create an energetically favorable interaction with the sediment or chemicals within the sediment, such as carboxylic acids, aromatic rings, and alkyl chains (Reidel et al., 2013).

Prior studies of estuarine systems have shown that as DOC concentrations to decrease with increasing salinity, the relative proportion of the various compound classes, such as carbohydrates, amino acids, lipids, aromatic structures, lignin and molecularly uncharacterized carbon, shift depending on the characteristics of the sampling site and estuary (Abdulla et al., 2010; Harvey and Mannino 2001; Hermes and Sikes, 2006). These alterations are the sum of several removal processes including photooxidation, microbial respiration, salinity-induced flocculation, and sediment sorption, as well as inputs from autochthonous sources, such as primary production and degradation products.

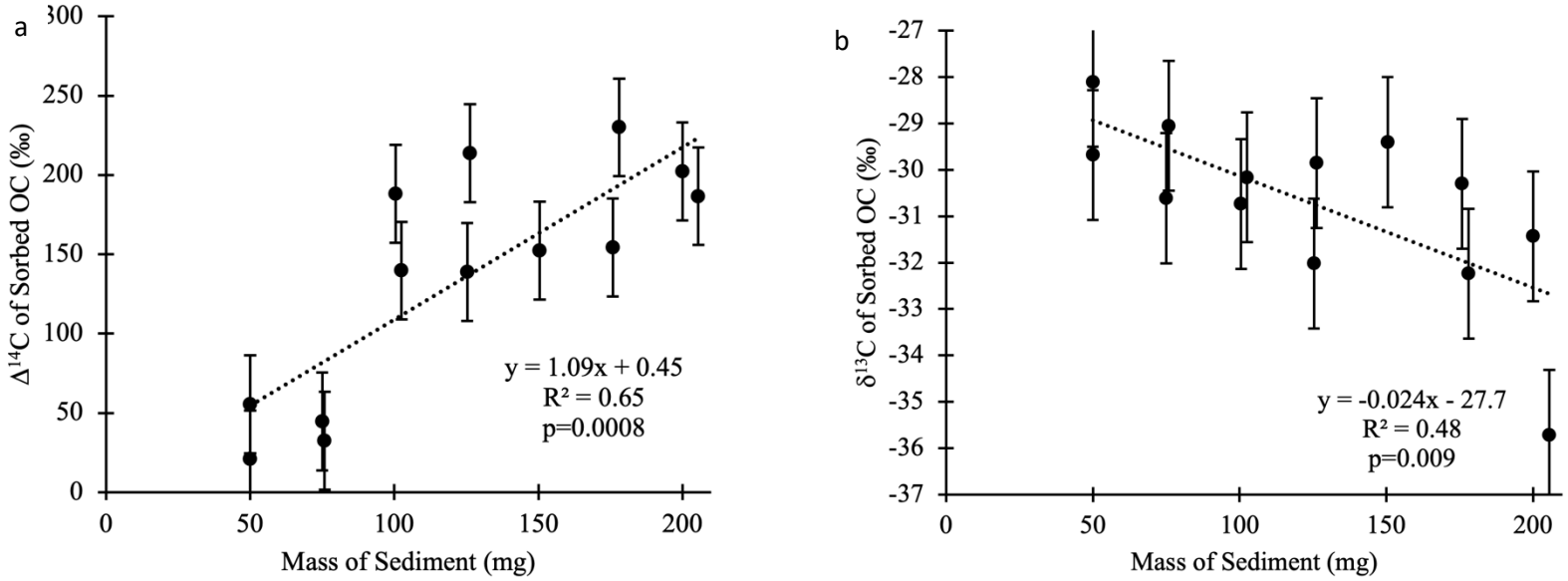

Figure 2.5: Calculated a) $\Delta^{14}C$ and b) $\delta^{13}C$ values of sorbed OC recovered after the sediment sorption experiments as a function of increasing sediment mass. Error bars show the pooled standard deviation of replicates. Experiments with masses below 50mg were excluded due to contamination from the freeze dryer

Studies of DOC compound classes in estuarine systems have reported $\Delta^{14}C$ values of total hydrolyzable carbohydrates that range from 148‰ higher to 86‰ lower and $\delta^{13}C$ values that range from 10.9‰ to 2.5‰ higher than those of bulk DOC (Loh et al., 2006; Wang et al., 2006). They also report that total hydrolyzable amino acids have $\Delta^{14}C$ values that are 129‰ to 24‰ higher and $\delta^{13}C$ that are 3.3‰ lower to 2.3‰ higher than those of the bulk DOC. It should be noted that the low $\delta^{13}C$ value is an outlier in this data set, with all the other samples having either higher or the same $\delta^{13}C$ as the bulk DOC (Loh et al., 2006; Wang et al., 2006). The reported $\delta^{13}C$ values of both carbohydrates and amino acids are higher than our measurements of sorbed SRNOM (Figure 2.5b). It is thus unlikely that these two compound classes are a major component of our sorbed SRNOM.

Studies have reported that lipid fractions of estuarine DOC also have $\Delta^{14}C$ that range from 60‰ to 925‰ lower and $\delta^{13}C$ values that 0.6‰ and 6.3‰ lower than those of the bulk DOC (Loh et al., 2006; Wang et al., 2006). These $\Delta^{14}C$ values are far lower than our measurements of the sorbed SRNOM (Figure 2.5a). Furthermore, as much as 17% of SRNOM was sorbed (Figure 2.1c). Because lipids are expected to constitute a very small fraction of DOC (Loh et al., 2006; Wang et al., 2006), it is unlikely that the sorbed SRNOM was predominantly lipid-like.

In complex natural organic matter, the molecularly uncharacterized component typically dominates the total OC pool (Hedges et al., 2000). This fraction contains all of the compounds not extracted with carbohydrates, amino acids, or lipids, and is sometimes termed “acid-insoluble” (Wang et al., 2006). Estimates of this fraction have $\Delta^{14}C$ values that range from 280‰ higher to 197‰ lower and $\delta^{13}C$ values that are 3.2‰ higher and 7.6‰ lower than those of the bulk DOC (Loh et al., 2006; Wang et al., 2006). This wide variation

in isotopic values suggests that a portion of the molecularly uncharacterized component could be in the sorbed SRNOM.

Beyond the major biomacromolecule fractions, a number of studies have examined the compound class specific isotopes of two important sources of aromatic carbon: lignin and black carbon. Lignin is characteristic of terrestrial organic matter, but it is almost absent in marine DOC. Benner and Opsahl (2001) found that lignin from rivers is quickly removed from solution as salinity of water increases. Lignin has lower $\delta^{13}C$ values than that of bulk plant material (Benner et al. 1987), and lignin from riverine DOC has been found to contain significant quantities of bomb ^{14}C (Benner et al., 1987; Feng et al., 2017; McNichol et al., 2000). This matches the isotopic profile of sorbed SRNOM from this experiment and the expected chemical profile of sorbed OC. Prior laboratory studies have shown that a significant portion of lignin derived phenols from plant samples can bind irreversibly with sediment and that this binding can alter the composition of these samples (Hernes et al., 2007; 2013). However, it is important to note that aromatic DOC compounds are easily photo-oxidized, and their solubility is sensitive to changes in salinity (Benner and Opsahl, 2001; Hernes and Benner, 2003). Even if lignin is a significant portion of the material sorbed in our experiments, these competing removal pathways might reduce the fraction of lignin sorbed to sediments in the field.

Black carbon accounts for 12 ± 2% of total SRNOM OC and has a $\Delta^{14}C$ of -148 ± 17‰ (Coppola et al., 2015), and has a variety of solubilities based on its source(s), charring temperature, and degradation state (Wagner et al., 2018). The addition of metals to water has been shown to promote the precipitation of black carbon, and it is found in riverine and estuarine sediments (Coppola et al., 2014; Masiello and Druffel, 1998; Reidel et al., 2012). It

is possible that the presence of black carbon lowers the $\Delta^{14}C$ of the sorbed SRNOM in the experiments with lower sediment masses (Figure 2.5a). We can estimate the amount of black carbon present in the system by mass balance. If we assume that the sorbed SRNOM is a mixture of black carbon ($\Delta^{14}C$ = - 148‰) and an enriched OC pool with the highest sorbed SRNOM $\Delta^{14}C$ value observed ($\Delta^{14}C$ = 230‰), then the experiments with ≤75 mg of sediment would be about half black carbon and half ^{14}C enriched carbon. This is equivalent to about 2% of the total SRNOM OC added to the system, which is less than the total amount of black carbon in SRNOM (12%) (Coppola et al., 2015). It is, thus, plausible that black carbon could be in the sorbed SRNOM pool.

2.5 Future work

Any further work towards understanding this phenomenon should consider how our laboratory conditions differ from the natural environment. 1) Our system used water with a salinity of 35‰. In any natural system, DOC will experience a gradient of salinities that will gradually change the solubility of compounds within the DOC and promote flocculation. Additionally, the salinity will change the redox state of sediment ions and alter the availability of binding sites there. 2) Our system was homogenized and then left relatively static. The water's movement in a system will control the amount of time that DOC can interact with sediment. 3) Our system was kept relatively dark. Photo-oxidation is one of the major removal pathways for DOC, especially for aromatic molecules, as they readily absorb photons in the ultraviolet spectrum. As aromatics are one of the possible compound classes that led to our observed fractionation, it may be difficult in the field to determine how many of the terrestrial aromatics were sorbed and how many were photo-

oxidized. 4) Our system assumes no microbial activity. SRNOM was passed through a 0.45μm filter upon collection, so there should be minimal microbes in the sample. This prevents most material loss due to heterotrophic respiration or most production of degradation by products. Labile compounds, such as carbohydrates and amino acids, have distinct isotopic contents, and microbial consumption of these compounds would alter the remaining DOC's $\Delta^{14}C$ and $\delta^{13}C$ values. 5) We used a specific DOC and a specific sediment. Other riverine DOC with different isotopic ranges and chemical compositions, and sediments with different binding capacities would result in a different isotopic shift.

While the conditions of these experiments are artificial, the data do demonstrate that the chemically selective process of OC sorption, can also be isotopically selective. We hypothesize that this occurred due to the chemical selectivity of the sorption process and the isotopic diversity of different compound classes. To investigate this phenomenon further we propose both laboratory experiments with increasing complexity and field studies. Salinity, temperature, mineral content, and DOC source are all variables to explore in similar experiments. Additionally, further chemical characterization techniques such as nuclear magnetic resonance and high-resolution mass spectrometry can be used to further explore the connection between chemically selective and isotopically selective sorption. Field measurements of DOC, POC, and SOC carbon isotopes in response to major carbon fluxes, such as run off or algae blooms, can be used to evaluate the significance of this phenomenon. Constraining the isotopic selectivity of carbon fluxes is a key step in studying the aquatic carbon cycle, and this study shows that sorption of DOC to sediments should be considered in that future work.

2.6 References

Abdulla, H. A. N.; Minor, E. C.; Dias, R. F.; Hatcher, P.G. 2010. "Changes in the Compound Classes of Dissolved Organic Matter along an Estuarine Transect: A Study Using FTIR and 13C NMR." *Geochim. Cosmochim. Acta* 74, no. 13: 3815–38. https://doi.org/10.1016/j.gca.2010.04.006.

Aufdenkampe, A. K.; Hedges, J. I.; Richey, J. E.; Krusche, A. V.; Llerena, C. A. 2001. Sorptive Fractionation of Dissolved Organic Nitrogen and Amino Acids onto Fine Sediments within the Amazon Basin. *Limnol. Oceanogr. 46:* (8), 1921–1935. https://doi.org/10.4319/lo.2001.46.8.1921.

Benner, R.; Fogel, M. L.; Sprague, E. K.; Hodson, R. E. 1987. Depletion of 13C in Lignin and Its Implications for Stable Carbon Isotope Studies. *Nature 329:* (6141), 708–710. https://doi.org/10.1038/329708a0.

Benner, R.; Opsahl, S. 2001. Molecular Indicators of the Sources and Transformations of Dissolved Organic Matter in the Mississippi River Plume. *Org. Geochem. 32:* (4), 597–611. https://doi.org/10.1016/S0146-6380(00)00197-2.

Chen, M.; Kim, S.; Park, J.-E.; Jung, H.-J.; Hur, J. 2016. Structural and Compositional Changes of Dissolved Organic Matter upon Solid-Phase Extraction Tracked by Multiple Analytical Tools. *Anal. Bioanal. Chem. 408:* (23), 6249–6258. https://doi.org/10.1007/s00216-016-9728-0.

Close, H. G. 2019 Compound-Specific Isotope Geochemistry in the Ocean. *Annu. Rev. Mar. Sci. 11:* (1), 27–56. https://doi.org/10.1146/annurev-marine-121916-063634.

Coppola, A. I.; Walker, B. D.; Druffel, E. R. M. 2015. Solid Phase Extraction Method for the Study of Black Carbon Cycling in Dissolved Organic Carbon Using Radiocarbon. *Mar. Chem. 177*: 697–705. https://doi.org/10.1016/j.marchem.2015.10.010.

Coppola, A. I.; Ziolkowski, L. A.; Masiello, C. A.; Druffel, E. R. M. 2014. Aged Black Carbon in Marine Sediments and Sinking Particles. *Geophys. Res. Lett. 41:* (7), 2427–2433. https://doi.org/10.1002/2013GL059068.

Druffel, E. R. M.; Griffin, S. 2015 Radiocarbon in Dissolved Organic Carbon of the South Pacific Ocean. *Geophys. Res. Lett. 42:* (10), 4096–4101. https://doi.org/10.1002/2015GL063764.

Druffel, E.R.M.; Griffin, S.; Walker, B.D.; Coppola A.I.; Glynn, D.S. 2013. "Total Uncertainty of Radiocarbon Measurements of Marine Dissolved Organic Carbon and Methodological Recommendations." *Radiocarbon* 55: no. 3, 1135–41. https://doi.org/10.1017/S0033822200048049.

Druffel, E. R. M.; Beaupré, S. R.; Grotheer, H.; Lewis, C. B.; McNichol, A. P.; Mollenhauer, G.; Walker, B. D. 2022. Marine Organic Carbon and Radiocarbon—Present and Future Challenges. *Radiocarbon* 1–17. https://doi.org/10.1017/RDC.2021.105.

Druffel, E. R. M.; Griffin, S.; Lewis, C. B.; Rudresh, M.; Garcia, N. G.; Key, R. M.; McNichol, A. P.; Hauksson, N. E.; Walker, B. D. 2021 Dissolved Organic Radiocarbon in the Eastern Pacific and Southern Oceans. *Geophys. Res. Lett. 48:* (10), e2021GL092904. https://doi.org/10.1029/2021GL092904.

Feng, X.; Vonk, J. E.; Griffin, C.; Zimov, N.; Montluçon, D. B.; Wacker, L.; Eglinton, T. I. 2017. 14C Variation of Dissolved Lignin in Arctic River Systems. *ACS Earth Space Chem., 1:* (6), 334–344. https://doi.org/10.1021/acsearthspacechem.7b00055.

Fox, L. E. 1983. The Removal of Dissolved Humic Acid during Estuarine Mixing. *Estuarine, Coastal Shelf Sci. 16:* (4), 431–440. https://doi.org/10.1016/0272-7714(83)90104-X.

Green, N. W.; McInnis, D.; Hertkorn, N.; Maurice, P. A.; Perdue, E. M. 2015. Suwannee River Natural Organic Matter: Isolation of the 2R101N Reference Sample by Reverse Osmosis. *Environ. Eng. Sci. 32:* (1), 38–44. https://doi.org/10.1089/ees.2014.0284.

Hansell, D.; Carlson, C.; Repeta, D.; Schlitzer, R. 2009 Dissolved Organic Matter in the Ocean: A Controversy Stimulates New Insights. *Oceanog. 22:* (4), 202–211. https://doi.org/10.5670/oceanog.2009.109.

Harvey, H. R. and Mannino, A. 2001 "The Chemical Composition and Cycling of Particulate and Macromolecular Dissolved Organic Matter in Temperate Estuaries as Revealed by Molecular Organic Tracers." *Org. Geochem.* 32, no. 4 527–42. https://doi.org/10.1016/S0146-6380(00)00193-5.

Hedges, J. I.; Keil, R. G.; Benner, R. 1997 What Happens to Terrestrial Organic Matter in the Ocean? *Org. Geochem. 27:* (5), 195–212. https://doi.org/10.1016/S0146-6380(97)00066-1.

Hedges, J. I.; Keil, R. G. 1999. Organic Geochemical Perspectives on Estuarine Processes: Sorption Reactions and Consequences. *Mar. Chem. 65:* (1), 55–65. https://doi.org/10.1016/S0304-4203(99)00010-9.

Hedges, J. I.; Eglinton, G.; Hatcher, P. G.; Kirchman, D. L.; Arnosti, C.; Derenne, S.; Evershed, R. P.; et al. 2000. "The Molecularly-Uncharacterized Component of Nonliving Organic Matter in Natural Environments." *Org. Geohem.* 31: no. 10, 945–58. https://doi.org/10.1016/S0146-6380(00)00096-6.

Hermes, A. L. and Sikes, E. L. 2016. "Particulate Organic Matter Higher Concentrations, Terrestrial Sources and Losses in Bottom Waters of the Turbidity Maximum, Delaware Estuary, U.S.A." *Estuarine Coastal Shelf Sci* 180: 179–89. https://doi.org/10.1016/j.ecss.2016.07.005.

Hernes, P. J.; Benner, R. 2003. Photochemical and Microbial Degradation of Dissolved Lignin Phenols: Implications for the Fate of Terrigenous Dissolved Organic Matter in Marine Environments. *J. Geophys. Res.: Oceans 108:* (C9). https://doi.org/10.1029/2002JC001421.

Hernes, P. J.; Kaiser K.; Dyda, R.Y.; Cerli, C. 2013. "Molecular Trickery in Soil Organic Matter: Hidden Lignin." *Environ. Sci. Tech.* 47: no. 16 9077–85. https://doi.org/10.1021/es401019n.

Hernes, P. J.; Robinson, A.C.; Aufdenkampe, A.K. 2007. "Fractionation of Lignin during Leaching and Sorption and Implications for Organic Matter 'Freshness.'" *Geophys Res Lett* 34: no. 17 https://doi.org/10.1029/2007GL031017.

Hwang, J.; Druffel, E. R. M. 2005. Blank Correction for Δ14C Measurements in Organic Compound Classes of Oceanic Particulate Matter. *Radiocarbon*, *47:* (1), 75–87. https://doi.org/10.1017/S0033822200052218.

J, C.; Je, B.; Erm, D. 1996: Utilization and Turnover of Labile Dissolved Organic Matter by Bacterial Heterotrophs in Eastern North Pacific Surface Waters. *Mar. Ecol. Prog. Ser.*, *139*, 267–279. https://doi.org/10.3354/meps139267.

Keiluweit, M.; Kleber, M. 2009 Molecular-Level Interactions in Soils and Sediments: The Role of Aromatic π-Systems. *Environ. Sci. Technol.*, *43:* (10), 3421–3429. https://doi.org/10.1021/es8033044.

Kleber, M.; Sollins, P.; Sutton, R. 2007. A Conceptual Model of Organo-Mineral Interactions in Soils: Self-Assembly of Organic Molecular Fragments into Zonal Structures on Mineral Surfaces. *Biogeochemistry 85:* (1), 9–24. https://doi.org/10.1007/s10533-007-9103-5.

Komada, T.; Anderson, M. R.; Dorfmeier, C. L. 2008. Carbonate Removal from Coastal Sediments for the Determination of Organic Carbon and Its Isotopic Signatures, Δ13C and Δ14C: Comparison of Fumigation and Direct Acidification by Hydrochloric Acid. *Limnol. Oceanogr.: Methods*, *6:* (6), 254–262. https://doi.org/10.4319/lom.2008.6.254.

Li, Y.; Harir, M.; Lucio, M.; Gonsior, M.; Koch, B. P.; Schmitt-Kopplin, P.; Hertkorn, N. 2016. Comprehensive Structure-Selective Characterization of Dissolved Organic Matter by Reducing Molecular Complexity and Increasing Analytical Dimensions. *Water Res. 106*: 477–487. https://doi.org/10.1016/j.watres.2016.10.034.

Loh, A. N.; Bauer J.E.; Canuel, E. A. 2006. "Dissolved and Particulate Organic Matter Source-Age Characterization in the Upper and Lower Chesapeake Bay: A Combined Isotope and Biochemical Approach." *Limnol. Oceanogr.* 51: no. 3 1421–31. https://doi.org/10.4319/lo.2006.51.3.1421.

Mahamat Ahmat, A.; Boussafir, M.; Le Milbeau, C.; Guegan, R.; Valdès, J.; Guiñez, M.; Sifeddine, A.; Le Forestier, L. 2016. Organic Matter-Clay Interaction along a Seawater Column of the Eastern Pacific Upwelling System (Antofagasta Bay, Chile): Implications for Source Rock Organic Matter Preservation. *Mar. Chem. 179*: 23–33. https://doi.org/10.1016/j.marchem.2016.01.003.

Masiello C. A.; Druffel E. R. M. 1998. Black Carbon in Deep-Sea Sediments. *Science*, *280:* (5371), 1911–1913. https://doi.org/10.1126/science.280.5371.1911.

Matiasek, S. J.; Hernes, P. J. 2019 The Chemical Fingerprint of Solubilized Organic Matter from Eroded Soils and Sediments. *Geochim. Cosmochim. Acta 267:* 92–112. https://doi.org/10.1016/j.gca.2019.09.016.

McNaught AD, Wilkinson A. 1997 *IUPAC Compendium of Chemical Terminology. 2nd Edition, The Gold Book*. Oxford: Blackwell Scientific Publications.

McNichol, A. P.; Ertel, J. R.; Eglinton, T. I. 2000. The Radiocarbon Content of Individual Lignin-Derived Phenols: Technique and Initial Results. *Radiocarbon 42:* (2), 219–227. https://doi.org/10.1017/S0033822200059026.

Nwosu, U. G.; Cook, R. L. 2015.13C Nuclear Magnetic Resonance and Electron Paramagnetic Spectroscopic Comparison of Hydrophobic Acid, Transphilic Acid, and Reverse Osmosis May 2012 Isolates of Organic Matter from the Suwannee River. *Environmental Engineering Science 32:* (1), 14–22. https://doi.org/10.1089/ees.2014.0261.

Raymond, P. A.; Spencer, R. G. M. 2015 Chapter 11 - Riverine DOM. In *Biogeochemistry of Marine Dissolved Organic Matter (Second Edition)*; Hansell, D. A., Carlson, C. A., Eds.; Academic Press: Boston, pp 509–533. https://doi.org/10.1016/B978-0-12-405940-5.00011-X.

Reed, W. E.; Kaplan, I. R. 1997. The Chemistry of Marine Petroleum Seeps. *Journal of Geochemical Exploration 7*: 255–293. https://doi.org/10.1016/0375-6742(77)90084-X.

Riedel, T.; Biester, H.; Dittmar, T. 2012. Molecular Fractionation of Dissolved Organic Matter with Metal Salts. *Environ. Sci. Technol. 46:* (8), 4419–4426. https://doi.org/10.1021/es203901u.

Riedel, T.; Zak, D.; Biester, H.; Dittmar, T. 2013. Iron Traps Terrestrially Derived Dissolved Organic Matter at Redox Interfaces. *Proc. Natl. Acad. Sci. U. S. A. 110:* (25), 10101–10105. https://doi.org/10.1073/pnas.1221487110.

Santos, G. M.; Southon, J. R.; Drenzek, N. J.; Ziolkowski, L. A.; Druffel, E.; Xu, X.; Zhang, D.; Trumbore, S.; Eglinton, T. I.; Hughen, K. A. 2010. Blank Assessment for Ultra-Small Radiocarbon Samples: Chemical Extraction and Separation Versus AMS. *Radiocarbon 52:* (3), 1322–1335. https://doi.org/10.1017/S0033822200046415.

Smith, K. L.; Huffard, C. L.; Ruhl, H. A. 2020. Thirty-Year Time Series Study at a Station in the Abyssal NE Pacific: An Introduction. *Deep Sea Res., Part II 173:* 104764. https://doi.org/10.1016/j.dsr2.2020.104764.

Sternberg, L. O.; Deniro, M. J.; Johnson, H. B. 1984. Isotope Ratios of Cellulose from Plants Having Different Photosynthetic Pathways. *Plant Physiol. 74:* (3), 557–561. https://doi.org/10.1104/pp.74.3.557.

Stuiver, M.; Polach, H. A. 1997. Discussion Reporting of 14C Data. *Radiocarbon 19:* (3), 355–363. https://doi.org/10.1017/S0033822200003672.

Wagner, S., Brandes, J., Spencer, R. G. M., Ma, K., Rosengard, S. Z., Moura, J. M. S., & Stubbins, A. (2019). Isotopic composition of oceanic dissolved black carbon reveals non-riverine source. Nature Communications, 10(1), Article 1. https://doi.org/10.1038/s41467-019-13111-7

Walker, B. D.; Xu, X. 2019. An Improved Method for the Sealed-Tube Zinc Graphitization of Microgram Carbon Samples and 14C AMS Measurement. *Nucl. Instrum. Methods Phys. Res., Sect. B 438*: 58–65. https://doi.org/10.1016/j.nimb.2018.08.004.

Wang, X.C.; Druffel, E.R.M.; Griffin, S.; Lee C.; and Kashgarian, M. 1998. Radiocarbon Studies of Organic Compound Classes in Plankton and Sediment of the Northeastern Pacific Ocean. *Geochim et Cosmochim Acta* 62: no. 8 1365–78. https://doi.org/10.1016/S0016-7037(98)00074-X.

Wang, X.C.; Callahan, J.; Chen, R. F. 2006. Variability in Radiocarbon Ages of Biochemical Compound Classes of High Molecular Weight Dissolved Organic Matter in Estuaries. *Estuarine Coastal Shelf Sci.* 68: no. 1 188–94. https://doi.org/10.1016/j.ecss.2006.01.018.

Williams, P. M.; Gordon, L. I. 1970Carbon-13: Carbon-12 Ratios in Dissolved and Particulate Organic Matter in the Sea. *Deep-Sea Res. Oceanogr. Abstr. 17:* (1), 19–27. https://doi.org/10.1016/0011-7471(70)90085-9.

Xing, L.; Zhang, H.; Yuan, Z.; Sun, Y.; Zhao, M. 2011. Terrestrial and Marine Biomarker Estimates of Organic Matter Sources and Distributions in Surface Sediments from the East China Sea Shelf. *Cont. Shelf Res. 31:* (10), 1106–1115. https://doi.org/10.1016/j.csr.2011.04.003.

Xu, X.; Trumbore, S. E.; Zheng, S.; Southon, J. R.; McDuffee, K. E.; Luttgen, M.; Liu, J. C. 2007. Modifying a Sealed Tube Zinc Reduction Method for Preparation of AMS Graphite Targets: Reducing Background and Attaining High Precision. *Nucl. Instrum. Methods Phys. Res., Sect. B 259:* (1), 320–329. https://doi.org/10.1016/j.nimb.2007.01.175.

Chapter 3. Time Series of Surface Water Dissolved Inorganic Carbon Isotopes from the Southern California Bight

3.1 Abstract

Dissolved inorganic carbon (DIC) in ocean water is a major sink of fossil fuel derived CO_2. Carbon isotopes in DIC serve as tracers for oceanic water masses, biogeochemical processes, and air-sea gas exchange. We present a timeseries of surface DIC $\delta^{13}C$ and $\Delta^{14}C$ values from 2011 to 2022 from Newport Beach, California. This is a continuation of previous timeseries (Hinger et al. 2010; Santos et al. 2011) that together provide an 18-year record. These data show that DIC $\Delta^{14}C$ values have declined by 42‰ and that DIC $\delta^{13}C$ values have declined by 0.4‰ since 2004. By 2020, DIC $\Delta^{14}C$ values were within analytical error of nearby clean atmospheric CO_2 $\Delta^{14}C$ values. These long-term trends are likely the result of significant fossil fuel derived CO_2 in surface DIC from air-sea gas exchange. Seasonally, $\Delta^{14}C$ values varied by 3.4‰ between 2011 and 2022, where seasonal $\delta^{13}C$ values varied by 0.7‰. The seasonal variation in $\Delta^{14}C$ values is likely driven by variations in upwelling, surface eddies, and mixed layer depth. The variation in $\delta^{13}C$ values appears to be driven by isotopic fractionation from marine primary producers. The DIC $\delta^{13}C$ and $\Delta^{14}C$ values record the influence of the drought that began in 2012, and a major upwelling event in 2016.

3.2 Introduction

Marine dissolved inorganic carbon (DIC) is the largest exchangeable reservoir of carbon in the surface ocean, and it exchanges with atmospheric CO_2 on annual to decadal

timescales (Broecker and Peng, 1982). As humans have released additional CO_2 into the atmosphere, DIC has acted as a major sink for some of this additional carbon (Sabine et al., 2004, Gruber et al., 2019). This increase in DIC lowers the ocean's pH, which has profound impacts on ocean ecosystems (Feely et al., 2004). A key tool used to track DIC are its carbon isotopes (^{13}C and ^{14}C), as they are reflective of the circulation and biogeochemistry of the water mass in which DIC is dissolved. These isotopes also reflect the anthropogenic impact on the global carbon cycle. First, above-ground thermonuclear bomb testing nearly doubled the ^{14}C content of atmospheric CO_2 by the early 1960s. Due to the relatively long isotopic equilibration time of CO_2, this resulted in a smaller, but longer-lived increase in surface marine DIC $\Delta^{14}C$ (Druffel, 1989). Second, the burning of fossil fuels since 1890 released CO_2 with no ^{14}C and less ^{13}C than atmospheric CO_2 that has reduced the overall isotopic ratios, the so called the Suess effect (Suess 1953). The decrease in $^{14}C/^{12}C$ and $^{13}C/^{12}C$ ratios have also been observed in marine DIC (Andrews et al., 2016; Brooks, 2020). Thus, that attempts by the international community to curb CO_2 emissions will likely be reflected in future DIC isotopic records.

The $^{13}C/^{12}C$ ratio of DIC is the result of equilibrium isotope effect and kinetic isotope effect acting on the sources and sinks of DIC. For example, the $^{13}C/^{12}C$ of surface DIC ($\delta^{13}C \approx 1‰$) is higher than that of atmospheric CO_2 ($\delta^{13}C \approx -8‰$), because equilibrium processes favor a higher proportion of the heavier isotope in the more condensed phase (Mook, 1986). A non-equilibrium process, like biological uptake, favors the lighter isotope due to its higher diffusivity. Marine phytoplankton are thus, depleted in ^{13}C ($\delta^{13}C \approx -21‰$) relative to surface DIC (Mook, 1986). In regions with significant phytoplankton growth, this can also measurably raise the $^{13}C/^{12}C$ ratio of the remaining DIC (Kroopnik, 1985). Conversely,

remineralization of sinking marine phytoplankton by zooplankton and microbes releases ^{13}C-depleted DIC, which then lowers the overall $^{13}C/^{12}C$ of the subsurface DIC (Kroopnik, 1985).

While ^{14}C also undergoes isotopic fractionation, reported $^{14}C/^{12}C$ ratios are corrected for any fractionation (Stuiver and Polach, 1977). Therefore, the primary control on a measured $^{14}C/^{12}C$ ratio is the radioactive decay of ^{14}C and the mixing of carbon pools with different $^{14}C/^{12}C$ ratios. In the surface ocean, newly dissolved CO_2 mixes with DIC from the surface water. In the pre-bomb era, this resulted in surface DIC with $^{14}C/^{12}C$ ratios ($\Delta^{14}C \approx -60$) lower than that of atmospheric CO_2 ($\Delta^{14}C \approx 0$) (Stuiver et al., 1986). The equilibration time of ^{14}C by air-sea exchange of CO_2 is about 10 years, which is far longer than the mixing time of surface waters (Broecker and Peng, 1982). Thus, shifts in the $^{14}C/^{12}C$ ratio in surface DIC during this period are almost entirely due to mixing of surface and upwelled waters within a region. The introduction of bomb radiocarbon to the atmosphere produced a large isotopic gradient with the ocean that increased the $\Delta^{14}C$ of surface DIC by ~200‰ (Druffel et al., 2016). As the $^{14}C/^{12}C$ of atmospheric CO_2 has declined due to redistribution of bomb-derived ^{14}C and the ^{14}C-free CO_2 from fossil fuels, the surface DIC $^{14}C/^{12}C$ ratios have also declined, albeit at a slower rate (Hinger at al., 2010, Santos et al., 2011, Andrews et al., 2016). In the last few years, atmospheric CO_2 reached its pre-bomb $^{14}C/^{12}C$ ratio ($\Delta^{14}C \approx 0$‰) (Graven et al., 2022). How this ratio and the resulting change in surface DIC carbon isotope ratios will change in the coming years will require continuous monitoring of these carbon pools.

One such monitoring site is located at Newport Beach, California in the Southern California Bight (SCB). The SCB is home to productive marine ecosystems and is

characterized by complex circulation of local currents. The northern end of the SCB is at Point Conception (~34.4°N), where the North American coastline turns almost 90° westward and then begins curving southwards (Figure 3.1). The SCB ends 236 km south of the Mexican-American border, in Baja California (~32°N). The eastern boundary current of the North Pacific Gyre, the California Current, flows southward from Point Conception and dominates the western portion of the SCB (Hickey, 1979). This current begins in the subarctic region west of Washington state and is relatively low in temperature and salinity. Closer to the coast, there is the poleward flowing Southern California Countercurrent that brings warmer, nutrient-depleted waters from Baja California. These two currents create a domain scale gyre that can be subdivided into 3 cyclonic eddies (Dong et al., 2009). These eddies can transport warmer, nutrient-poor water east from the North Pacific Gyre to the SCB (Dong et al., 2009). The Southern California Countercurrent dissipates in the spring when wind-driven upwelling creates a westward flow that brings colder, nutrient-rich waters to the surface and stimulates phytoplankton growth (Bray et al., 1999). However, the upwelling in this region is generally weaker than at other points along the Eastern North Pacific (Hickey, 1992). The proportions these different water masses present in the SCB at a given time vary based on the prevailing winds (Hickey et al., 2003).

The main subsurface flow in the SCB is the California Undercurrent. This current is formed in the Eastern Equatorial Pacific and is characterized by warm, salty, nutrient-replete, and low-oxygen water (Hickey, 1979). Its core generally resides from 200-300 m depth and rises to 100 m during the spring upwelling (Dong et al., 2009; Brogard et al., 2019). CFC-ages between 200-300 m in the SCB indicate that the California Undercurrent's ventilation age is around 50-125 years (Jeanson et al., 2021, Figure B.1). DIC $\Delta^{14}C$ values

from this depth in the SCB have been observed to be 40-90‰ lower than surface DIC values (Figures S2a and S2b) (Key et al., 2015, Olsen et al., 2016). This offset cannot be translated directly into a radiocarbon age due to the presence of bomb radiocarbon. Upwelling results in surface DIC in the SCB with $\Delta^{14}C$ values that are 50‰ lower than those of surface DIC from the North Pacific Gyre (Figures S3a and S3b) (Key et al., 2015, Olsen et al., 2016). As expected, $\delta^{13}C$ values of DIC are lower within the California Undercurrent than those in the surface waters of the SCB (Figure B.2c) (Key et al., 2015, Olsen et al., 2016). However, the surface DIC $d^{13}C$ values in the SCB are higher than those in the North Pacific Gyre, suggesting that upwelling is not the primary driver of $d^{13}C$ values in the SCB (Figure B.3c) (Key et al., 2015, Olsen et al., 2016).

Figure 3.1: Google Earth image of the Southern California Bight. Arrows show surface currents as described in Hickey (1992). Google, Data LDEO-Columbia, NSF, NOAA, Landsat / Copernicus Data SIO, NOAA, U.S. Navy, NGA, Gebco Data MBARI

During the past decade, the SCB has had unusually warm temperatures and low rainfall (Frankson et al., 2022). In 2012, the region entered a drought, due to the formation of a persistent ridge of high atmospheric pressure over the Northeast Pacific (Seager et al., 2015). Sea surface temperatures (SST) also abruptly rose due to ocean heat waves between 2013-2015 and 2018-2020 (Bond et al., 2015, Weber et al., 2021). Due to anthropogenic climate change, the region is expected to continue to warm and to oscillate between extreme dry and extreme wet periods (Berg and Hall, 2015). The distinct water masses that contribute to the SCB and the region's sensitivity to climate change make it valuable for understanding both the natural variability of DIC carbon isotopes and the human impact on them.

Hinger et al. (2010) and Santos et al. (2011) reported DIC $\Delta^{14}C$ and $\delta^{13}C$ measurements of seawater from the Newport Beach Pier in the Southern California Bight between 2004-2010. Here, we present a continuation of this time series that contains monthly records from the Newport Beach Pier between 2011-2022. Combined, the nearly two decades of data reflect the natural variability of DIC, the response of DIC to a changing climate, and the effect of fossil fuel CO_2 emissions on the carbon isotopes in DIC.

3.3 Methods

3.3.1. Sample collection

Sampling was performed monthly at the Newport Beach Pier in Orange County, California (33°36'21"N, 117°55'52"W). Sampling has been conducted since August 2004, with varying gaps in 2009, 2016, 2018, and 2020.

Glass bottles (0.25 L media bottles) were acidified in 10% HCl for two hours, rinsed with Milli-Q water, baked at 540°C for two hours, and then stored in plastic bags. Sea water was collected via a surface cast of a plastic bucket on a nylon line. The bucket was fitted with a spigot and Teflon tubing that was used to fill the sample bottles. Sample bottles were rinsed three times with sea water and then filled and overflowed for one volume. Samples were poisoned with two drops of saturated mercuric chloride solution and inverted several times after closure. Duplicates were collected for each sampling.

3.3.2 DIC extraction

The DIC extraction for ^{14}C samples was performed according to the procedure described by Gao et al. (2014). Briefly, ~45mL of seawater was subsampled into a 60 mL vial fitted with a Teflon and a Viton septa inside a He-filled glove box. The samples were then acidified with 0.5 mL 85% H_3PO_4 administered using a Hamilton glass syringe with a Sub-Q 26G5/8-gauge needle. The sample vials were then heated on a heatblock at 75 °C for two hours to convert all DIC to gaseous CO_2. The CO_2 from the headspace of the sample vial was extracted by a 60 mL syringe with a one-way stopcock. The CO_2 was then loaded onto a vacuum line through a septum for cryogenic purification. Samples were converted to graphite using the sealed tube zinc reduction method over iron catalyst as described by Xu et al. (2007).

The DIC extraction for ^{13}C samples was performed according to a modified procedure described by Torres et al. (2005). One mL of seawater was subsampled into a Labco exetainer vial fitted with a Labco septa in a He gas-filled glove box. The samples were then acidified with 50µL of 85% H_3PO_4 administered with a BD Falcon 1mL syringe with a

26G5/8-gauge needle. Samples were allowed to equilibrate at room temperature for 12 hours to prevent ^{13}C fractionation of the CO_2.

3.3.3 Isotope analyses

The ^{14}C analyses of the graphite samples were performed at the Keck Carbon Cycle Accelerator Mass Spectrometry (KCCAMS) Laboratory at the University of California, Irvine (Beverly et al., 2010). Processed standards and blank were performed by dissolving modern coral standard (CSTD), IAEA-C2 and radiocarbon-dead calcite in separate aliquots of previously acidified and stripped sea water using the ^{13}C DIC extraction described above. The results from the calcites were used to correct for sample preparation backgrounds added during DIC extraction and graphitization of samples (Gao et al, 2014). Radiocarbon results are reported as $\Delta^{14}C$ corrected for collection date (Stuiver and Polach, 1977). Uncertainty of $\Delta^{14}C$ was estimated as ±2.6‰ (±1σ, 31 data points) using the pooled, standard deviation of replicate measurements (McNaught and Wilkinson 1997).

The ^{13}C analysis was performed at UCI using a Gas Bench II coupled with a Thermo Scientific Delta Plus XL isotope ratio mass spectrometer. CO_2 from the sample preparation vials was directly transferred into the Gas Bench via an auto-sampler. DIC concentration was determined with the same IRMS, using a calibration curve derived from calcite standards with various weights. The pooled standard deviation of repeat measurements of $\delta^{13}C$ was estimated as ±0.05‰ (±1σ, 14 data points). However, due to uncertainties in the $\delta^{13}C$ values of the standards, we report an uncertainty of 0.1‰ for $\delta^{13}C$ values. Uncertainty of the concentrations was ±0.01 mM C based on the pooled standard deviation of repeat measurements (±1σ, 14 data points).

3.3.4 Sea surface characteristics

Sea surface temperature (SST) and salinity data were obtained from the Scripps Shore Stations program (Carter et al., 2022). Newport Beach lifeguards collected temperatures and water samples daily and sent the samples to Scripps for analysis. The water samples were analyzed for salinity at Scripps Institution of Oceanography (https://sccoos.org/autoss). The Coastal Upwelling Transport Index (CUTI), from NOAA Pacific Fisheries Environmental Laboratory, was used to determine wind-driven upwelling rates at the site (https://oceanview.pfeg.noaa.gov/products/upwelling). CUTI uses satellite and in situ wind measurements to estimate the vertical transport of water (Jacox et al., 2018). Our site is very close to the boundary between the 33°N and 34°N CUTI grid boxes. We selected the 33°N box to remain consistent with prior studies (Santos et al., 2011).

3.4 Results

3.4.1 DIC concentration and isotopes

The DIC $\Delta^{14}C$, $\delta^{13}C$ values and DIC concentrations are shown in Table 3.1 and Figures 2a-c. The DIC $\Delta^{14}C$ values ranged from 22.1‰ in March 2012 to -8.4‰ in April 2022 (Figure 3.2a). The DIC $\delta^{13}C$ values ranged from 2.14‰ in April 2014 to -0.3‰ in October 2015 (Figure 3.2b). Concentrations varied from 2.04 ± 0.01 mM C in October 2020 to 2.68 mM C in August 2013 and the average concentration was 2.29mM C (n=89) (Figure 3.2c). The samples collected did not coincide with any major precipitation or runoff events.

3.4.2 Oceanographic Conditions in the Surface Waters

The 15-day moving average of CUTI ranged from 1.5 m^2/s to -0.2 m^2/s (Figure 3.2d). Upwelling was typically elevated in the spring and summer months and lowered during the winter months. SST ranged from 10.0°C in the winter to 25.2 °C in the summer (Figure 3.2e). Lows in SST during the summers of 2010 and 2017 are likely due to enhanced upwelling or intrusion of the colder California Current water towards the coast. SST increased markedly in 2014 and remained elevated throughout 2020. Surface salinities ranged from 23.39 practical salinity units (PSU) to 34.87 PSU throughout the 2011-2022 period (Figure 3.2f). Salinity was lowest and most variable during the winter months and highest during the summer and early fall.

Table 3.1. $\Delta^{14}C$ values, $\delta^{13}C$ values, and concentrations of surface DIC samples

Date Collected	UCI AMS#	$\Delta^{14}C$ (‰)	±[1]	$\delta^{13}C$ (‰)[2]	Concentration (mM C)[3]
1/10/11	136164	8.3	2.3		
1/10/11	136161	10.6	2.5	0.67	2.34
2/13/11	99410	15.5	1.9		
2/13/11	99411	19.6	1.9		
4/12/11	129994	17.5	2.6		
4/12/11	129995	14.4	2.6		
5/12/11	99412	17.1	1.8		
5/12/11	99413	15.8	2.0		
6/13/11	99414	15.1	1.8		
6/13/11	99415	16.0	2.1		
7/13/11	99416	15.9	1.8		
7/13/11	99417	16.9	1.8		
8/11/11	99418	16.5	1.9		
8/11/11	99419	16.5	2.2		
9/13/11	136165	15.9	2.5		
9/13/11	99420	13.7	1.9	1.49	2.22
9/13/11	99421	16.3	2.0		
10/15/11	133972	10.1	1.9		
11/15/11	128696	11.8	1.9	1.41	2.21
11/15/11	128697	11.6	1.9		
11/15/11	128698	10.5	1.8		
11/15/11	128699	7.2	2.0		
11/15/11	136158	14.3	2.4		
12/14/11	129997	15.3	2.6		
12/14/11	129998	15.3	2.6		
12/14/11	129999	16.4	2.9		
1/12/12	130003	15.3	2.6		
1/12/12	130004	11.4	2.6		
1/12/12	130005	14.3	2.6		
1/12/12	130006	17.4	2.7		
3/15/12	136160	22.1	2.6		
4/12/12	129996	20.9	2.6		
4/12/12	130001	12.6	2.7	0.49	2.35
5/17/12	136166	15.4	2.4	1.04	2.35

6/14/12	136159	16.7	2.4	1.49	2.26
7/23/12	136167	16.8	2.4	1.63	2.22
8/17/12	136168	15.5	2.4	1.44	2.23
8/17/12				1.51	2.27
9/19/12	136169	17.7	2.6	1.62	2.29
11/14/12	136167	18.8	2.4	1.06	2.28
1/10/13	136643	12.6	3.3	1.22	2.29
2/7/13	136654	16.0	2.7		
2/7/13	136655	9.5	2.7		
3/12/13	136151	19.4	2.4	0.91	2.28
4/18/13	136152	9.2	2.7		
4/18/13	136161	10.6	2.5	0.67	2.34
5/9/13	136153	17.1	2.8	1.37	2.26
6/6/13	136644	13.0	2.7		
7/6/13	136645	14.8	2.7		
7/6/13	136646	14.2	2.7		
8/2/13	136647	4.4	3.0	1.28	2.68
8/27/13	136648	15.5	2.7	1.61	2.26
10/9/13	136649	22.0	2.7	1.71	2.21
11/4/13	136650	14.7	2.7		
12/4/13	136651	12.3	2.7	1.14	2.26
1/9/14	136652	11.1	2.7		
1/9/14	136656	9.2	2.7		
2/10/14	164582	12.2	2.9	1.18	2.27
3/13/14	164583	12.4	2.7	1.47	2.22
4/7/14	164584	12.2	2.6	2.14	2.17
5/8/14	164585	10.3	2.5	1.19	2.28
6/3/14	164586	12.4	2.6	1.40	2.25
7/7/14	164587	10.3	2.6	1.73	2.24
8/4/14	164588	9.2	2.8	1.50	2.26
9/16/14	164589	7.6	2.6	1.53	2.26
10/7/14	164590	10.1	2.7	1.50	2.24
11/25/14	164591	10.1	2.6	1.39	2.24
1/9/15	164592	9.2	2.6	1.32	2.26
2/6/15	164593	10.3	2.7	1.14	2.24
3/23/15	164594	10.1	2.8		

4/29/15	164595	10.2	2.8	1.38	2.22
5/27/15	164596	5.2	2.6	1.33	2.33
5/27/15				1.26	2.3
6/17/15	164597	10.0	2.7	1.44	2.24
7/24/15	191748	5.2	1.5	1.38	2.26
8/28/15	191743	5.2	1.5	1.63	2.29
9/22/15	191749	8.6	1.6	1.41	2.22
10/30/15	191744	6.7	1.6	-0.30	2.32
11/30/15	191745	11.1	1.6	1.45	2.23
12/18/15	191746	5.6	2.0	1.33	2.30
1/29/16	191747	7.1	1.5		
1/29/16	262143	3.2	1.6	1.05	2.39
3/28/16	171954	2.3	1.6		
3/28/16	227518	-2.9	2.6	1.15	2.39
3/28/16	229231	-3.9	2.4		
3/28/16	262144	3.2	1.6	1.11	2.37
4/29/16	191755	4.7	1.6		
4/29/16	262145	4.5	1.9	1.21	2.38
5/27/16	191758	-1.1	1.4		
5/27/16	265836	5.3	1.9	1.34	1.99
6/24/16	191759	1.8	1.4	1.15	2.29
7/28/16	191763	-4.1	1.6		
9/1/16	191764	-1.4	1.6	1.25	2.23
4/20/17	262147	9.5	1.6	1.33	2.34
4/20/17	262148	12.7	1.7	1.30	2.33
6/1/17	262151	1.7	1.6	1.44	2.35
6/1/17	262152	2.7	1.6		
7/18/17	262153	6.3	1.8	2.12	2.27
8/23/17	262154	6.6	1.7	1.56	2.34
10/31/17	262155	3.1	1.6	1.43	2.33
12/5/17	262156	7.8	1.6	1.02	2.35
10/18/18	262158	8.6	1.6	1.14	2.29
11/21/18	227508	7.2	2.7	1.08	2.26
11/21/18				1.11	2.24
12/20/18	262158	4.0	1.6	0.87	2.33
12/20/18	265837	7.6	1.7		

1/24/19	262160	8.0	1.8		
1/24/19	262161	2.2	1.6	0.98	2.32
3/19/19	262163	3.9	2.3	1.14	2.30
4/18/19	262164	3.0	2.2	1.09	2.29
6/26/19	262166	2.5	1.8	1.03	2.31
8/28/19	229270	4.0	2.3		
8/28/19	227505	5.4	2.6		
8/28/19	227506	8.8	2.6		
8/28/19	227509	5.3	2.8		
8/28/19	262169	-4.6	1.8	2.09	2.23
9/29/19	262170	5.7	1.8		
9/29/19	262584	7.0	2.3	1.43	2.28
10/29/19	227510	5.3	2.6		
11/19/19	229233	6.2	2.3		
11/19/19	229234	1.6	2.2		
11/19/19	262171	1.5	1.9	1.10	2.25
1/20/20	262172	-2.7	2.0	0.93	2.42
2/27/20	262173	2.4	1.9	0.93	2.30
6/16/20	262174	2.0	1.7	1.34	2.59
6/16/20	262175	3.3	1.7	1.50	2.27
7/30/20	262176	-5.5	1.7	1.10	2.62
8/24/20	262177	-7.2	1.8	1.80	2.25
9/18/20	262178	-8.0	2.0	1.72	2.31
9/18/20	162585	-2.6	1.6	1.66	2.26
10/20/20	262179	1.6	1.7	1.52	2.04
3/11/21	262180	-6.3	2.1	0.61	2.67
3/11/21	265842	-0.3	1.8		
3/11/21	265843	-2.0	1.8		
4/20/21	262181	-2.3	1.7	1.05	2.29
4/20/21	262182	1.2	2.3	1.04	2.36
5/14/21	262183	-0.3	2.2	1.08	2.67
6/25/21	262184	-5.3	1.7	1.39	2.26
8/17/21	262185	-5.4	1.7	1.61	2.22
9/30/21	262186	-7.1	1.4	1.34	2.26
9/30/21				1.40	2.26
9/30/21	262586	-4.7	1.6		

10/7/21	262187	-5.6	1.6	1.39	2.24
10/15/21	262188	-5.8	1.6	1.12	2.25
10/28/21	262189	-4.7	1.7	1.69	2.17
12/21/21	262190	-12.6	1.7	1.07	2.26
12/21/21	265844	-4.0	1.8		
1/19/22	262587	-4.8	1.6	1.23	2.23
2/18/22	262588	-4.8	1.6	1.17	2.23
3/17/22	262191	-5.7	1.5	0.89	2.25
4/13/22	262141	-8.4	1.9	1.19	2.24
4/13/22	262582	-3.0	1.8	1.04	2.30
5/16/22	265845	-4.7	1.7	1.24	2.19

[1]Listed values represent AMS error. Pooled standard deviation of replicates is 2.6‰
[2]Pooled standard deviation of replicates is 1‰
[3]Pooled standard deviation of replicates is 0.01 mM C.

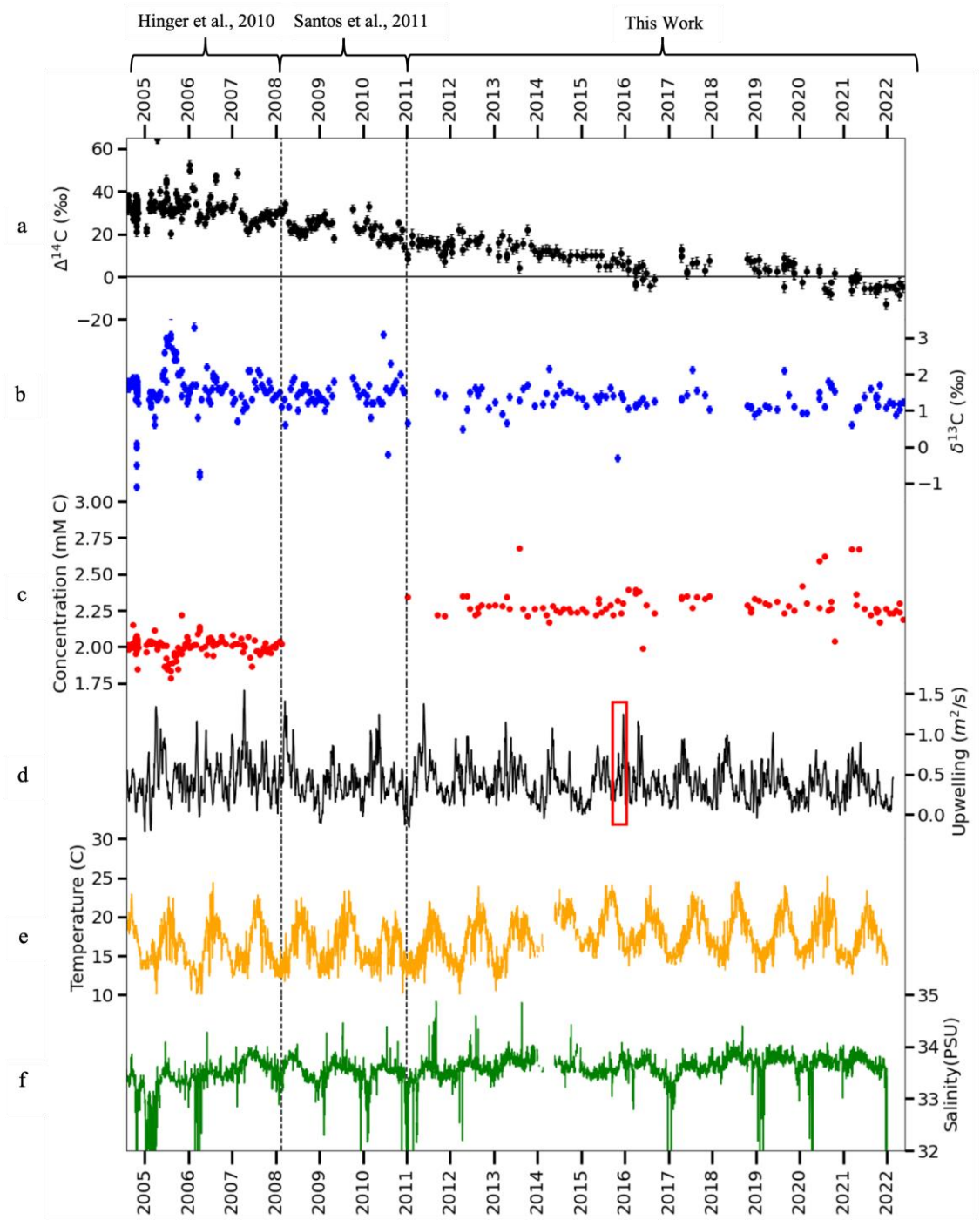

Figure 3.2: Time series of a) $\Delta^{14}C$ values, b) $\delta^{13}C$ values, and c) concentration of surface DIC, d) the 15-day moving average of CUTI, e) sea surface temperature, and f) surface salinity of water samples. Error bars from this work represent the pooled standard deviations of repeated analyses of samples. Error bars for DIC concentration are smaller than the sizes of the symbols. Samples with salinity < 32 PSU are not shown. Dashed lines indicate the different sources of data. The red box on the upwelling axis indicates the period of abnormal upwelling discussed in section 4.3.

3.5 Discussion

We present the discussion in three parts. First, we discuss the possible reasons for the decline of the DIC $\Delta^{14}C$ and $\delta^{13}C$ values over the past two decades. Second, we discuss the seasonal trends in the DIC $\Delta^{14}C$ and $\delta^{13}C$ values and the driving factors behind these trends. Third, we discuss how major climate events between 2011-2022 may have affected the DIC $\Delta^{14}C$ and $\delta^{13}C$ values and their trends.

3.5.1 Decline of DIC $\Delta^{14}C$ and $\delta^{13}C$ values

The long-term trends in $\Delta^{14}C$ and $\delta^{13}C$ values were evaluated by performing model 2 geometric regressions of the average annual isotopic values versus the number of years since measurements began in 2004. The regressions were performed using the python package Scipy (Virtanen et al., 2020). These analyses included years with sampling gaps because omission of these years did not change the slope coefficients of the trendlines by more than one standard error.

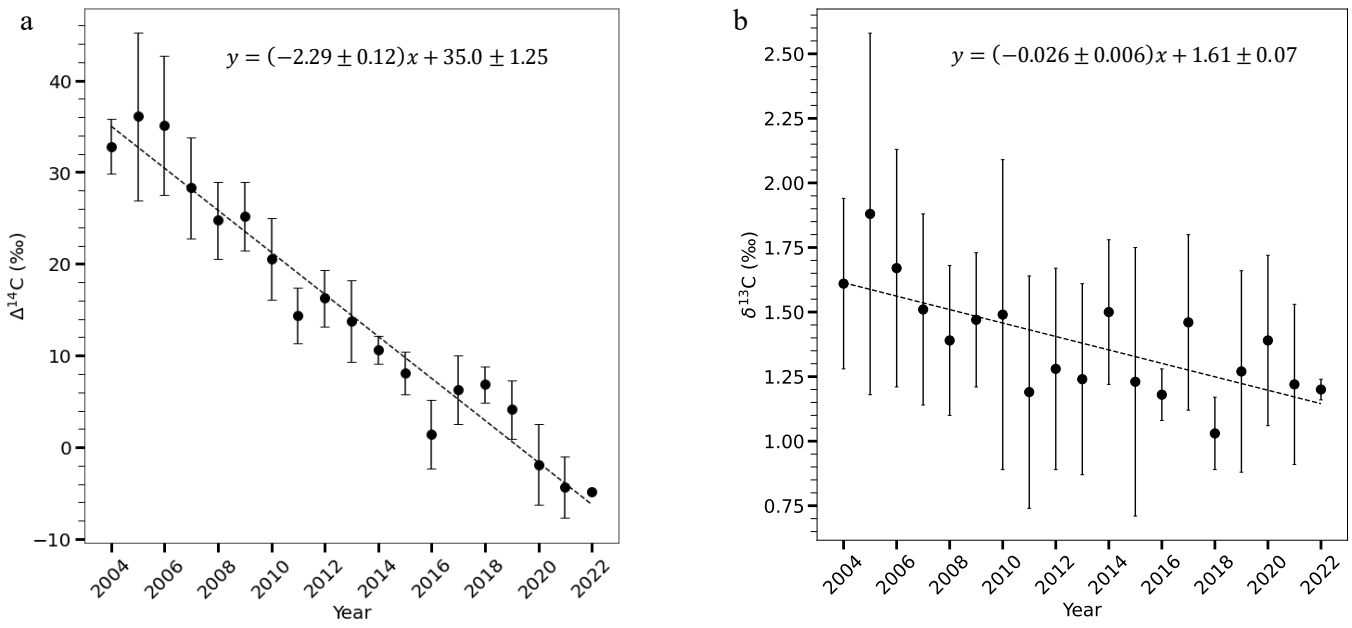

Figure 3.3: Annual average of a) $\Delta^{14}C$ and b) $\delta^{13}C$ values of DIC samples from Newport Beach Pier. Dashed lines show model 2 geometric regressions. Error bars represent standard deviation of analyzed samples from that year.

Annual average DIC $\Delta^{14}C$ values decreased linearly from 35‰ in 2004 to -6‰ in 2022 (R^2=0.96, p<<0.001) (Figure 3.3a). This is consistent with atmospheric CO_2 observations from La Jolla, California, (32.9ºN, 117.3ºW), also in the SCB, where atmospheric CO_2 $\Delta^{14}C$ decreased from 60‰ to -5‰ over this same time period (Graven et al., 2022). This indicates that air-sea CO_2 exchange is a significant factor in the long-term trend of surface DIC $\Delta^{14}C$. Prior to anthropogenic influence, surface DIC $\Delta^{14}C$ values were lower than those of atmospheric CO_2 due to mixing of surface water with aged water masses and the slow equilibration time (~10 years) of atmospheric and dissolved $^{14}CO_2$ (Broecker and Peng, 1982). This mixing with aged subsurface waters means that the surface DIC $\Delta^{14}C$ has a lagged and dampened response to the anthropogenic disturbances in atmospheric CO_2 $\Delta^{14}C$. In recent years, these two reservoirs have converged. In 2000,

annual coral bands in the North Pacific Gyre had $\Delta^{14}C$ values that were higher than atmospheric CO_2 values (86‰) (Andrews et al. 2016), and higher surface water DIC $\Delta^{14}C$ than maritime air in 2014 from the South China Sea was reported by Gao et al. (2018). Our coastal site has lower DIC $\Delta^{14}C$ values than surface gyre water due to the local upwelling. As of 2020, DIC $\Delta^{14}C$ values at Newport Beach pier and atmospheric $^{14}CO_2$ values are both below 0‰ and within experimental error of one another (Graven et al., 2022). The future relationship of DIC and CO_2 $\Delta^{14}C$ values at this site is highly dependent on the magnitude of fossil fuel CO_2 emissions in the coming years. Thus, continued monitoring of this site will be invaluable for understanding the magnitude of the ocean carbon sink and the efficacy of our efforts to mitigate climate change.

Annual average DIC $\delta^{13}C$ values decreased from 1.6‰ in 2004 to 1.2‰ in 2022 (R^2=0.50, p=0.001) (Figure 3.3b). This trend is consistent with decreasing $\delta^{13}C$ of atmospheric CO_2 (Quay et al., 2017) and in the North Pacific Gyre (Brooks, 2020). This is likely a further demonstration of the $\delta^{13}C$ Suess effect as fossil fuel CO_2 emissions continue. It should be noted that the annual variability of $\delta^{13}C$ (0.7‰) is greater than the total decline observed during this 18-year period (0.4‰). This suggests the possibility that strong seasonality or significant changes in local carbon cycling could mask the Suess effect on DIC $\delta^{13}C$ in small data sets.

3.5.2 Seasonality of DIC $\Delta^{14}C$ and $\delta^{13}C$ values

Seasonality was evaluated by comparing the average monthly $\Delta^{14}C$ and $\delta^{13}C$ values for the entire data set. As the change in $\Delta^{14}C$ from 2004-2022 was found to be larger than the annual variation during this time, the $\Delta^{14}C$ values were detrended assuming a linear

trend using Scipy (Virtanen et al., 2020). The annual variation in $\delta^{13}C$ values was larger than the change in annual averages from 2004-2022, so detrending was not performed. Each year was given equal weight when determining monthly averages to account for some years with multiple samples in a single month. Samples on days with salinity <32 PSU were omitted from this analysis. This was done to remove the effect of precipitation events, because changes from these events are highly variable and short-lived (Hinger et al., 2010). These analyses were performed separately for data from Hinger et al. (2010) and Santos et al. (2011) (Figures 3.4a and 3.4c) and for the data from this study (Figures 3.4b and 3.4d).

Between 2004-2010 (Figure 3.4a), detrended $\Delta^{14}C$ values are elevated throughout the winter and early spring, followed by a sharp drop in May and gradual rise in the summer and autumn. Hinger at al. (2010) attributed the elevated $\Delta^{14}C$ values in the winter to an increase in the number and clustering of small eddies during the winter months. They hypothesized that these eddies transported North Pacific gyre water with higher $\Delta^{14}C$ values to our site. After 2011, the elevated winter values are not present (Figure 3.4b). We hypothesize that this could have occurred for two reasons. First, there was less transport of gyre water to our site. During our study period, an atmospheric ridge of persistent high-pressure was formed over the Northeast Pacific (Seager et al., 2015). This ridge drastically reduced the magnitude of the winter winds that possibly could have reduced the eddy strength during this time (Seager et al., 2015). Second, the DIC $\Delta^{14}C$ values of the Gyre waters have also decreased during this period (Figure B.3, Appendix B) (Key et al., 2015, Olsen et al., 2016). As the $\Delta^{14}C$ values of the surface and upwelled waters converge, this may reduce the strength of the seasonal cycle.

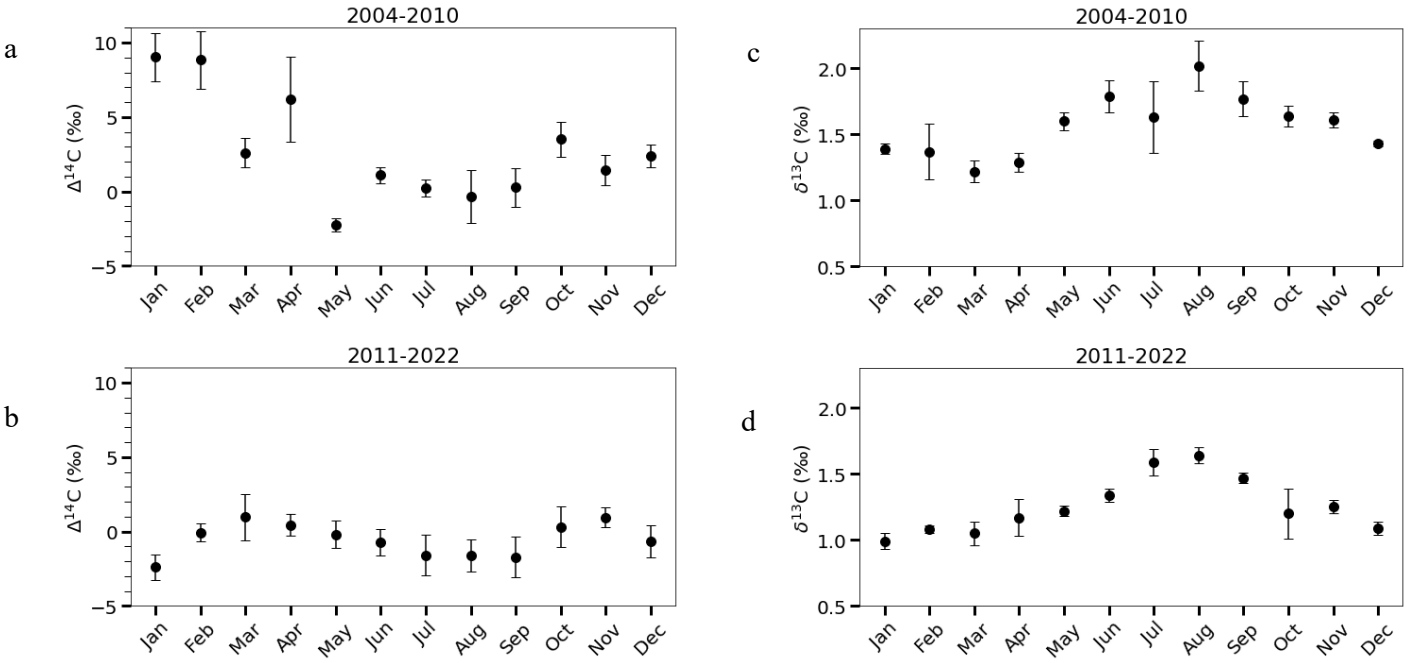

Figure 3.4: Monthly average of a) and b) $\Delta^{14}C$ and c) and d) $\delta^{13}C$ values of DIC samples from Newport Beach Pier from the a) and c) prior timeseries and this work b) and d). Error bars represent standard error of the mean for samples available from each month. Samples from 2004-2010 are from Hinger et al. (2010) and Santos et al. (2011). Samples from 2011-2022 are from this work.

The detrended DIC $\Delta^{14}C$ values from this study period (Figure 3.4b) display semiannual seasonality with small peaks in March and November and troughs in January and September. The DIC $\Delta^{14}C$ values vary by 3.4‰ during these cycles, which is less than 2 times the largest standard error in March (2.1‰). The lower DIC $\Delta^{14}C$ values in winter and summer are likely indicative of mixing between surface water and deeper, older water masses. Upwelling is at its maximum during the late spring, and we observe a decrease in DIC $\Delta^{14}C$ values during this time. Upwelling is stronger further North in the California Current, and transport of these upwelled waters to the SCB may have continued to keep the $\Delta^{14}C$ values lower during the months after the upwelling maximum (Hickey, 1992). The

low $\Delta^{14}C$ values during the winter, when upwelling is weak, could be due to deepening of the mixed layer depth that allows for advection of the deeper, aged water to the surface. The peaks in spring and autumn likely then reflect an increase in the contribution of water from the North Pacific Gyre, which have higher $\Delta^{14}C$ values (Andrews et al., 2016). This trend overall suggests a steady composition of source waters at our site.

Average seasonal $\delta^{13}C$ values are strongly seasonal with a minimum during late winter and a maximum during late summer (Figures 3.4c and 3.4d). The seasonality of the two study periods is largely the same, except that, on average, the $\delta^{13}C$ values were 0.2‰ lower during 2011-2022 than in 2004-2010. The summer maximum suggests that mixing of surface and upwelled water is not the primary control of $\delta^{13}C$. Deep water DIC typically has lowered $\delta^{13}C$ due to the remineralization of particulate and dissolved organic matter (Kroopnick 1985). If mixing with upwelled water was the main driver of DIC $\delta^{13}C$ variability, then we would expect to see decreases in $\delta^{13}C$ values during the summer months, as we do with $\Delta^{14}C$ values. Instead, we find a pattern similar to atmospheric $\delta^{13}C$ CO_2 values. Atmospheric fluctuations in $\delta^{13}C$ CO_2 values are due to fractionation during terrestrial photosynthesis, which preferentially removes ^{12}C atoms. We hypothesize that the surface DIC $\delta^{13}C$ at our site fluctuates due to a similar mechanism. As nutrient-rich waters from spring and summer upwelling stimulate primary productivity, the phytoplankton and kelp take up DIC with lower $\delta^{13}C$ values and thereby increase the $\delta^{13}C$ of DIC remaining in the water.

The average increase in $\delta^{13}C$ between March and August is 0.7‰ (Figure 3.4d). Assuming a concentration of DIC in March of 2.25 mM C (Figure 3.2c), a DIC $\delta^{13}C$ of 1.0‰,

and a $\delta^{13}C$ of phytoplankton of -21.0‰, we calculated that 3% (0.07 mM C) of the DIC would need to be fixed by the phytoplankton to produce this increase. Particulate organic carbon concentrations at this site vary seasonally by about 0.03 mM C (Fagan et al., 2019). Assuming a dissolved organic carbon production of a similar magnitude, which is typical in marine settings (Carlson et al., 1998), this suggests that there is sufficient biological fractionation to account for the seasonal variation of DIC $\delta^{13}C$. This seasonality may be a coastal phenomenon because coasts typically have much higher phytoplankton concentrations than the rest of the ocean (Antione et al., 1996).

3.5.3 Major upwelling event reflected in DIC $\Delta^{14}C$ and $\delta^{13}C$

During the late winter and spring of 2016, we observe an increase in DIC concentration and salinity and decreases in the $\Delta^{14}C$ and SST (Figures 3.2a, 3.2c, 3.2e, 3.2f). These features are all consistent with a period of strong upwelling. The CUTI index does show strong fall and winter upwelling during this time period (Figure 3.2d). This has been attributed to the abrupt end of the 2015-2016 El Niño, which resulted in strong upwelling winds (Frischknecht et al., 2017). This unseasonal upwelling created a large positive nutrient anomaly in the region, which stimulated higher than normal phytoplankton growth during the winter and early spring. This reduced the amount of nutrients available during the 2016 summer and consequently reduced the phytoplankton abundance during that summer (Frischknecht et al., 2017). During the summer of 2016, the DIC $\delta^{13}C$ values are lower than other summers (Figure 3.2d). This is consistent with the hypothesis that primary productivity is the dominant control of $\delta^{13}C$ in this region.

3.6 Conclusion

This work provides an extended timeseries of surface DIC $\delta^{13}C$ and $\Delta^{14}C$ from the Newport Beach pier for two decades. This series demonstrates the seasonality due to changes in ocean circulation and the continued dilution of these isotopes due to CO_2 from fossil fuel sources. DIC $\delta^{13}C$ values decreased by 0.03‰ per year with a total decrease of 0.4‰ from 2004 to 2020. DIC $\Delta^{14}C$ values decreased by 2‰ per year with a total decrease of 42‰ from 2004 to 2020. Between 2004 and 2010, seasonal monthly average $\Delta^{14}C$ values varied by 11‰ and between 2011 and 2022, monthly average $\Delta^{14}C$ values varied by 3.4‰. The $\Delta^{14}C$ variability was likely driven by vertical mixing bringing ^{14}C-depleted waters to the surface and offshore eddies bringing ^{14}C-enriched waters from the gyres to the coastline. Monthly averaged $\delta^{13}C$ values vary by 0.7‰, likely driven by marine primary productivity, similar to atmospheric CO_2. The seasonal signal in $\Delta^{14}C$ is smaller during 2011-2022 than during 2004-2010, but the signal does still correspond to seasonal upwelling, including a major upwelling event in 2016. As $\delta^{13}C$ and $\Delta^{14}C$ of both atmospheric CO_2 and surface DIC continue to decline, their relative values may provide vital insight to the rate and magnitude of the fossil fuel CO_2 sink in the ocean, as well as climatic shifts that affect ocean circulation.

3.7 References

Andrews AH, Siciliano D, Potts DC, DeMartini EE, Covarrubias S. 2016. Bomb Radiocarbon and the Hawaiian Archipelago: Coral, Otoliths, and Seawater. *Radiocarbon* 58(3): 531–48.

Antoine D, André J, and Morel A. 1996. Oceanic Primary Production: 2. Estimation at Global Scale from Satellite (Coastal Zone Color Scanner) Chlorophyll. *Global Biogeochemical Cycles* 10(1):57–69.

Berg N, and Hall A. 2015. Increased Interannual Precipitation Extremes over California under Climate Change. *Journal of Climate* 28(16):6324–34.

Bond, NA., Cronin MF, Freeland H, and Mantua N. 2015. Causes and Impacts of the 2014 Warm Anomaly in the NE Pacific. *Geophysical Research Letters* 42(9):3414–20.
Beverly, RK, Beaumont W, Tauz D, Ormsby KM, von Reden KF, Santos GM, and Southon JR. 2010. The Keck Carbon Cycle AMS laboratory, University of California, Irvine: Status report. Radiocarbon 52(2):301-309.
Bray NA, Keyes A, Morawitz WML. 1999 The California Current System in the Southern California Bight and the Santa Barbara Channel. *Journal of Geophysical Research: Oceans* 104(C4): 7695–7714
Broecker WS and Peng TH. 1982. Tracers in the Sea, 705.
Bograd SJ, Schroeder ID, Jacox MG. 2019 A Water Mass History of the Southern California Current System. *Geophysical Research Letters* 46(12): 6690–98.
Brooks MK. 2020. Time-Series of Stable Isotopes in Dissolved Inorganic Carbon of Surface Seawater Near Bermuda and Hawaii. Ph.D., University of California, San Diego
Carlson CA, Ducklow HW, Hansell DA, Smith Jr WO. 1998 Organic Carbon Partitioning during Spring Phytoplankton Blooms in the Ross Sea Polynya and the Sargasso Sea. *Limnology and Oceanography* 43(3): 375–86.
Carter ML, Flick RE, Terrill E, Beckhaus EC, Martin K, Fey CL, Walker PW, Largier JL, McGowan JA. 2022. Shore Stations Program, Newport Beach - Balboa Pier (Newport Beach Archive, 2022-10-24). In Shore Stations Program Data Archive: Current and Historical Coastal Ocean Temperature and Salinity Measurements from California Stations. UC San Diego Library Digital Collections.
Dong, C, Idica EY, and McWilliams JC. 2009. Circulation and Multiple-Scale Variability in the Southern California Bight. *Progress in Oceanography* 82(3):168–90.
Druffel ERM, Beaupré SR, and Ziolkowski LA. 2016. Radiocarbon in the Oceans. In *Radiocarbon and Climate Change: Mechanisms, Applications and Laboratory Techniques*, edited by Edward A.G. Schuur, Ellen Druffel, and Susan E. Trumbore, 139–66. Cham: Springer International Publishing.
Druffel ERM. 1989. Decade Time Scale Variability of Ventilation in the North Atlantic: High-Precision Measurements of Bomb Radiocarbon in Banded Corals. *Journal of Geophysical Research: Oceans* 94(C3):3271–85.
Fagan AJ, Moreno AR, and Martiny AC. 2019. Role of ENSO Conditions on Particulate Organic Matter Concentrations and Elemental Ratios in the Southern California Bight. *Frontiers in Marine Science* 6:386
Feely RA., Sabine CL, Lee K, Berelson W, Kleypas J, Fabry VJ, Millero FJ. 2004. Impact of Anthropogenic CO2 on the CaCO3 System in the Oceans. *Science* 305(5682): 362–66.
Frankson R, Stevens LE, Kunkel KE, Champion SM, Easterling DR, Sweet W, and Anderson M. 2022. California State Climate Summary 2022. NOAA Technical Report. NOAA NESDIS
Frischknecht M, Münnich M, Gruber N. 2017. Local Atmospheric Forcing Driving an Unexpected California Current System Response during the 2015–2016 El Niño. *Geophysical Research Letters* 44(1):304–11.
Gao P, Xu X, Zhou L, Pack MA, Griffin S, Santos GM, Southon JR, Liu K. 2014. Rapid Sample Preparation of Dissolved Inorganic Carbon in Natural Waters Using a Headspace-Extraction Approach for Radiocarbon Analysis by Accelerator Mass Spectrometry. *Limnology and Oceanography: Methods* 12(4):174–90.

Gao P, Zhou L, Liu K, Xu X. 2018. Radiocarbon in the Maritime air and sea surface water of the South China Sea. *Radiocarbon* 61(2):461-72

Graven H, Keeling R, Xu X. 2022. Radiocarbon Dating: Going Back in Time. *Nature* 607(7919):449–449.

Gruber N, Clement C, Carter BR, Feely RA, van Heuven S, Hoppema M, Ishii M, Key RM, Kozyr A, Lauvset SK, et al. 2019. The Oceanic Sink for Anthropogenic CO2 from 1994 to 2007. *Science* 363(6432):1193–99.

Hickey BM. 1992. Circulation over the Santa Monica-San Pedro Basin and Shelf. *Progress in Oceanography* 30(1):37–115.

Hickey BM. 1979. The California Current System—Hypotheses and Facts. *Progress in Oceanography* 8(4):191–279.

Hinger EN, Santos GM, Druffel ERM, and Griffin S. 2010. Carbon Isotope Measurements of Surface Seawater from a Time-Series Site Off Southern California. *Radiocarbon* 52(1):69–89.

Jacox MG, Edwards CA, Hazen EL, Bograd SJ. 2018. Coastal Upwelling Revisited: Ekman, Bakun, and Improved Upwelling Indices for the U.S. West Coast. *Journal of Geophysical Research: Oceans* 123:7332–50.

Jeansson E, Steinfeldt R, Tanhua T. 2021. Water mass ages based on GLODAPv2 data product (NCEI Accession 0226793). Gv2 PAC age. NOAA National Centers for Environmental Information. Dataset. Accessed May 2023.

Key RM, Olsen A, van Heuven S, Lauvset SK, Velo A, Lin X, Schirnick C, Kozyr A, Tanhua T, Hoppema M, et al. 2015. Global Ocean Data Analysis Project, Version 2 (GLODAPv2), ORNL/CDIAC-162, NDP-093. Carbon Dioxide Information Analysis Center, Oak Ridge National Laboratory, US Department of Energy, Oak Ridge, Tennessee. Accessed May 2023

Kroopnick PM. 1985 The Distribution of 13C of ΣCO2 in the World Oceans. *Deep Sea Research Part A. Oceanographic Research Papers* 32, (1):57–84.

McNaught AD, Wilkinson A. 1997 *IUPAC Compendium of Chemical Terminology. 2nd Edition, The Gold Book*. Oxford: Blackwell Scientific Publications.

Mook WG. 1986 13C in Atmospheric CO2. *Netherlands Journal of Sea Research* 20(2/3): 211-223

Olsen A, Key RM, van Heuven S, Lauvset SK, Velo A, Lin X, Schirnick C, Kozyr A, Tanhua T, Hoppema M, et al. 2016. The Global Ocean Data Analysis Project version 2 (GLODAPv2) – an internally consistent data product for the world ocean, Earth Syst. Sci. Data, 8, 297–323,

Quay P, Sonnerup R, Munro D, Sweeney C. 2017. Anthropogenic CO2 Accumulation and Uptake Rates in the Pacific Ocean Based on Changes in the 13C/12C of Dissolved Inorganic Carbon. *Global Biogeochemical Cycles* 31(1)59–80.

Sabine CL, Feely RA, Gruber N, Key RM, Lee K, Bullister JL, Wanninkhof R, Wong CS, Wallace DWR, Tilbrook B, et al. 2004. The Oceanic Sink for Anthropogenic CO2. *Science* 305(5682):367–71.

Santos, G M, Ferguson J, Acaylar K, Johnson KR, Griffin S, Druffel ERM. 2011. D ^{14}C and D ^{13}C of Seawater DIC as Tracers of Coastal Upwelling. *Radiocarbon*, 53(4): 6690677.

Seager RI, Hoerling M, Schubert S, Wang H, Lyon B, Kumar A, Nakamura J, Henderson N. 2015. Causes of the 2011–14 California Drought. *Journal of Climate* 28(18):6997–7024.

Stuiver M, Polach HA. 1977. Discussion Reporting of 14C Data. *Radiocarbon* 19(3):355–63.
Stuiver M, Pearson GW, Braziunas T. 1986. Radiocarbon Age Calibration of Marine Samples Back to 9000 Cal Yr BP. *Radiocarbon* 28, no. 2B: 980–1021.
Suess, HE. 1953. Natural Radiocarbon and the Rate of Exchange of Carbon Dioxide between the Atmosphere and the Sea. *Aldrich, L. T., Ed., Proceedings of Conference on Nuclear Processes in Geological Settings. National Research Council, Commission on Nuclear Science* 1:52–56.
Torres, ME, Mix AC, Rugh WD. 2005. Precise $\Delta^{13}C$ Analysis of Dissolved Inorganic Carbon in Natural Waters Using Automated Headspace Sampling and Continuous-Flow Mass Spectrometry. *Limnology and Oceanography: Methods* 3(8)349–60.
Virtanen P, Gommers R, Oliphant TE, Haberland M, Reddy T, Cournapeau D, Burovski E, Peterson P, Weckesser W, Bright J, et al. 2020., SciPy 1.0 Contributors. SciPy 1.0: Fundamental Algorithms for Scientific Computing in Python. *Nature Methods* 17(3):261–72.
Weber ED, Auth TD, Baumann-Pickering S, Baumgartner TR, Bjorkstedt EP, Bograd SJ, Burke BJ, Cadena-Ramírez JL, Daly EA, de la Cruz M, et al. 2021. State of the California Current 2019–2020: Back to the Future With Marine Heatwaves? *Front. Mar. Sci.* 8:709454.
Xu X, Trumbore SE, Zheng S, Southon JR, McDuffee KE, Luttgen M, Liu JC. 2007. Modifying a Sealed Tube Zinc Reduction Method for Preparation of AMS Graphite Targets: Reducing Background and Attaining High Precision. *Nuclear Instruments and Methods in Physics Research Section B: Beam Interactions with Materials and Atoms*, Accelerator Mass Spectrometry, 259(1)320–29.

Chapter 4. Carbon Isotopes Show a Consistent Composition of Particulate Organic Carbon from Mouth of Santa Clara River Across Precipitation Extremes

4.1 Abstract

Small mountains rivers transport large quantities of sediment and organic carbon (OC) relative to their total water discharge to coastal oceans, and the majority of the discharge occurs during short-lived precipitation events. The Santa Clara River, the largest and least developed river in Southern California, is a small mountainous river with a geologically diverse watershed. While OC export from this river has been studied before, the effect of drought conditions on the magnitude and composition on OC export has not been quantified. We collected particulate organic carbon (POC) from the river and riverbank sediment from the estuary during the 2021-2022 rainy season and measured their OC content and C isotopes to determine the magnitude and the composition of OC exported by the river. We found that similar to previous studies, the POC contained significant portion of petrogenic OC. Riverbank sediment displayed highly variable OC compositions that depended on the sediment type and whether sampling occurred during a precipitation event. The drought conditions of 2021-2022 resulted in ~3000 times less POC exported than during the El Niño year 1997-1998 (Masiello and Druffel, 2001). However, the exported POC had a flow-weighted average composition of ~40% petrogenic OC and ~60% modern plant OC in both years. This suggests that the composition of POC exported in small mountainous rivers may be somewhat resilient to changes in river discharge.

4.2 Introduction

Rivers are the main system that transports terrestrial organic carbon (OC) to most coastal waters. Small mountainous rivers, characterized by steep catchments and storm driven outflow, cover about 14% of the ocean-draining land surface, yet are responsible for over 40% of the total sediment input from rivers to the ocean (Milliman and Syvitski, 1991). These large, concentrated pulses of sediment and OC result in high burial efficiency of OC in the near-shore sediments (Blair et al., 2004). A growing body of evidence suggests that transport and burial of terrestrial OC by small mountainous rivers is a pathway for the drawdown of atmospheric CO_2 (Hilton and West, 2020). The precipitation dependence of OC export in these rivers suggests that this export will be sensitive to disruptions in local climate. As regions undergo natural and anthropogenic climatic shifts, we need to monitor the change in magnitude and composition of exported riverine OC to determine the significance of this feedback.

The Santa Clara River (SCR) is a typical small mountainous river located in Southern California and is the largest and least dammed river within that region (Biroski, 2006). It flows into the Santa Barbara Basin, located in the northern section of the Southern California Bight. Sediment cores from the Santa Barbara Basin contain terrestrial OC from major flood events (Hwang et al., 2005, Sarno et al., 2020). Particulate OC (POC) from the SCR has been examined in prior decades during El Niño events (Masiello and Druffel 2001; Komada et al., 2004). These studies showed that significant quantities of both modern POC and petrogenic POC were exported during the winter rainy season. Since these prior occupations, Southern California has experienced severe drought (Frankson et al., 2022).

How this drought has affected the quantity and composition of OC exported by the river has not been directly studied.

The SCR catchment is in the Western Transverse Ranges in Southern California. This region contains young, active faults and marine terraces that have been formed over the last 140,000 years (Dibblee and Ehrenspeck, 1992; DeVecchio et al., 2012a). The watershed includes the Monterey Shale formation, which has significant quantities of marine biogenic shale (Dibblee and Ehrenspeck, 1992; Komada et al., 2004). This formation contains both mineral-bound kerogen and oil seeps that release significant quantities of petroleum to the SCR and its tributaries (Komada et al., 2004; Aronson et al., 2022). These petrogenic sources of OC comprise a substantial portion of the OC exported by the SCR (Masiello and Druffel 2001; Komada et al., 2004). Unlike most rivers in Southern California, the SCR has not been channelized and much of the surrounding land remains undeveloped with plentiful native vegetation (Biroski, 2006). However, there are several wastewater treatment plants that discharge secondary and tertiary treated water into the SCR (Biroski, 2006). This treated wastewater is a significant portion of the river discharge during the dry season (Biroski, 2006). The size of the SCR Estuary has, however, been reduced by the construction of levees and the vast majority of the river flow is directed to the nature preserve at McGrath State Beach (Biroski, 2006). For most of the year, the estuary is separated from the ocean by a sand berm. This berm is eroded during storms and allows for rapid draining of the estuary into the Pacific Ocean. The variability of potential organic carbon sources and river discharge means that intensive sampling is required to capture the full picture of OC exported by the SCR.

Carbon isotopes (^{13}C and ^{14}C) are valuable tools for determining the composition of environmental OC samples. The $\Delta^{14}C$ and $\delta^{13}C$ values of a heterogenous sample represents the weighted average of the isotope values of its endmembers. If the $\Delta^{14}C$ and $\delta^{13}C$ values of the endmembers are known, then the relative abundance of each endmember can be estimated. Stable carbon isotope values ($\delta^{13}C$) are representative of the photosynthetic pathway of the OC; values for C3, C4, CAM and marine pathways are -23‰ to -28‰, -12‰ to -16‰, -11‰ to -13‰, and -18‰ to -23‰, respectively (Sternberg et al., 1984; Mook, 1986). Petrogenic OC is derived from either C3 or marine sources and has similar $\delta^{13}C$ values (-22‰ to -27‰) (Reed and Kaplan, 1977). Radiocarbon values ($\Delta^{14}C$) of living organisms reflect the radiocarbon content of the CO_2 used for photosynthesis. Above ground nuclear weapons testing nearly doubled the $\Delta^{14}C$ values of atmospheric CO_2 in the 1960s but since that time, the $\Delta^{14}C$ values of atmospheric CO_2 have declined due to the mixing of bomb-generated ^{14}C into the biosphere and the ocean, as well as the emission of ^{14}C-free fossil fuel derived CO_2 (Hua et al., 2013). Thus, a present-day living plant has a significantly lower $\Delta^{14}C$ value than a plant growing thirty years ago. After an organism dies, its radiocarbon content will decrease due to radioactive decay. C sources older than ~60,000 years, such as shale deposits, have no measurable ^{14}C. Together, ^{14}C and ^{13}C can be used to identify at least three isotopically distinct endmembers in a sample. This tool is well suited to the SCR given the diversity of the OC sources in the watershed.

In this study, we conducted a field campaign during the 2021-2022 rainy season of a drought to collect and measure the concentration and carbon isotopes of POC and sedimentary OC at the SCR Estuary. The goals of this study were to 1) determine the magnitude and composition of exported OC change during a low precipitation year, 2)

determine the composition of the OC stored in the estuarine sediments, and 3) analyze how these results compare to those from prior studies conducted under wetter conditions at this site. Together these results help to constrain the variability of this system across precipitation extremes.

4.3 Research Site and Methods

4.3.1 Sample site description

The SCR, located in Southern California, is a small mountainous river with a watershed area of 4232 km^2 (Birosik, 2006) (Figure 4.1a). The river is in Ventura and Los Angeles Counties and is the largest undeveloped river in Southern California, as only 37% of the basin is controlled by dams (Brownlie and Taylor, 1981). Rainfall events occur in the winter, resulting in high streamflow during December to March, and dry periods during the rest of the year (Ventura County Public Works; Birosik, 2006).

Sediment and particulate samples were collected from the SCR after high flow periods from three precipitation events (12-17-2021, 1-5-2022, 3-29-2022) and three low flow dry periods (3-5-2022, 4-22-2022, 6-20-2022). Due to flooding, sediment was collected only once on 1-5-2022 at site Silt 1.

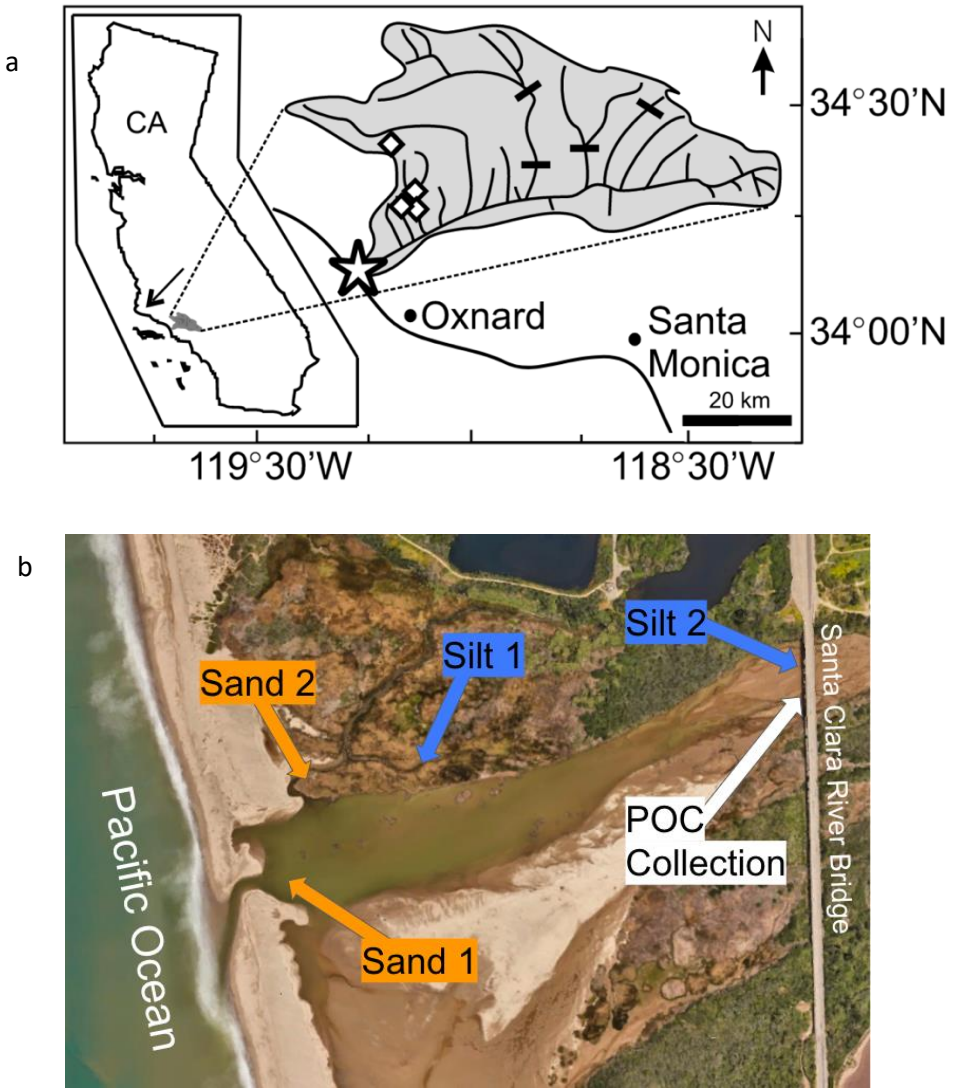

Figure 4.1: a) Map of the SCR watershed. The star indicates the sampling site. (After Komada et al., 2004). b) Collection sites of particulate matter and sediment samples. Sedmiment samples were collected at Sand 1, Sand 2, Silt 1, and Silt 2, and particulate matter samples were collected near Silt 2 from the SCR Bridge. Satellite image from Google Earth. Imagery ©2023 Airbus, CNES / Airbus, Data CSUMB SFML, CA OPC, Maxar Technologies, U.S. Geological Survey, USDA/FPAC/GEO, Map data ©2023

4.3.2 Particulate matter collection and sample processing

All glass sampling equipment was soaked in 10% HCl for at least two hours, rinsed with Milli-Q water, and baked at 540˚C for two hours prior to use. Metal sampling

equipment was baked at 540˚C for two hours prior to use. Bottle and jar lids were lined with Teflon tape that had been cleaned in Chromerge.

River water was collected by submerging a 2.5 L glass bottle hanging by a rope from the SCR Bridge on Harbor Boulevard (POC collection site in Figure 4.1b). The samples were stored on ice for up to 24 hours until vacuum filtered in the laboratory using pre-combusted 2.2 µm quartz fiber filters. The filters were frozen in glass petri dishes wrapped in aluminum foil and plastic bags. For isotope analyses, filters were cut into sections using a razor blade cleaned with methanol, transferred into quartz combustion tubes, then acidified with 3% H_3PO_4 for how long and dried in vacuo.

Prior work by collaborators raised the possibility that carbonates from the POC samples from 1997-1998 (Masiello and Druffel, 2001) might have not been fully removed possibly (Komada et al., 2004). To test this, a full set of duplicate 1997-1998 samples was analyzed using a more aggressive acidification approach of HCl fumigation, as described for the riverbank sediment samples (see section 4.3.3) (Komada et al., 2008). The samples were then processed in the same manner as the other POC samples.

4.3.3 Riverbank sediment collection and processing

Sediment from the top 3 cm of the riverbank at sites Sand 1, Sand 2, Silt 1, and Silt 2 (Figure 4.1b) were collected in glass jars and stored in plastic bags on ice for up to 24 hours until transported to the laboratory, and then frozen. Sub-samples were taken by first thawing at room temperature, then weighing approximately 200 mg of wet sediment in a petri dish before fumigation with concentrated HCl for 3 to 4 hours (Komada et al., 2008). Samples were then either refrigerated overnight or were immediately transferred into

quartz combustion tubes with quartz wool and dried in vacuo. Moisture content of sediment samples was determined by drying samples at 40˚C to a constant mass.

4.3.4 ^{14}C analysis

All samples were transferred to quartz combustion tubes containing cupric oxide and silver wire and were vacuum sealed and combusted to CO_2 at 850˚C for 2 hours. The CO_2 was then cryogenically purified from water using dry ice/isopropyl alcohol slush, and from other gasses using liquid nitrogen (-196˚C). The extracted CO_2 was converted to graphite on iron catalyst for ^{14}C analyses using reduction with zinc (Xu et al. 2007, Walker and Xu 2019). ^{14}C analyses were performed at the Keck Carbon Cycle AMS (KCCAMS) Laboratory at the University of California, Irvine (UCI) by members of our lab group. Uncertainty for river POC and sediment OC samples was determined by pooled standard deviation of replicates (McNaught and Wilkinson, 1977). Uncertainty for river POC $\Delta^{14}C$ values was ± 4‰ and uncertainty for riverbank sediment OC $\Delta^{14}C$ values was ± 45‰ and were high due to heterogeneity of the samples.

4.3.5 ^{13}C analysis

The CO_2 obtained from combusted samples for ^{14}C analysis were split on the vacuum line after equilibrating for at least 2 minutes to avoid fractionation. The split was analyzed for $\delta^{13}C$ using a Finnigan Delta Plus mass spectrometer at UCI. Uncertainty was determined using pooled standard deviation of replicates (McNaught and Wilkinson, 1977). River POC samples have an uncertainty of ± 0.1 ‰; riverbank sediment OC samples have an uncertainty of ± 0.5 ‰ and were high due to heterogeneity of the samples.

4.3.6 Blank Corrections

Blank corrections for River POC and sediment OC samples were made using the indirect method (Santos et al 2010) with tannic acid ($\Delta^{14}C$ = 5 ± 2 ‰; n=4) and salicylic acid ($\Delta^{14}C$=-863 ± 8‰; n=4) as secondary standards. The process blanks were determined by processing the secondary standards in the same manner as river POC and sediment OC samples and measuring their $\Delta^{14}C$ values. We then calculated the mass and $\Delta^{14}C$ of extraneous C required to produce the difference between $\Delta^{14}C$ value of the processed standard and the consensus $\Delta^{14}C$ value of the unprocessed standard. We found process blanks of 8 ± 4 µgC with $\Delta^{14}C$ value of -1000‰ for POC, and 4 ± 2 µgC with $\Delta^{14}C$ values of -1000‰ for riverbank sediment OC.

4.3.7 Stream discharge and salinity

Stream discharge data for December 2021 to June 2022 were obtained from the U.S. Geological Survey National Water Dashboard (Miller et al., 2022). The discharge gauges record measurements every 15 minutes and gauges from the SCR (location 11109000) and three of its tributaries (locations 11109800, 11113000, 11113500) were used. The sum of the flow from the gauges are reported in Figure 4.3. Salinity of river water was determined using a salinity refractometer (Science First NO.:611-2275) with a measurement error of ±0.1‰.

4.3.8 Source apportionment

To estimate the proportions of the endmembers of OC we found are most important (terrestrial plants, marine algae, and petroleum or dead carbon e.g., shale) in the POC samples, we used the MixSAIR Bayesian stable isotope mixing model with two isotopes ($\Delta^{14}C$ and $\delta^{13}C$) and endmembers (Stock et al., 2018). While ^{14}C is not a stable isotope, its half-life is long enough compared to the process of interest (mixing of OC during a precipitation event) that it can be assumed there is no change in $\Delta^{14}C$ due to decay. The $\Delta^{14}C$ and $\delta^{13}C$ values of the endmembers were estimated using Keeling plots of our data (where the inverse of OC concentration is plotted against the isotopic value) (Pataki et al., 2003).

4.4 Results

4.4.1 River physical characteristics

Stream discharge was highest after large rain events, with stream gauge measurements of 5300 ft^3/s on 12-14-2021, 4600 ft^3/s on 12-24-2021, 7400 ft^3/s on 12-30-2021, 120 ft^3/s on 3-05-2022, and 800 ft^3/s on 3-29-2022. The salinity measurements ranged from 0 ‰ to 5 ‰ (Table 4.1a).

4.4.2 POC filter observations

Microscopic examination of one POC filter from each sample day are shown in Figure 4.2. The filters from 12-17-2021, 1-2-2022, and 3-29-2022 contained predominantly sediment (<0.05mm diameter) (Figure 4.2a, 4.2b, and 4.2d). The filter from 1-2-2022

consisted of large debris pieces, such as wood, plant roots, and tar (Figure 4.2b). The filter from 3-29-2022 also consisted of large woody debris, and a microplastic piece (Figure 4.2d). Filters from 3-5-2022 and 6-20-2022 showed varying cell shapes (Figures 4.2c and 4.2f), including a 2mm long organism on the 6-20-2022 filter. The filter from 4-22-2022 consisted of small, circular green cells (dia. 0.2 mm - 0.5 mm) (Figure 4.2e).

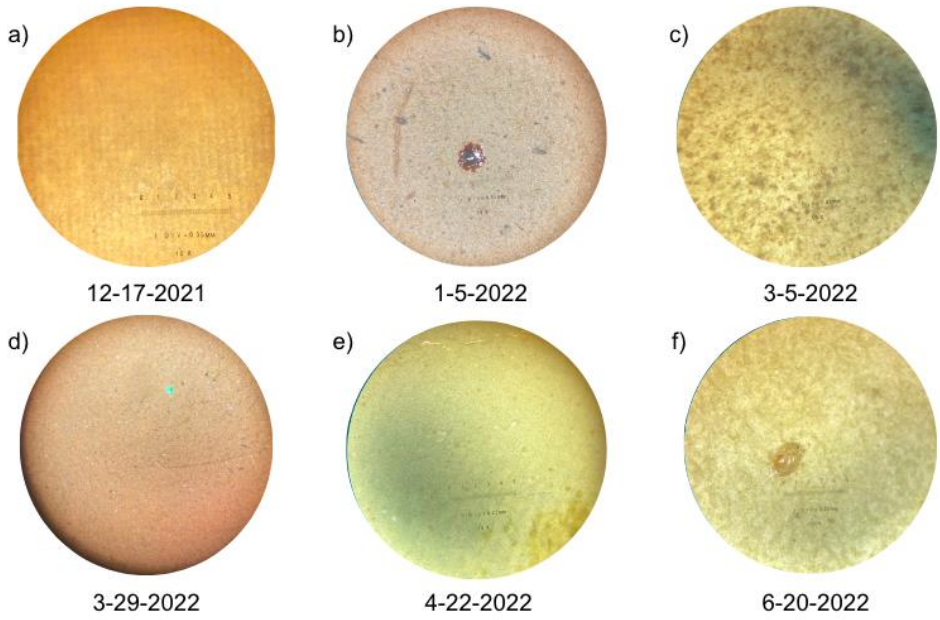

Figure 4.2: Images of POC filters under the microscope from a) 12-17-2021, b) 1-5-2022, c) 3-5-2022, d) 3-29-2022, e) 4-22-2022, and f) 6-20-2022. Images were magnified 10x.

Table 4.1: Streamflow, salinity, POC sample analyses ($\Delta^{14}C$ values, $\delta^{13}C$ values, percent OC, and POC concentrations) for a) 2021-2022 and b) 1997-1998.

a

Date Collected	Flow	Salinity (‰)	[Sediment] (mg/L)	UCID #	[POC] (mM)	% OC (wt/wt)	$\Delta^{14}C$ (‰)	$\delta^{13}C$ (‰)
12/17/21	High	0	11	23815	0.06	8.0	-190	-27.8
				23816	0.06	8.0	-191	-27.8
1/2/22	High	0	285	23817	0.27	2.8	-519	-24.8
				23818	0.28	3.0	-505	-24.9
3/5/22	High	5	190.	23819	0.37	5.9	-107	-27.1
				23820	0.48	7.6	-110	-26.9
3/29/22	High	2	383	23821	0.18	1.4	-301	-25.9
				23822	0.20	1.6	-303	-25.8
4/22/22	Low	5	40.	23835	0.37	19.8	-97	-20.8
				23865	0.36	19.2	-103	-20.7
6/20/22	Low	4	10.	23866	0.08	25.7	-100	-30.0
				23867	0.10	30.8	-101	-29.9

b

Date Collected	Flow	UCID #	[POC] (mM)	% OC *(wt/wt)	$\Delta^{14}C$ (‰)	$\delta^{13}C$ (‰)
11/22/97	Low	24042			14	-33.3
12/5/97	High	24043A	0.66	0.33	-130	-25.7
1/2/98	Low	24043B			7	-20.9
1/28/98	High	24044	4.74	1.15	-215	-25.3
2/14/98	High	24039	9.77	0.44	-565	-25.5
2/14/98	High	24040	10.57	0.47	-584	-25.5
2/24/98	High	24046A	15.36	0.99	-322	-24.7
2/24/98	High	24046B	13.92	0.78	-316	-24.6
3/25/98	High	24047A	13.58	0.91	-458	-24.3
3/25/98	High	24046B	13.52	0.75	-454	-24.3

*%OC was calculated by assuming that it would change by the same proportion that the POC concentration changed relative to the originally published data (Masiello and Druffel, 2001).

Table 4.2. Carbon content and isotope values of riverbank sediment samples ($\Delta^{14}C$ values, $\delta^{13}C$ values, and OC content per dry weight) at the SCR.

Date	Site	Flow	Jar	UCID #	%OC (wt/wt)	$\Delta^{14}C$ (‰)	$\delta^{13}C$ (‰)
1/5/22	Sand 1	High	A	23759	2.62	-947	-21.9
				23760	0.79	-862	-22.0
				23761	0.55	-830	-22.3
			B	23763	0.50	-746	-22.8
				23764	0.53	-577	-22.4
3/5/22	Sand 1	High	A	23793	0.39	-767	-22.8
				23794	0.18	-660	-22.8
			B	23795	0.21	-658	
				23796	0.48	-838	
3/29/22	Sand 1	High	A	23797	0.68	-878	
				23798	0.27	-653	
				23829	0.50	-896	
			B	23830	0.17	-700	
				23843	0.11	-655	-22.5
				23844	0.17	-641	-22.3
4/22/22	Sand 1	Low	A	23823	1.67	-222	-23.6
				23824	1.30	-293	-22.6
				23837	4.20	-143	-24.5
				23838	1.46	-266	-22.8
	Sand 2	Low	B	23825	1.09	-139	-25.4
				23826	1.14	-160	-25.3
				23839	1.17	-240	-25.2
				23840	1.19	-173	-25.2
6/20/22	Sand 1	Low	A	23857	0.60	-170	-21.0
				23858	0.62	-208	-22.7
				23871	0.50	-206	-26.7
				23872	0.58	-286	-26.3
	Sand 2	Low	B	23859	0.47	-309	-20.8
				23860	0.63	-222	-24.5
				23873	0.39	-231	-25.3
				23874	0.40	-177	-24.7
1/5/22	Silt 1	High	A	23691	1.15	-365	-26.1
				23693	1.48	-427	-25.8
			B	23694	4.40	-136	-27.6
				23695	4.06	-105	-28.2
				23696	3.36	-110	-27.9
3/29/22	Silt 2	High	A	23849	2.40	-307	-25.4
				23850	4.47	-245	-25.8
			B	23851	14.74	-118	-26.2
				23852	11.31	-169	-25.4
4/22/22	Silt 2	Low	A	23855	2.43	-206	-25.7
				23856	2.15	-213	-25.3
6/20/22	Silt 2	Low	A	23861	1.08	-536	-25.5
				23862	1.14	-682	-24.2
			B	23875	1.57	-601	-24.4
				23876	1.39	-658	-24.0

4.4.3 POC content and isotopes

The sediment load, concentration of POC in river water, weight percent of OC, $\Delta^{14}C$ values, $\delta^{13}C$ values of river particulate samples are shown in Table 4.1a and Figure 4.3. Sediment load ranged from 10 mg/L on 12-17-2021 to 383 mg/L on 1-2-2022, both during high streamflow (Figure 4.3d). The POC concentrations ranged from 0.06 mM after the first precipitation event of the season on 12-17-2021 to 0.38 mM during low streamflow on 3-5-2022 (Figure 4.3c). The percent OC in the POC ranged from 1.4% and 1.6% on 3-05-2022 to 19.2% and 19.8% on 4-22-2022 (Figure 4.3e). The POC $\Delta^{14}C$ values ranged from -519 ‰ on 1-5-2022 during high stream flow to -97 ‰ (n=4) on 4-22-2022 during low streamflow (Figure 4.3a). $\delta^{13}C$ values ranged from -20.7 ‰ on 4-22-2022 to -30.0 ‰ on 6-20-2022, both at times of low streamflow (Figure 4.3b).

The concentration of POC in river water, weight percent of OC in filtered sediment, $\Delta^{14}C$ values, $\delta^{13}C$ values of river particulate samples from 1997-1998 are shown in Table 4.1b. The POC concentrations ranged from 0.66 mM on 12-5-1997 to 15.36 on 2-24-2022 (Table 4.1b). The $\Delta^{14}C$ values ranged from -584 ‰ on 2-14-1998 to 14 ‰ on 11-22-1997 (Table 4.1b). The $\delta^{13}C$ values ranged from -33.3 ‰ on 11-22-1997 to -20.9 ‰ on 1-2-1998 (Table 4.1b).

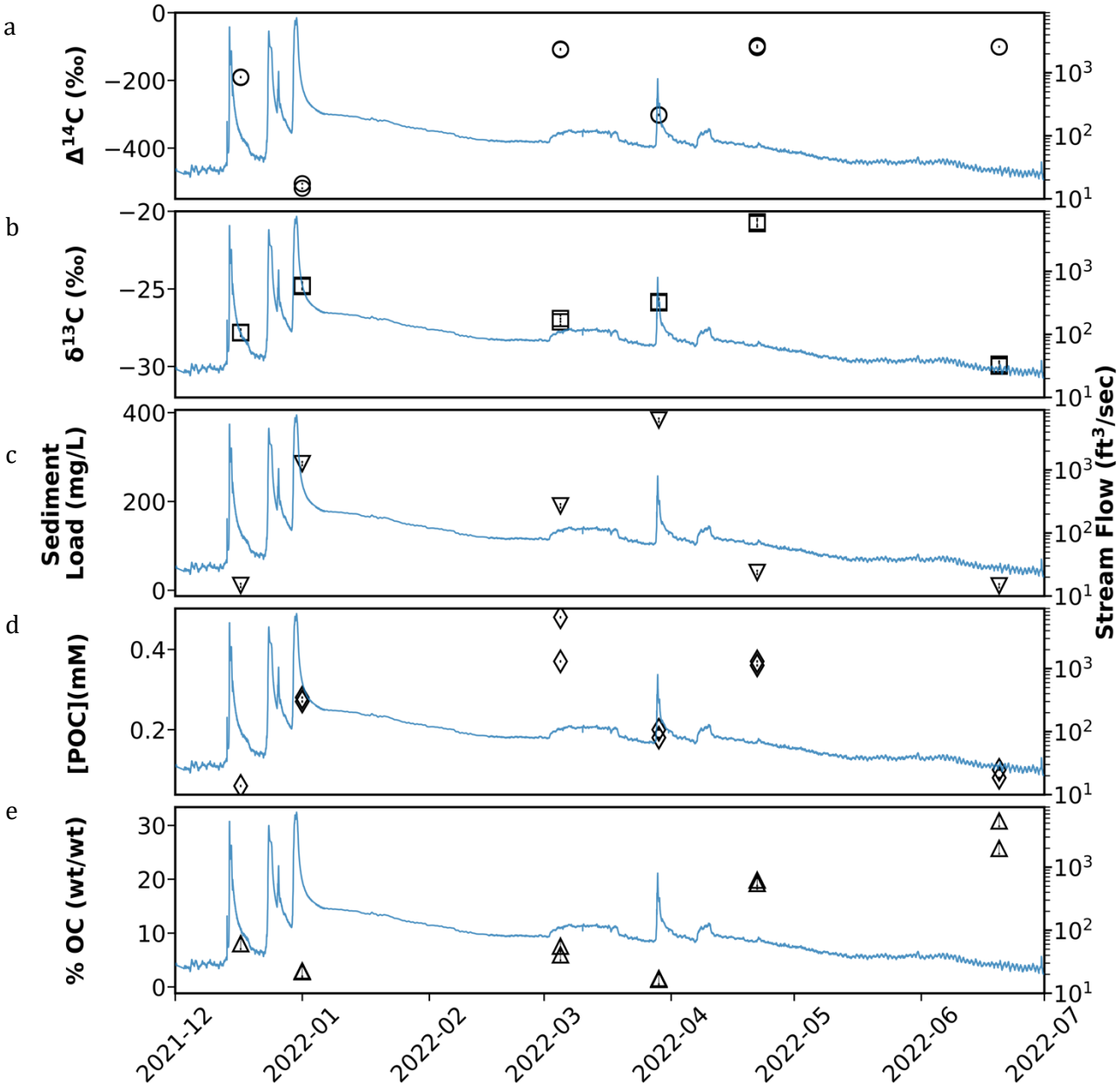

Figure 4.3: Logarithmic scale of stream discharge in blue from November 2021 to June 2022 with a) $\Delta^{14}C$ values, b) $\delta^{13}C$ values, c) sediment load, d) POC concentration, and e) %OC all POC samples collected at the SCR Bridge. Error bars represent the standard deviation, and most error bars are smaller than the symbols on the plot.

4.4.4 Riverbank sediment OC content and isotopes

The $\Delta^{14}C$ values, $\delta^{13}C$ values, soil moisture content, and percent OC of riverbank sediment samples are shown in Table 4.2 and the $\Delta^{14}C$ versus $\delta^{13}C$ values of riverbank sediment samples are shown in Figure 4.4. At Sand sites, the average $\Delta^{14}C$ values ranged from -139 ‰ on 4-22-2022 to -947 on 1-5-2022 (Table 4.2, Figure 4.4). At Silt sites, the average $\Delta^{14}C$ values ranged from -105 ‰ on 1-5-2022 to -682 ‰ on 6-20-2022 (Table 4.2, Figure 4.4). Some sampling dates do not have both Sand and Silt site samples. At the Sand sites, the $\delta^{13}C$ values ranged from -20.8 ‰ to -26.7 ‰, both on 6-20-2022 and at the Sand 1 site from different sampling jars (Table 4.2, Figure 4.4). At the Silt sites, the average $\delta^{13}C$ values ranged from -23.8 ‰ on 6-20-2022 to -28.2 ‰ on 1-5-2022 (Table 4.2, Figure 4.4). The average percent OC in the sediment varied from 0.11 ± 0.03 % (mg/mg dry weight) to 2.1 ± 1.5 % at the Sand sites and from 0.53 ± 0.05 % to 6.75 ± 1.26 % at the Silt sites (Table 4.2).

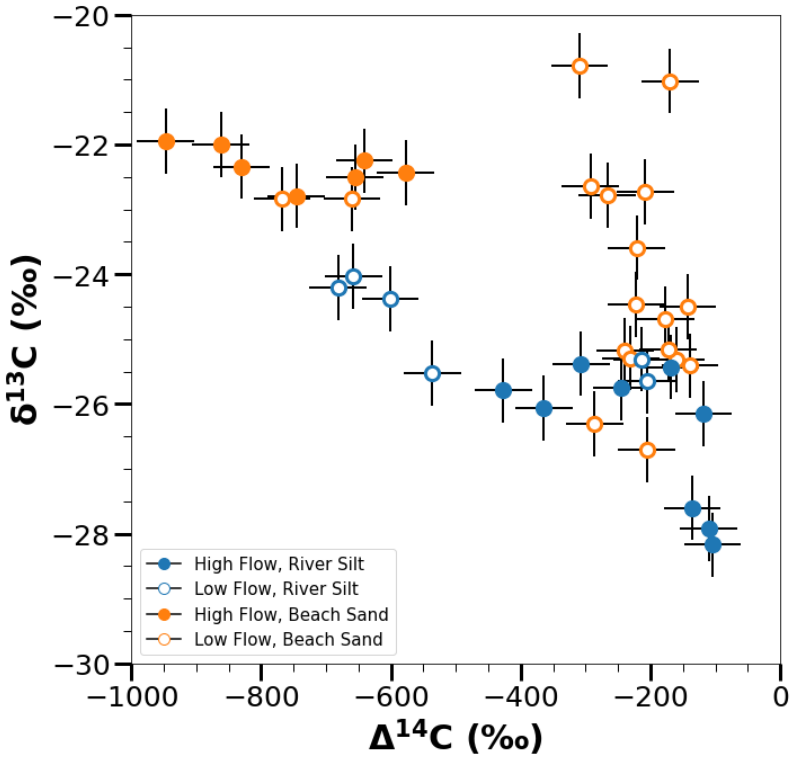

Figure 4.4: Average $\Delta^{14}C$ vs $\delta^{13}C$ values of OC from riverbank sediment samples collected at the mouth of the SCR from sites consisting primarily of either sand (orange symbols) or silt (blue symbols), and on days of either high (filled circles) or low (empty circles) flow. High flow days were defined as days with stream discharge greater than 10^2 ft^3/s.

4.5 Discussion

The objective of this study was to examine the composition of POC transported to and retained by the SCR Estuary during a low stream flow year. Carbon isotope values of both the POC and riverbank sediment OC span a wide range. This is indicative of multiple isotopically distinct pools of OC present within the samples. We discuss the findings in three parts. First, we discuss the composition of the SOC and how it shows evidence for three distinct pools of OC. Second, we discuss the composition of the river POC and how it

relates to the precipitation events. Third, we compare the river POC data with results from prior years during higher stream flows.

4.5.1 Riverbank sediment OC composition

The $\Delta^{14}C$ and $\delta^{13}C$ values of the SOC samples can be well characterized using three end members (Figure 4.4). These endmembers were estimated using Keeling plots (Section 4.3.8) to be the following: recent C3 plant material ($\Delta^{14}C$ = -72 ± 19 ‰, and $\delta^{13}C$ = -29.0 ± 1.8 ‰), recent marine algae ($\Delta^{14}C$ = -105 ± 3 ‰, and $\delta^{13}C$ = -20.9 ± 0.2 ‰), and petrogenic material ($\Delta^{14}C$ = -956 ± 138 ‰, and $\delta^{13}C$ = - 22.4 ± 0.3 ‰). The $\Delta^{14}C$ values of recent C3 and algae endmembers are lower than those of atmospheric CO_2 (Graven et al., 2022). We hypothesize that the $\Delta^{14}C$ values of the C3 endmember may also be slightly lower due to the presence of eroded, aged soils from upstream. Additionally, algae in the SCR estuary may have used DIC with lower $\Delta^{14}C$ values for photosynthesis. This DIC may have had lower $\Delta^{14}C$ values due to remineralization of the abundant, aged organic matter in the estuary or from fossil fuel combustion from vehicles in the nearby, busy roads. The petrogenic endmember has a marine-like $\delta^{13}C$ value (-22‰). This is consistent with the prior observations of shale in this watershed (Komada et al., 2004).

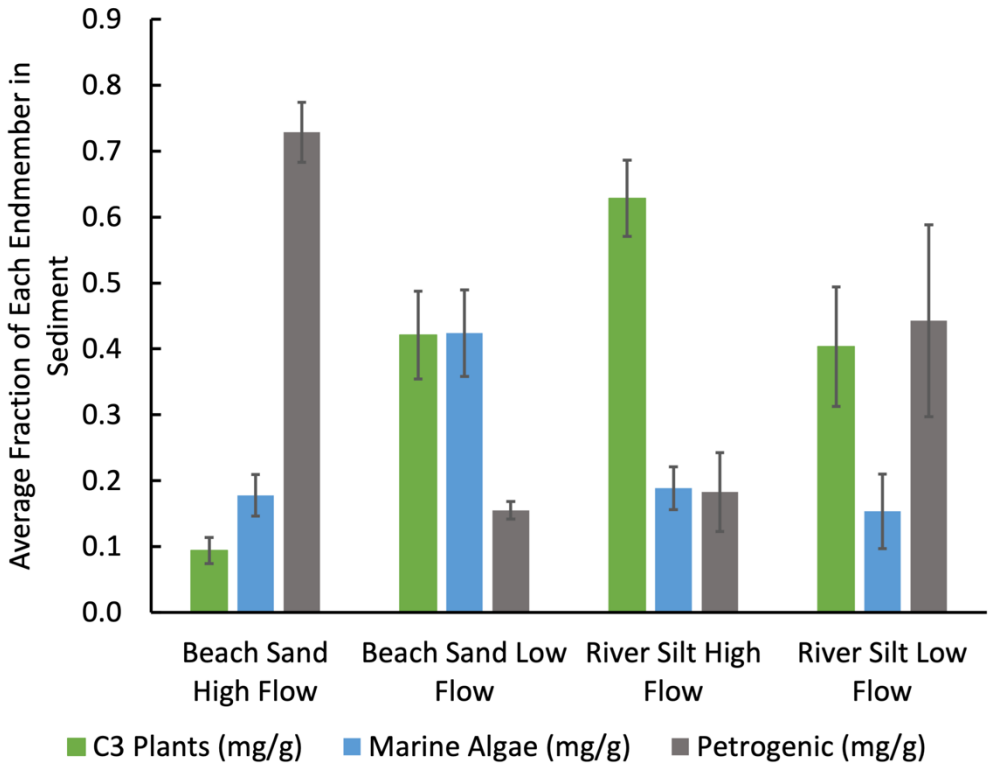

Figure 4.5. Histograms showing the average fraction of each endmember in sediment. Error bars show 1 standard error.

Table 4.3 The average fraction OC content of each end member in sediment samples.

Site	Time Period	C3 Plants	± (s.e.)	Marine Algae	±	Petrogenic	±
Beach Sand	High Flow	0.09	0.02	0.18	0.03	0.73	0.05
	Low Flow	0.42	0.07	0.42	0.07	0.16	0.01
River Silt	High Flow	0.63	0.06	0.19	0.03	0.18	0.06
	Low Flow	0.40	0.09	0.15	0.06	0.44	0.15

The beach sand OC during high flow periods was predominantly petrogenic material (Figure 4.5 and Table 4.3). During the low flow periods, C3 plants and marine algae contribute the more OC to the sediment than petrogenic OC (Figure 4.5 and Table 4.3). During the low flow periods, the estuary is separated from the sea by a sand berm, which allows plant and algal OC to accumulate in the estuary. Pieces of algae could be observed with the naked eye in the sand throughout the sampling depth (3 cm). Precipitation events

form a channel between the estuary and the sea that reduces the size of the lagoon and increases the flow rate through the estuary. Because most of the freshly produced algae is not present in the high-flow samples, it was likely either remineralized, buried to a depth >3 cm, or delivered to the ocean.

During both high and low flow periods, the river silt OC appears to be predominantly C3 plant material and has the highest OC concentrations of all the sediments tested (Figure 4.5 and Table 4.2). During the low flow period, river silt apparently contains lower recent C3 OC than the high flow period (Figure 4.5 and Table 4.3). This suggests that the modern OC deposited during the rainy season may not have been retained (e.g. remineralized, remobilized, diluted, or buried). During the dry periods with large algae blooms, relatively little algae was observed in the silt compared to that in the beach sand. This may have been due to increased turbulence in the water observed at this site compared to the beach sand site when the estuary was separated from the ocean.

Overall, the carbon isotopes of sediment OC suggest mixing of three isotopically distinct pools. Furthermore, each combination of river discharge and sediment type has a distinct OC composition. High flow sand contains mostly petrogenic OC, low flow sand contains mostly marine algae OC and C3 OC, high flow river silt contains mostly petrogenic C3 OC, and low flow river silt contains mostly C3 and petrogenic OC (Figure 4.5). Overall, this system displays highly dynamic OC cycling on monthly timescales.

4.5.2 SCR POC composition

During high flow periods, the POC can be described as a linear mixture of petrogenic OC and recently produced C3 plant OC (Figure 4.6). During high flow, more petrogenic

material was observed in the POC. This corresponded with higher sediment loads and lower percent OC in the sediment (Table 4.1a and Figure 4.2). The carbon isotope values of the POC were highly variable with stream flow. Visual inspection of the POC filters revealed oil drops and microplastics in the high flow samples. This is consistent with previous studies of the SCR and other small mountainous rivers, wherein precipitation mobilizes OC that is low in ^{14}C (Masiello and Druffel, 2001; Komada et al., 2004; Goñi et al., 2013). The petrogenic component of the POC appears to have a similar isotopic composition as that of the petrogenic OC in the sediment (Figure 4.4 and Figure 4.6). This suggests that there is a common source that contributes the majority of petrogenic OC to both pools.

Sampling of POC during the low flow periods coincided with algae blooms in the estuary. Notably the samples collected on 4/22/22 had a marine-like $\delta^{13}C$ value of -20.8 and -20.7‰ and the samples collected on 6/20/22 had a C3-like $\delta^{13}C$ value of -29.9 and -30.0‰ (Table 4.1a). Saltwater and freshwater algae species have different $\delta^{13}C$ values that resemble marine plankton and C3 plants respectively (Maberly et al., 1992). This large variation in $\delta^{13}C$ values suggests that the dominant species of algae in the estuary was changing on a month-to-month time scale.

All the remeasured samples from the high flow periods in 1997-1998 had higher $\Delta^{14}C$ values and lower $\delta^{13}C$ values than previously reported (Masiello and Druffel, 2001). We also remeasured samples from the Komada et al., 2004 study from 2002-2003 and our values were equal within error to the initial measurements. The remeasured samples from the low flow periods in 1997-1998 had $\Delta^{14}C$ and $\delta^{13}C$ values that were equal to the those previously reported (Masiello and Druffel, 2001). This is consistent with the hypothesis that the initial measurements were incompletely acidified (Masiello and Druffel, 2001;

Komada et al., 2004). The low flow samples' lower mineral loads could be adequately decarbonated using the weaker acidification method, while the high flow samples, with much higher mineral loads, required more aggressive acidification to completely remove the inorganic C.

4.5.3 POC loads and composition across varying precipitation

There are mass and isotopic data for SCR POC from three rainy seasons, each with different precipitation levels: 1997-1998 during extremely high precipitation, 2002-2003 during average precipitation, and 2021-2022 during low precipitation (Miller et al., 2022). There was less OC exported during 2021-2022 than that in 1997-1998 (Table 4.4). Despite this difference, the range of carbon isotopes is remarkably similar for the two periods (Figure. 4.6). The $\Delta^{14}C$ and $\delta^{13}C$ values for high flow POC samples appear be a mixture of recent C3 plant OC and petrogenic OC. The only outlier is the sample from 2-14-1998. It has a $\Delta^{14}C$ value of -584 ‰ and a $\delta^{13}C$ of -25.5 ‰ (Table 4.1b). This is inconsistent with marine shale as a source of low ^{14}C OC. These values could be explained by the presence of aged soils, which would have lower $\Delta^{14}C$ and similar $\delta^{13}C$ values to the recent C3 plant OC. If this point is excluded, all three years show a common petrogenic endmember with $\Delta^{14}C \approx$ -1000‰ and $\delta^{13}C \approx$-21.5‰ (Figure 4.6). If the modern endmember is assumed to have a C3 like $\delta^{13}C$ value (-23‰ to -28‰) then the $\Delta^{14}C$ values would be consistent with the ^{14}C content of atmospheric CO_2 near the time of collection (100 ‰ to 0 ‰) (Hua et al., 2013; Graven et al., 2022).

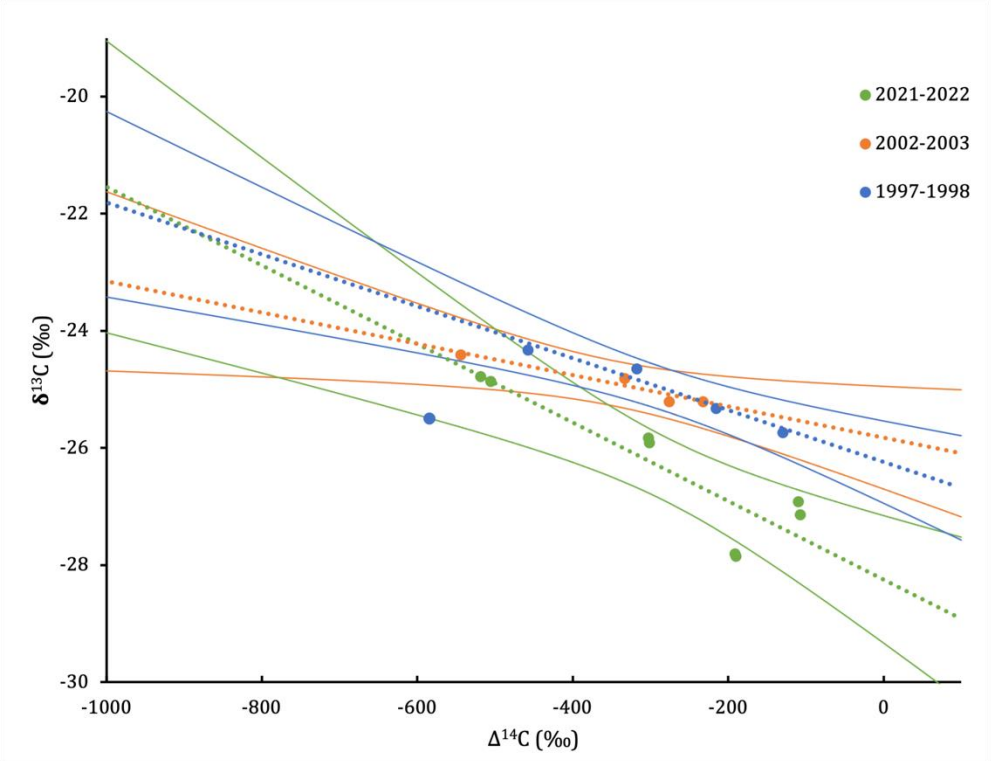

Figure 4.6. $\Delta^{14}C$ and ^{13}C values of POC collected during high flow events in 1997-1998 (blue), 2002-2003 (orange), and 2021-2022 (green). Dashed lines show linear regressions and solid lines show 95% confidence intervals. Error bars are smaller than the symbols.

We estimated the percent of petrogenic OC and recent C3 OC of the high flow POC samples using the mass balance equation (1).

$$\Delta^{14}C_{Total} M_{Total} = \Delta^{14}C_{Petrogenic} M_{Petrogenic} + \Delta^{14}C_{C3} M_{C3} \quad (1)$$

Petrogenic OC was assumed to have a $\Delta^{14}C$ value of -1000‰ and the modern OC was assumed to have a $\Delta^{14}C$ value equal to that of atmospheric CO_2 during the year of collection (1997-1998 $\Delta^{14}C$=101‰, 2002-2003 $\Delta^{14}C$=72‰, 2021-2022 $\Delta^{14}C$=0‰) (Hua et al., 2013; Graven et al., 2022). We then calculated the flow weighted average of the POC parameters. Weights of precipitation events were calculated by dividing the total flow for three days

after the beginning of each sampled precipitation event by the total flow of all precipitation events sampled during the occupation. Observed flow is the sum of the water discharge for each precipitation event during which samples were collected and total flow is the sum of the water discharged over the rainy season (December-March). Discharge outside of this time period is negligible due to low discharge rates and the separation of the estuary from the ocean. The weighted average values are summarized in Table 3.

Table 4.4 The flow weighted average characteristics of POC from high flow events sampled in 2021-22 (this work) and those published previously (Masiello and Druffel 2001; Komada et al., 2004).

Year	1997-1998	2002-2003	2021-2022
Weighted $\Delta^{14}C$ (‰)	-332 ± 76	-395 ± 102	-422 ± 202
Weighted $\delta^{13}C$ (‰)	-24.8 ± 0.8	-24.3 ± 0.5	-25.5 ± 1.7
Percent Petrogenic OC (%)	39 ± 6	44 ± 10.	42 ± 13
Percent C3 OC (%)	61 ± 6	56 ± 10.	58 ± 13
OC Concentration (mM)	14.0 ± 1.8	N.R.	0.2 ± 0.1
% OC (wt/wt) (%)	0.9 ± 0.3	1.4 ± 1.1	3.9 ± 1.8
Total Flow (L)	1.70×10^{12}	7.72×10^{11}	4.37×10^{10}
Observed Flow (L)	1.07×10^{12}	4.25×10^{11}	2.39×10^{10}

There were large differences in total and observed flow between the high flow years 1997-1998 and 2002-2003, and between 2002-2003 and 2021-2022 (Table 4.4). The weight % of OC in the sediment was inversely related to the total flow, indicating the mobilization of low-OC sediments (Table 4.4). This is consistent with other small mountainous rivers in the western United States (Goñi et al., 2013). The concentration of POC in river water in 1997-1998 was also 70 times greater than that in 2021-2022 (14.0 mM/0.2 mM) (Table 4.4). This resulted in ~3000 times as much POC exported during 1997-

1998 than that during 2021-2022 ($(1.70x10^{12}$ L * 14.0mM)/($4.37x^{10}$ L * 0.2 mM))(Table 4.4).

Despite the difference in streamflow and POC concentrations, the annual ratios of flow-weighted percent petrogenic OC to C3 OC are within error of each other for all years sampled (Table 4.4). This is a surprising and telling result. On average, a consistent mixture of ~40% petrogenic OC and ~60% C3 OC is exported by the SCR across a large range of precipitation levels (Table 4.4). This result is remarkable because of the extreme differences in total discharge and POC concentrations. We must first acknowledge the fact that we lack the data required to capture the full variability of this system. The variability in the chemical nature of sediment over the entire course of a rain event has not been adequately studied and the results from sampling once per precipitation event may not be representative of the entire flow. If the samples are representative, then this finding indicates that the annual average ratio of petrogenic OC and C3 OC is not dependent on the total stream flow over the rainy season. This contrasts with the fact that stream flow is clearly related to the total amount of exported POC. A possible explanation is that both petrogenic OC and C3 OC in this region are similarly mobilized by precipitation. The C3 OC likely comes from plant litter and soils. The SCR catchment features mostly grasslands, which have loosely held soils that are eroded each rainy season, and coastal sage scrub, which have tightly held soils that are mobilized by landslides (Gabet et al., 2005). Petrogenic OC can be found both as mineral bound shale that requires physical erosion to mobilize, and as oil seeps in the tributaries that are mobilized by any precipitation (Dibblee and Ehrenspeck, 1992; Aronson et al., 2022). Thus, increased precipitation and the

associated erosion from landslides, can mobilize both additional petrogenic and additional C3 OC.

4.6 Conclusion

The POC from the SCR and the OC from riverbank sediment displayed a wide range of $\Delta^{14}C$ and $\delta^{13}C$ values that is consistent with the substantial presence of petrogenic OC and modern OC. In the sediment samples, there was a relatively constant background of petrogenic OC with seasonably variable modern marine algae and C3 OC. During rain events, the exported POC from the SCR was a mixture of the petrogenic and C3 OC pools. When the estuary was separated from the ocean (low flow period), almost all of the OC appeared to be from the local algae. While the amount of POC exported in 2021-2022 was ~3000 times less than 1997-1998, the POC surprisingly contained ~40% petrogenic OC and ~60% modern C3 OC in all years with data. This work improves our understanding of the carbon cycle in small mountainous rivers across different climatic conditions. It is valuable for predicting the response of the C cycle in this region as anthropogenic climate change continues to disrupt the regional hydrological cycle.

4.7 References

Aronson, H. S., Monteverde, D. R., Barnes, B. D., Johnson, B. R., Zawaski, M. J., Speth, D. R., Wang, X. T., Wu, F., Webb, S. M., Trower, E. J., and others; (2022). Sulfur cycling at natural hydrocarbon and sulfur seeps in Santa Paula Creek, CA. Geobiology, 20, 707–725. https://doi.org/10.1111/gbi.12512

Birosik, S. (2006). *State of the Watershed – Report on Surface Water Quality: The Santa Clara River Watershed* (RB-AR22181). California Regional Water Quality Control Board, Los Angeles Region.

Blair, N. E., Leithold, E. L., & Aller, R. C. (2004). From bedrock to burial: The evolution of particulate organic carbon across coupled watershed-continental margin systems. *Marine Chemistry*, *92*(1), 141–156. https://doi.org/10.1016/j.marchem.2004.06.023

Brownlie, William R., and Brent D. Taylor. 2009. "Sediment Management for Southern California Mountains, Coastal Plains and Shoreline. Part C: Coastal Sediment Delivery by Major Rivers in Southern California". California Institute of Technology.

Dibblee, T.W., and Ehrenspeck, H.E., ed., 1992, Geologic map of the Santa Paula quadrangle, Ventura County, California: Dibblee Geological Foundation, Dibblee Foundation Map DF-41, scale 1:24,000

DeVecchio, D. E., Heermance, R. V., Fuchs, M., & Owen, L. A. (2012). Climate-controlled landscape evolution in the Western Transverse Ranges, California: Insights from Quaternary geochronology of the Saugus Formation and strath terrace flights. *Lithosphere*, *4*(2), 110–130. https://doi.org/10.1130/L176.1

Environmental Quality Laboratory. (1981). *Sediment Management for Southern California Mountains, Coastal Plains and Shoreline. Part C: Coastal Sediment Delivery by Major Rivers in Southern California*. https://doi.org/10.7907/Z9VT1Q1R

Frankson, R., Stevens, L. E., Kunkel, K. E., Champion, S. M., Easterling, D. R., Sweet, W., & Anderson, M. (2022). *California State Climate Summary 2022* (150-CA; NOAA Technical Report). NOAA NESDIS. https://statesummaries.ncics.org/chapter/ca

Goñi, M. A., Hatten, J. A., Wheatcroft, R. A., & Borgeld, J. C. (2013). Particulate organic matter export by two contrasting small mountainous rivers from the Pacific Northwest, U.S.A. *Journal of Geophysical Research: Biogeosciences*, *118*(1), 112–134. https://doi.org/10.1002/jgrg.20024

Graven, H., Keeling, R., & Xu, X. (2022). Radiocarbon dating: Going back in time. Nature, 607(7919), 449–449. https://doi.org/10.1038/d41586-022-01954-y

Hilton, R. G., & West, A. J. (2020). Mountains, erosion and the carbon cycle. *Nature Reviews Earth & Environment*, *1*(6), Article 6. https://doi.org/10.1038/s43017-020-0058-6

Hua, Q., Barbetti, M., & Rakowski, A. Z. (2013). Atmospheric Radiocarbon for the Period 1950–2010. *Radiocarbon*, *55*(4), 2059–2072. https://doi.org/10.2458/azu_js_rc.v55i2.16177

Hwang, J., Druffel, E. R. M., & Komada, T. (2005). Transport of organic carbon from the California coast to the slope region: A study of Δ14C and δ13C signatures of organic compound classes. *Global Biogeochemical Cycles*, *19*(2). https://doi.org/10.1029/2004GB002422

Komada, T., Anderson, M. R., & Dorfmeier, C. L. (2008). Carbonate removal from coastal sediments for the determination of organic carbon and its isotopic signatures, δ13C and Δ14C: Comparison of fumigation and direct acidification by hydrochloric acid. *Limnology and Oceanography: Methods*, *6*(6), 254–262. https://doi.org/10.4319/lom.2008.6.254

Komada, T., Druffel, E. R. M., & Trumbore, S. E. (2004). Oceanic export of relict carbon by small mountainous rivers. *Geophysical Research Letters*, *31*(7). https://doi.org/10.1029/2004GL019512

Maberly, S.C., Raven, J.A. & Johnston, A.M. Discrimination between ^{12}C and ^{13}C by marine plants. *Oecologia* **91**, 481–492 (1992). https://doi.org/10.1007/BF00650320

Masiello, C. A., & Druffel, E. R. M. (2001). Carbon isotope geochemistry of the Santa Clara River. *Global Biogeochemical Cycles*, *15*(2), 407–416. https://doi.org/10.1029/2000GB001290

McNaught, A. D., & Wilkinson, A. (1997). IUPAC Compendium of Chemical Terminology. 2nd Edition, The "Gold Book. Blackwell Scientific Publications.

Miller, M.P., Burley, T.E., and McCallum, B.E., 2022, Visit the U.S. Geological Survey's National Water Dashboard: U.S. Geological Survey General Information Product 213, 2 p., https://doi.org/10.3133/gip213.

Milliman, J. D., & Syvitski, J. P. M. (1992). Geomorphic/Tectonic Control of Sediment Discharge to the Ocean: The Importance of Small Mountainous Rivers. *The Journal of Geology*, *100*(5), 525–544.

Mook, W. G. (1986). 13C in atmospheric CO2. Netherlands Journal of Sea Research, 20(2), 211–223. https://doi.org/10.1016/0077-7579(86)90043-8

Reed, W. E., & Kaplan, I. R. (1977). The chemistry of marine petroleum seeps. *Journal of Geochemical Exploration*, *7*, 255–293. https://doi.org/10.1016/0375-6742(77)90084-X

Pataki, D. E., Ehleringer, J. R., Flanagan, L. B., Yakir, D., Bowling, D. R., Still, C. J., Buchmann, N., Kaplan, J. O., & Berry, J. A. (2003). The application and interpretation of Keeling plots in terrestrial carbon cycle research. Global Biogeochemical Cycles, 17(1). https://doi.org/10.1029/2001GB001850

Santos, G.M. J.R. Southon, N.J. Drenzek, L. Ziolkowski, E.R.M. Druffel, X. Xu, D. Zhang, S.E. Trumbore T.I. Eglinton and K.A. Hughen (2010). Blank assessment for ultra–small radiocarbon samples: chemical extraction and separation vs. AMS. *Radiocarbon* 52(3), 1322–1335.

Sarno, C. T., Benitez-Nelson, C. R., Ziolkowski, L. A., Hendy, I. L., Davis, C. V., Tappa, E. J., & Thunell, R. C. (2020). The Impacts of Flood, Drought, and Turbidites on Organic Carbon Burial Over the Past 2,000 years in the Santa Barbara Basin, California. *Paleoceanography and Paleoclimatology*, *35*(7), e2020PA003849. https://doi.org/10.1029/2020PA003849

Sternberg, L. O., Deniro, M. J., & Johnson, H. B. (1984). Isotope Ratios of Cellulose from Plants Having Different Photosynthetic Pathways. Plant Physiology, 74(3), 557–561. https://doi.org/10.1104/pp.74.3.557

Stock, B. C., Jackson, A. L., Ward, E. J., Parnell, A. C., Phillips, D. L., & Semmens, B. X. (2018). Analyzing mixing systems using a new generation of Bayesian tracer mixing models. *PeerJ*, *6*, e5096. https://doi.org/10.7717/peerj.5096

Walker, B. D., & Xu, X. (2019). An improved method for the sealed-tube zinc graphitization of microgram carbon samples and 14C AMS measurement. *Nuclear Instruments and Methods in Physics Research Section B: Beam Interactions with Materials and Atoms*, *438*, 58–65. https://doi.org/10.1016/j.nimb.2018.08.004

Xu, X., Trumbore, S. E., Zheng, S., Southon, J. R., McDuffee, K. E., Luttgen, M., & Liu, J. C. (2007). Modifying a sealed tube zinc reduction method for preparation of AMS graphite targets: Reducing background and attaining high precision. *Nuclear Instruments and Methods in Physics Research Section B: Beam Interactions with Materials and Atoms*, *259*(1), 320–329. https://doi.org/10.1016/j.nimb.2007.01.175

Chapter 5. Conclusions and Future Work

This thesis has improved our understanding of mechanisms that underlie coastal carbon cycling. It explored a variety of processes and environmental settings, and it points towards several possible future avenues of research. The following topics were addressed.

5.1 Summary of the dissertation

The second chapter sought to examine how the sorption of riverine DOC to marine sediments affects the isotopic content of the DOC. The experiments determined that sorption to the sediments was indeed isotopically selective and resulted in significant changes to the isotopic content of the remaining DOC. Organic carbon with higher $\Delta^{14}C$ and lower $\delta^{13}C$ than those of the bulk DOC was retained by the sediment. This suggests that material from the molecularly uncharacterized pool of DOC was sorbed to the sediment. This chapter serves as a proof of concept that demonstrates the importance of understanding this phenomenon in natural settings.

The third chapter reported a 12-year DIC $\Delta^{14}C$ record from the Newport Beach Pier in Orange County, CA. Seasonal upwelling and primary productivity were the most likely driving factors for seasonal variability of $\Delta^{14}C$ and $\delta^{13}C$ values, respectively. In addition, variability in the seasonal $\Delta^{14}C$ values declined compared to previous seasons, suggesting that less water from the North Pacific Gyre entered the Southern California Bight during the study period. Average annual values of both $\Delta^{14}C$ and $\delta^{13}C$ significantly declined during the study period indicating that the change in atmospheric CO_2 isotopic values was likely controlling the $\Delta^{14}C$ and $\delta^{13}C$ values of the surface DIC. Notably, in 2022, the $\Delta^{14}C$ of

atmospheric CO_2 and the Newport Beach Pier surface DIC were nearly equal. This record sets the stage for monitoring changes in the coastal C sink in the coming decades.

The fourth chapter reports the POC exported by the Santa Clara River and the OC from the sediments of its estuary during the 2021-2022 rainy season. Significant quantities of both plant-derived and petrogenic OC were transported by the river and found in the estuarine sediments. During the dry season significant quantities of algae-derived OC were present in the sediments. This material was not present during the wet season in the estuary and was likely either remineralized or transported offshore. Despite the significant differences in total stream flow between the study year and previous records, an equivalent mixture of ~40% petrogenic C and modern ~60% plant derived C was exported by the river for the years studied (Masiello and Druffel, 2001; Komada et al., 2004). However, the POC was far more concentrated in the high precipitation year, which resulted in ~3000 times more OC being exported in 1997-1998 than in 2021-2022. Examination of the sedimentary OC stored at the Santa Clara River estuary showed predominant storage of petrogenic OC and rapid cycling of algae OC produced during the dry season.

5.2 Future research

In my future work, I plan to continue examining the role of coastal systems in connecting terrestrial C with that in the ocean. Continuous monitoring of these sites is crucial for two main reasons: (1) human activity and climate change is continuing to alter the sediment and OC flux of rivers (Maavara et al., 2017), and (2) the $\Delta^{14}C$ of atmospheric CO_2 is now lower than that of the biosphere and surface ocean and is continuing to decline (Graven et al., 2022). The offset between these pools provides a valuable opportunity for

tracing carbon fluxes among them. The rate of equilibration between these pools will provide us with vital information about the rates of photosynthesis, air-sea CO_2 exchange, and CO_2 emissions. The more samples we can collect in the coming years, the better we will be able to disentangle these processes.

Our research group has obtained a RAPID National Science Foundation grant to examine the C export from the Santa Clara River during the 2023-2024 wet season. Due to the rapid shift to El Niño conditions (Trenberth et al., 2023), we anticipate that heavy rains will begin in late 2023, as they did in 1997-1998 (Masiello and Druffel, 2001; Jong et al., 2016). We hope to significantly improve the sampling resolution to better document the OC exported during heavy precipitation. We will also examine the variability in the POC export over the course of a single rain event, which has not been done previously. This variability is currently unknown and could have significant impact on interpreting measurements from small mountainous rivers.

I plan to also examine the reactivity of the petrogenic C exported by the Santa Clara River. The main source of petrogenic C in the watershed includes the Monterey Formation (Dibblee and Ehrenspeck, 1992). This formation contains both kerogen that has mineral bound OC, and oil seeps that produce free OC (Aronson et al., 2022). The free OC is likely far more reactive than the mineral bound OC and therefore more likely to be remineralized and contribute to outgassing to the atmospheric. I aim to quantify several biogeochemical parameters of these two sources, including $\Delta^{14}C$ values, $\delta^{13}C$ values, $\delta^{34}S$ values, and lipid profiles. These parameters can then be applied to the OC that reaches the estuary to obtain estimates of the reactivity of the exported POC.

We have also continued our monitoring of the dissolved inorganic C at Newport Beach Pier. The year 2023 was fascinating because of the extreme atmospheric rivers (NOAA, 2023) in the winter and because of the rapid switch from La Niña to El Niño conditions in the summer (Trenberth et al., 2023). We have increased the sampling frequency during these events and plan to examine how these events impact upwelling and water mass mixing at our sampling site. Additionally, we plan to use the current 18-year record of C isotope data to estimate the storage of anthropogenic C in the Southern California Bight. This effort would provide another method of examining the marine anthropogenic C sink to compare with more traditional methods.

Overall, the cycling of C in coastal waters is a dynamic topic that is critical for adequate evaluation of the global C cycle. These regions face major impacts from human activities and support vital marine ecosystems. Their complexity and heterogeneity call for continued study with a variety of techniques. I am excited and humbled to contribute to that effort.

5.3 References

Aronson, H. S., Monteverde, D. R., Barnes, B. D., Johnson, B. R., Zawaski, M. J., Speth, D. R., Wang, X. T., Wu, F., Webb, S. M., Trower, E. J., and others; (2022). Sulfur cycling at natural hydrocarbon and sulfur seeps in Santa Paula Creek, CA. Geobiology, 20, 707–725. https://doi.org/10.1111/gbi.12512

Dibblee, T.W., and Ehrenspeck, H.E., ed., 1992, Geologic map of the Santa Paula quadrangle, Ventura County, California: Dibblee Geological Foundation, Dibblee Foundation Map DF-41, scale 1:24,000

Komada, T., Druffel, E. R. M., & Trumbore, S. E. (2004). Oceanic export of relict carbon by small mountainous rivers. *Geophysical Research Letters*, *31*(7). https://doi.org/10.1029/2004GL019512

Maavara, T., Lauerwald, R., Regnier, P., & Van Cappellen, P. (2017). Global perturbation of organic carbon cycling by river damming. Nature Communications, 8(1), Article 1. https://doi.org/10.1038/ncomms15347

Masiello, C. A., & Druffel, E. R. M. (2001). Carbon isotope geochemistry of the Santa Clara River. Global Biogeochemical Cycles, 15(2), 407–416. https://doi.org/10.1029/2000GB001290

Jong, B.-T., Ting, M., & Seager, R. (2016). El Niño's impact on California precipitation: Seasonality, regionality, and El Niño intensity. Environmental Research Letters, 11(5), 054021. https://doi.org/10.1088/1748-9326/11/5/054021

NOAA National Centers for Environmental Information, Monthly National Climate Report for March 2023, published online April 2023, retrieved on November 11, 2023, from https://www.ncei.noaa.gov/access/monitoring/monthly-report/national/202303.

Trenberth, Kevin & National Center for Atmospheric Research Staff (Eds). Last modified 2023-07-25 "The Climate Data Guide: Nino SST Indices (Nino 1+2, 3, 3.4, 4; ONI and TNI)." Retrieved from https://climatedataguide.ucar.edu/climate-data/nino-sst-indices-nino-12-3-34-4-oni-and-tni on 2023-11-11.

Appendix A. Quantifying carbon recovery in sorption experiments

A.1 Recovered OC in sorption experiments

The percent recovery of OC was estimated for both the total OC in each experiment and the SRNOM OC in each experiment. The amount of OC present in the experiments was estimated using the results of the control experiments (table 1) and the initial mass of sediment and SRNOM present in each experiment (table 2), as shown in equation a.1.

$$M_{\text{Total OC}} = 0.0121 \frac{mg\ OC}{mg\ sediment} \cdot m_{sediment} + 0.428 \frac{mg\ OC}{mg\ SRNOM} \cdot m_{SRNOM} \qquad \text{Equation A.1}$$

Total OC recovery was determined by summing the masses of OC collected in each experiment, as shown in equation A.2.

$$M_{\text{Recovered OC}} = M_{\text{POC}} + M_{\text{DOC}} \qquad \text{Equation A.2}$$

Total SRNOM OC in each experiment was determined in the same manner as equation A.1 and is shown in equation A.3.

$$M_{\text{SRNOM OC}} = 0.428 \frac{mg\ OC}{mg\ sediment} \cdot m_{SRNOM} \qquad \text{Equation A.3}$$

Soluble SRNOM recovery was determined by subtracting the mass of soluble sediment OC from the mass of total DOC (tables 1 and 2), as shown in equation A.4.

$$M_{\text{Total Recovered OC}} M_{\text{soluble SRNOM}} = M_{\text{DOC}} - 0.00008 \frac{mg\ OC}{mg\ sediment} \cdot m_{Sediment} \quad \text{Equation A.4}$$

Insoluble SRNOM recovery was determined by multiplying the initial mass of SRNOM by the ratio of insoluble SRNOM OC (table 1), as shown in equation A.5.

$$M_{\text{insoluble SRNOM}} = 0.047 \frac{mg\ OC}{mg\ SRNOM} \cdot m_{SRNOM} \quad \text{Equation A.5}$$

Sorbed SRNOM recovery was determined by subtracting the mass of insoluble SRNOM OC from the mass of POC and then multiplying the remainder by percent increase in OC/mg of sediment (6%) as described in the results section of the main text, as shown in equation A.6.

$$M_{\text{sorbed SRNOM}} = (M_{\text{POC}} - M_{\text{insoluble SRNOM}}) \cdot 0.06 \quad \text{Equation A.6}$$

The results of these calculations are shown in figure 2.2. Average total OC recovery for samples where both DOC and POC were measured was 88.7±12.4% and ranged from 47.6% to 100.0%. Average SRNOM recovery for samples where both DOC and POC were measured was 81.0±13.2% and ranged from 47.5% and 99.0%

A.2 Estimating POC isotopes with 2 and 3 endmember models

As described in figure 2.1, we assume that the POC is made of three endmembers: insoluble sediment OC, insoluble SRNOM, and sorbed SRNOM. To determine whether

SRNOM sorbed to the sediment, we created two simple models. The first assumed that no sorption took place and thus, the isotopes of the POC can be described by the mixing of insoluble sediment OC and insoluble SRNOM. The model is described below using equations A.7 and A.8.

$$^{14}C_{\mathrm{POC}} = ((-432‰ \cdot \frac{12.1\mu gOC}{mg\ sediment}) + (37‰ \cdot 115\mu gOC))\frac{1}{\mathrm{M_{POC}}}$$ Equation A.7

$$^{13}C_{\mathrm{POC}} = ((-22.2‰ \cdot \frac{12.1\mu gOC}{mg\ sediment}) + (-28.0‰ \cdot 115\mu gOC))\frac{1}{\mathrm{M_{POC}}}$$ Equation A.8

These equations were derived from equation 2, by using the mass of sediment OC and the isotopic values of insoluble sediment OC and insoluble SRNOM derived from the control experiments, and the mass of insoluble sediment OC from equation 3. The mass of sor bed carbon is assumed to be zero.

The second model assumed that sorption did occur and therefore the POC can be described as the sum of insoluble sediment OC, insoluble SRNOM, and sorbed SRNOM. The model is described below using equations A.9 and A.10

$$^{14}C_{\mathrm{POC}} = ((-432‰ \cdot \frac{12.1\mu gOC}{mg\ sediment}) + (37‰ \cdot 115\mu gOC) + (130‰ \cdot \frac{0.8\mu gOC}{mg\ sediment}))\frac{1}{\mathrm{M_{POC}}}$$

Equation A.9

$$^{13}C_{\mathrm{POC}} = ((-22.2‰ \cdot \frac{12.1\mu gOC}{mg\ sediment}) + (-28.0‰ \cdot 115\mu gOC) + (-30‰ \cdot \frac{0.8\mu gOC}{mg\ sediment})\frac{1}{\mathrm{M_{POC}}}$$

Equation A.10

The equations were derived in the same manner as A.7 and A.8 with the addition of the mass and isotopic values of sorbed SRNOM as derived in the discussion section of the main text.

These equations were plotted against mass of sediment and compared to the observations and shown in figure A.1. When sediment masses were >50mg, the observed data agreed more with the 3-endmember model than with the 2-endmember model for both isotopes. We interpret this as showing that sorption of SRNOM explains the observed isotope values of the POC.

a

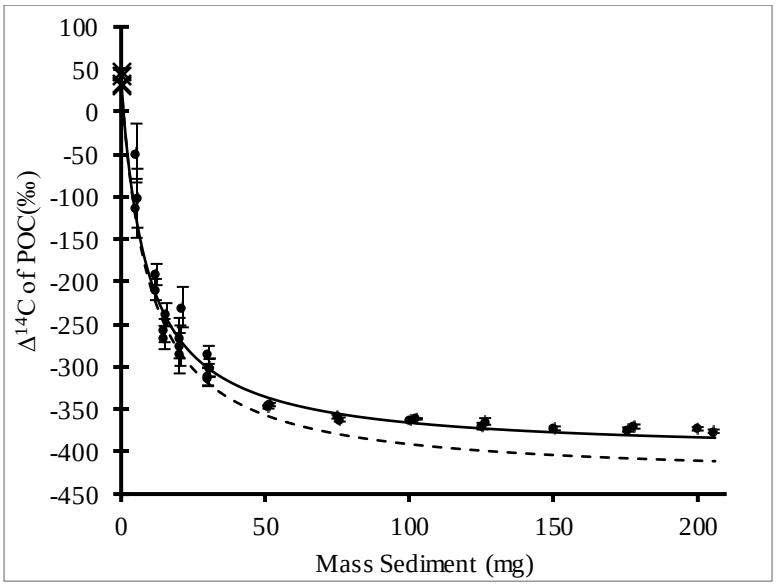

b

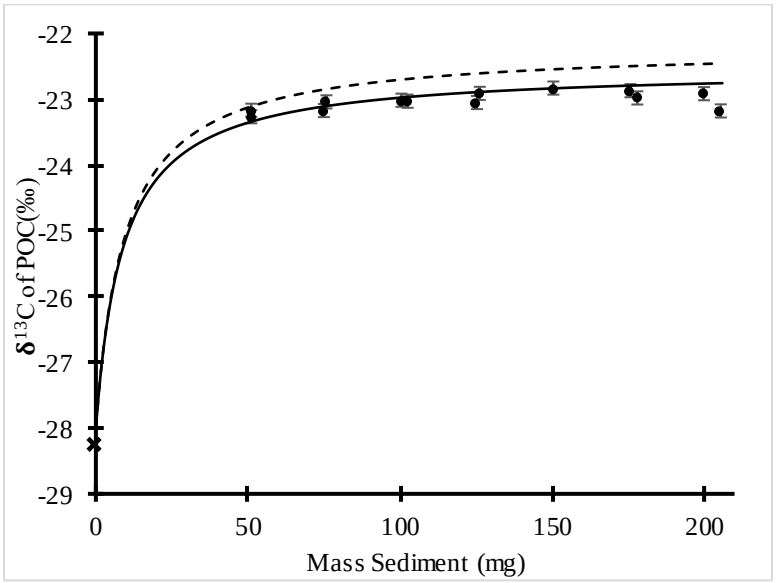

Figure A.1: a) $\Delta^{14}C$ and b) $\delta^{13}C$ of the 2-endmember (dashed line) and 3-endmember (solid line) compared to the isotopic values of POC recovered after control experiments (crosses) and sorption experiments (circles) as a function of increasing sediment mass used. Error bars show uncertainty as described in the text. Any error bars not visible are smaller than the size of the symbol. Initial masses of SRNOM were kept constant throughout the experiment.

Appendix B. Ventilation time of the California Undercurrent

B.1 Chemical tracers in the waters near the sampling site.

In this section we show ventilation age and DIC isotope values from the waters of the Southern California Bight (SCB) close to our sampling site. This is done to provide the reader with further background and context for the source waters described in the main text.

CFC age data was obtained from the National Oceanic and Atmospheric Administration NCEI Accession 0226793 data set (https://www.ncei.noaa.gov/data/oceans/ncei/ocads/metadata/0226793.html). CFC ages were calculated based on samples from the Global Ocean Data Analysis Project (GLODAP) V2.

Dissolved inorganic carbon (DIC) $\Delta^{14}C$ and $\delta^{13}C$ data were obtained from the GLODAP V2 data set (https://www.glodap.info/index.php/merged-and-adjusted-data-product-v2-2022/). The data is obtained from two cruises: 318M20040615 that occurred during August 2004, and 318M20130321 that occurred during August 2013.

Figures S1 and S2 show depth profiles from stations between latitudes 32°N to 32.63°N and longitudes 117.38°W to 119.77°W. This encompasses stations on the continental shelf and slope within the SCB. Figure B.3 shows zonal transects from the two cruises and the transects are located between 29.977°N and 32.63°N.

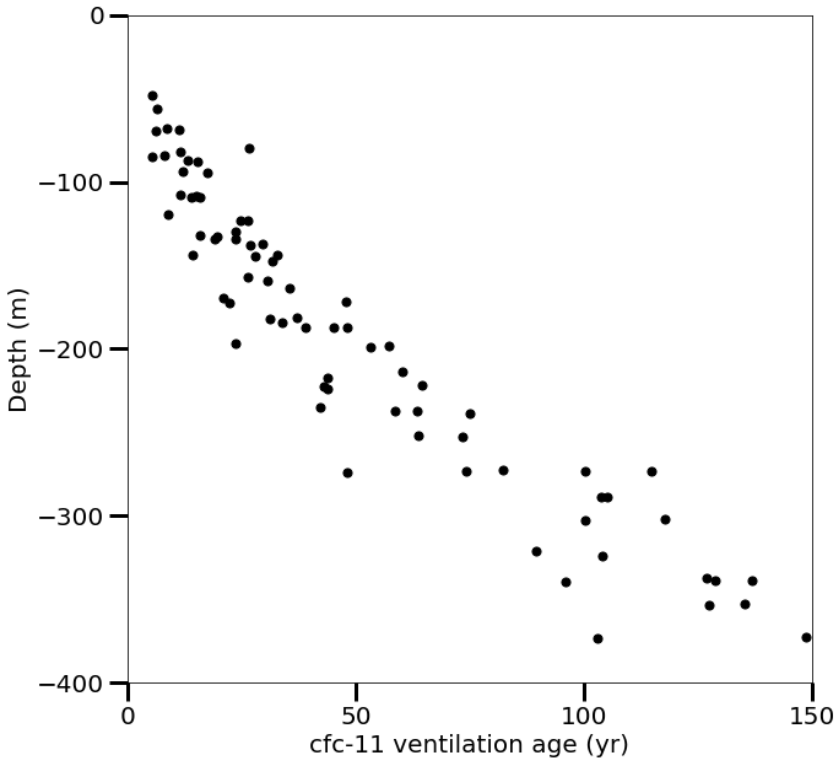

Figure B.1. CFC-11 ventilation age calculated using the transit time distribution method as described in (Jeansson et al., 2021) vs depth within the Southern California Bight.

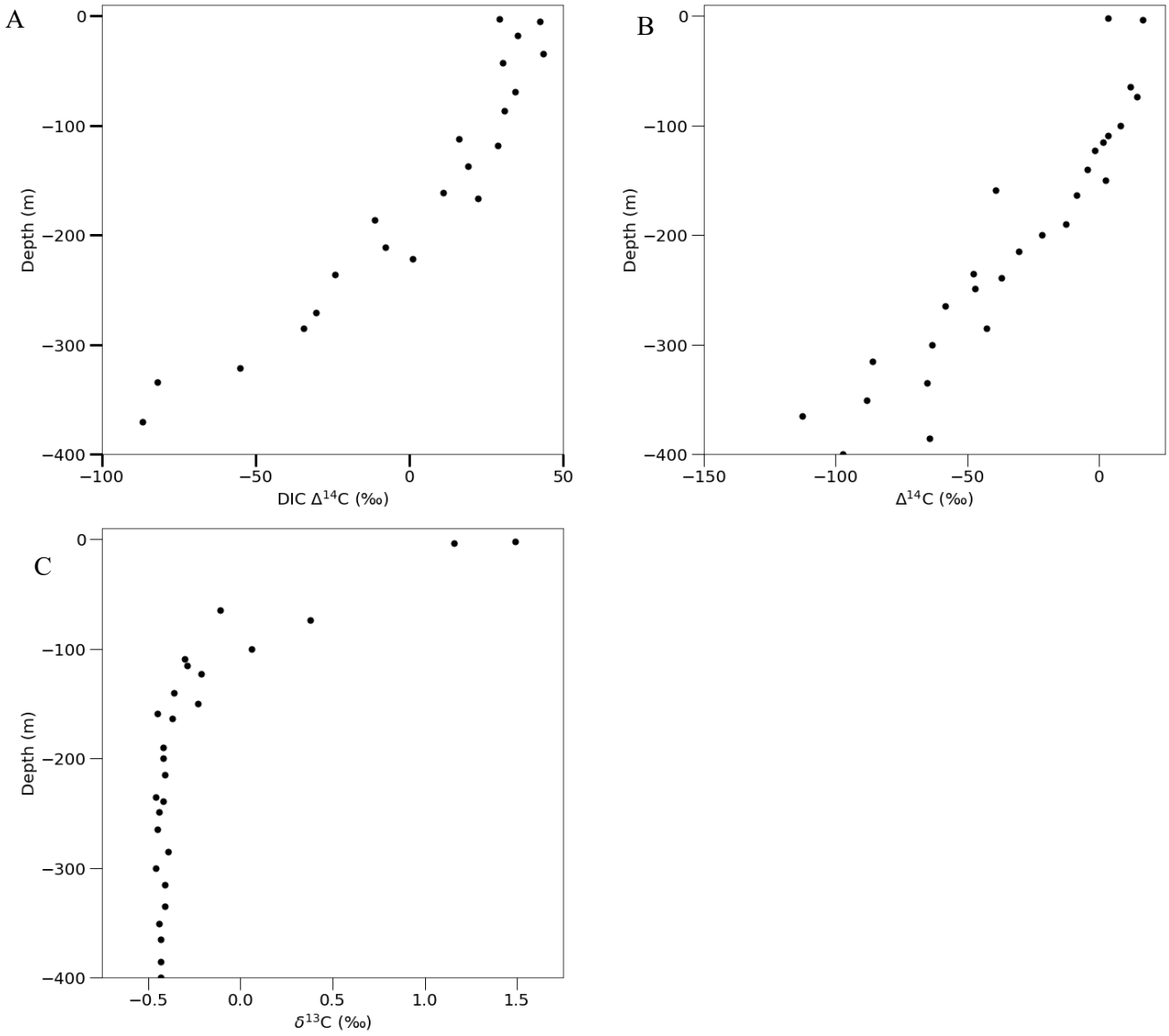

Figure B.2: Depth profiles DIC $\Delta^{14}C$ values from 2004 (a) and 2013 (b) and DIC $\delta^{13}C$ values from 2013 (c).

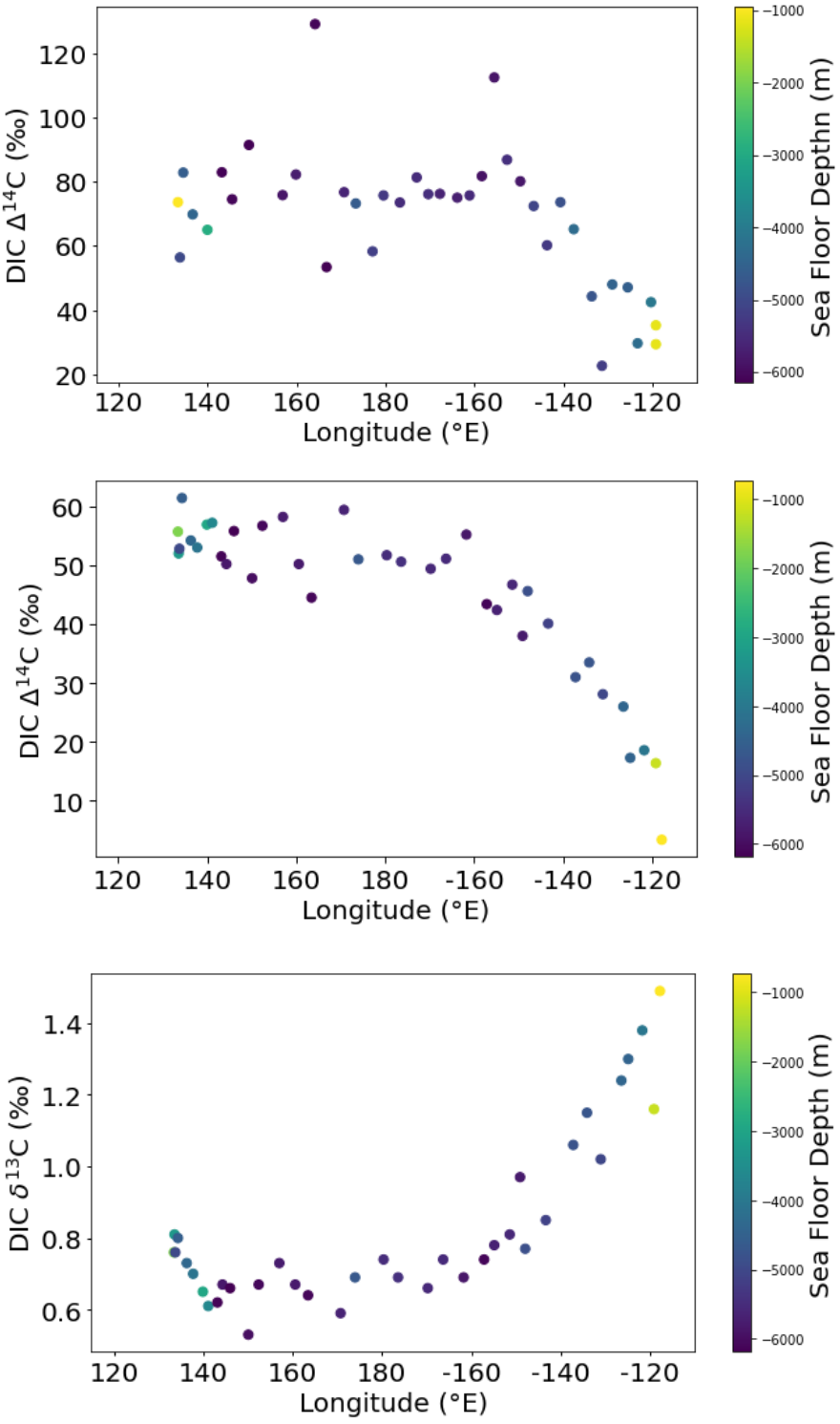

Figure B.3: Zonal transects showing surface (>20m) DIC $\Delta^{14}C$ values from 2004 (a) and 2013 (b) and DIC $\delta^{13}C$ values from 2013 (c).